CHAPTER 3

ASSESSMENT OF SOLAR PHOTOVOLTAIC POTENTIAL IN RURAL ASSAM

3.1 Introduction

As outlined in the preceding Chapters, the adoption and growth of solar energy in Assam, India, remain notably slow despite the region's abundant solar resources, increasing demand for sustainable energy solutions, and promotional efforts by the government (Chapter 1). This disparity highlights the critical need for a precise and comprehensive understanding of the solar energy generation potential in the region. A robust framework to understand the potential of solar energy sharable among stakeholders including end-users, policymakers and energy promoters is essential for facilitating widespread adoption of solar energy technologies. Assessment of the solar photovoltaic (PV) potential in a region, particularly in rural areas, necessitates a spatial framework that integrates diverse and dynamically variable input parameters (elaborately discussed in Chapters 1 and 2). Precise data for representing spatially and temporally variable parameters are essential inputs for generating accurate and actionable insights. Existing tools and methodologies, while effective in specific contexts, are limited in their ability to accommodate the dynamic variability and diverse requirements of stakeholders. To address the critical gap, this study develops and applies a novel spatial and temporal framework for assessing solar photovoltaic energy potential in rural Assam, demonstrating its utility in localized energy planning.

In addition to PV potential assessment, this study addresses the environmental impacts associated with the deployment of SPV systems by estimating Lifecycle Greenhouse Gas (GHG) emissions. It underscores the ecological aspects of transitioning from conventional energy sources to solar technologies, highlighting their contribution to environmental sustainability.

This Chapter is organized in two parts to present both the above aspects systematically as elaborated below.

The **PART A** (Spatial and Temporal Assessment of Solar Photovoltaic Potential) details the development and subsequent application of a framework to assess solar energy generation potential at spatial and temporal scales. The methodology consisting of (i) conceptualising the physical framework, (ii) development of spatial-temporal models, (iii) application of the model for spatial and temporal assessment of solar energy potential, (iv) data sources, and (v) assumption and limitations is presented in this **PART A** along with results and discussions.

PART B (Lifecycle GHG Emission Estimation) presents the methodology of assessment of GHG emissions attributed to distinctive lifecycle phases of the three solar PV systems (viz., RTS, GMS, and SWP). The greenhouse gas (GHG) emission reduction potential of solar PV systems compared to conventional electricity has been highlighted in Chapters 1 and 2. However, the diversity in existing GHG assessment methodologies necessitates a tailored approach. Based on a comprehensive review of the existing literature, this study adopts a rationale lifecycle analysis framework to estimate GHG emissions associated with the solar energy systems under consideration and is presented in **Part B** of this Chapter.

By exploring the nexus among (i) solar energy availability (ii) space availability (iii) preference for generation option and (iv) system performance in connection with the deploying solar energy systems, this Chapter establishes a foundation for discussions in subsequent Chapters, integrating these analyses into the broader narrative of energy planning and sustainability. It contributes to strategic energy planning, promotes renewable energy integration, and supports the formulation of effective policies for achieving sustainability in rural energy systems.

PART A: SPATIAL AND TEMPORAL ASSESSMENT OF SOLAR PHOTOVOLTAIC POTENTIAL

3.2 Conceptualizing the physical framework

3.2.1 Energy potential of solar PV systems: description of physical framework

The central focus of this research is solar energy, with a specific emphasis on solar PV energy. Estimating solar energy potential is a multidimensional and dynamic challenge, influenced by spatial, temporal, and technological factors. Solar energy is inherently variable and uncertain, as its availability depends on geographical, meteorological, and land-use characteristics. **Fig. 3.1** illustrates a conceptual framework that traces the flow of solar energy from its source, the Sun, to its end use.

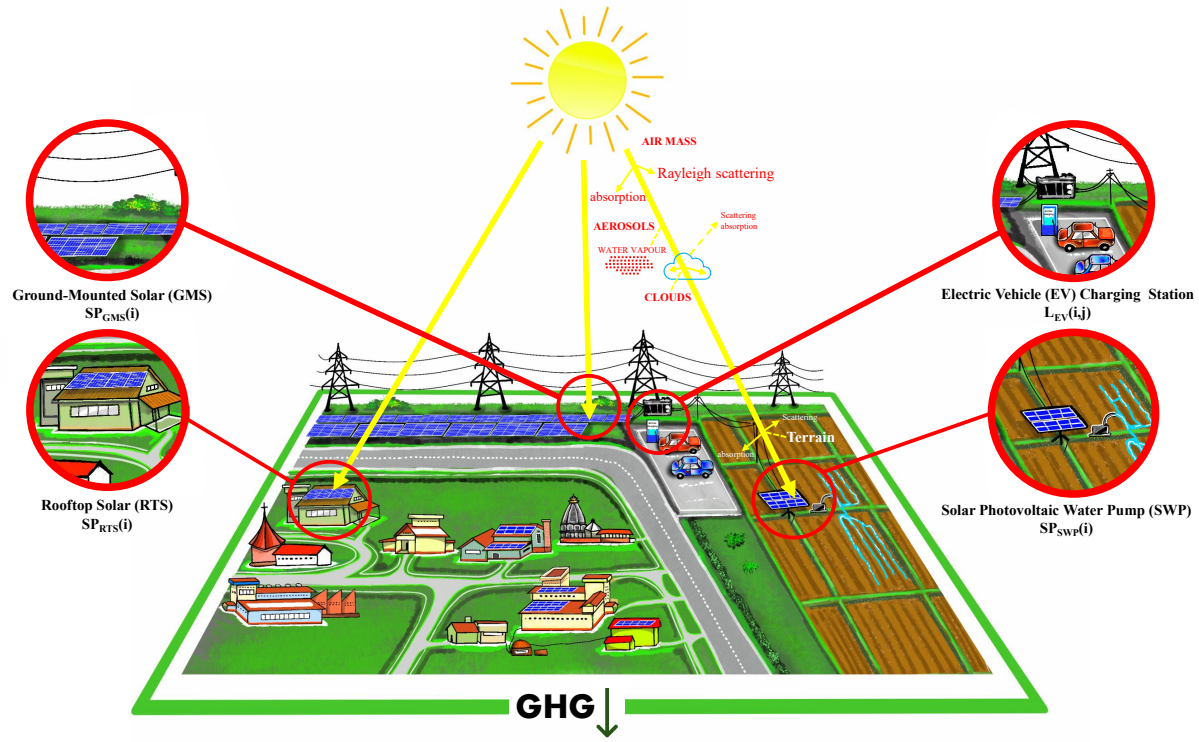

Fig 3.1: Conceptual framework representing a description of physical systems

Solar radiation intercepted by the Earth's surface is influenced by variations in land use, competing applications, and human activities. Accurate estimation of solar energy potential requires a thorough understanding of interrelated factors, including land-use and land-cover (LULC) classification, land applications, technological parameters of solar systems, and the

nature of transmission of harvested energy. LULC classification plays a pivotal role in identifying areas suitable for solar installations. Suitability depends on the type of system: RTS requires unshaded, structurally sound rooftops; GMS relies on large, barren, or fallow tracts of land; and SWP systems are suited to agricultural zones with specific water demand patterns. Evaluating solar potential requires consideration of current land use and anticipation of future changes driven by urbanisation, industrialization, or policy shifts. This dual focus ensures that solar energy planning is both effective and sustainable.

Solar radiation variability over time and space, combined with the performance of PV collectors, significantly affects the quantity of energy that can be harvested. The performance of PV modules depends on environmental conditions and technical characteristics, which need to be estimated precisely. Energy transmission to end users also presents challenges, such as transmission losses and fluctuating demand profiles. This research proposes an integrative methodology to represent the real-life representation of the complexities and uncertainties of physical systems concerned with the estimation of solar energy.

3.2.2 Key parameters for the assessment of solar PV energy potential

By utilising diverse data sources, including satellite imagery, ground-based observations, and field surveys, this study develops a comprehensive framework for evaluating solar energy potential. The proposed spatial-temporal model captures dynamic variations in solar radiation, land-use patterns, and system performance attributes. It also accounts for the heterogeneity of land surfaces, recognising diverse land-use types and competing applications. Temporal dynamics are incorporated to address fluctuations in solar radiation and their implications for energy generation. This multidimensional framework provides a detailed understanding of solar energy potential while guiding land-use and energy resource management decisions. By addressing the dynamic interplay of geographic and technological factors, the framework enhances the sustainability and efficacy of solar energy planning.

3.3 Development of the spatial-temporal model for solar PV potential assessment

Spatial-temporal modelling forms the backbone of solar PV potential assessment, offering a dynamic approach to capture variations in solar energy availability over time and across different locations. As discussed earlier, this model development integrates environmental factors, solar irradiance patterns, and land use characteristics to generate accurate and context-

specific insights. By incorporating advanced mathematical techniques and real-world parameters, the spatial-temporal model ensures robust predictions, aiding in optimizing solar installations and maximizing energy output across diverse geographic regions. The development of the framework is based on fundamental relationships expressed to capture spatial and temporal aspects as detailed below.

The solar energy generation potential of a region with given geographical boundary, during a specified period is estimated using fundamental relationships. However, for considering the variabilities concerning space and time, the region is divided into distributed spatial elements (smaller units). Similarly, the specified duration is also disintegrated into smaller temporal units. The assessed locational and temporal potential is then integrated over the entire region and duration.

3.3.1 Considerations for spatial variations

The geographical locations suitable for the installation of solar PV systems are identified using standard geospatial techniques. The administrative boundaries encompassing such variable locations are preferred to estimate the (i) solar energy potential and (ii) available land resources.

3.3.2 Considerations for temporal variations

When evaluating the potential for solar energy generation, it is crucial to consider the duration of sunlight available at a given location, as it directly impacts the overall energy yield. The sunrise, sunset, and day length can be calculated using specific equations that take into account the observer's latitude, the solar declination, and the time of year. Equation 3.1 is used for calculating sunrise and sunset times based on the solar hour angle [1]:

$$\cos \omega_{\circ} = -\tan \phi \times \tan \delta \tag{3.1}$$

where $\omega_{\circ}$ is the solar hour angle (negative for sunrise, positive for sunset); ϕ is the latitude of the observer; δ is the solar declination, which varies throughout the year and can be estimated using Eq. 3.2.

$$\delta = 23.44° \times sin\left(\frac{360}{365} \times (n + 10)\right) \tag{3.2}$$

where n is the day of the year.

The hour angle ($\omega_\circ$) is converted to time (Eq. 3.3) noting that the Earth rotates at 15° per hour:

$$t = \frac{\omega_\circ}{15^\circ} \tag{3.3}$$

The local sunrise or sunset times are adjusted by adding or subtracting this time from local noon. The length of daylight is then calculated by finding the difference between sunset and sunrise times as shown in Eq. 3.4.

$$t_{daylight} = t_e - t_s \tag{3.4}$$

3.3.3 Theoretical solar PV energy potential: assessment at spatial and temporal scales

The daily energy generation by a photovoltaic (PV) system at location i and time j is given by Eq. 3.5.

$$E(i) = \frac{\eta_{PV} \times A(i)}{1000} \times \int_{t_s}^{t_e} SI(i,j)dt \tag{3.5}$$

where $E(i)$ is the total energy generated by the PV system, kWh/day; η_{PV} is the efficiency of the solar PV module; $A(i)$ is the area of the PV system available for installation at location i, m²; $SI(i,j)$ is the solar irradiance incident at location i and time j, W/m²; t_s and t_e are the start and end times for solar irradiance (sunrise and sunset); and the factor $\frac{1}{1000}$ converts W to kW.

Consequently, the total solar energy $E_{sol}(i,j)$ available at location i and time j can be estimated using Eq. 3.6.

$$E_{sol}(i,j) = \sum_{j=t_s}^{t_e} (SI(i,j) \times \eta_{surf}(i,j) \times \Delta t) \tag{3.6}$$

where $E_{sol}(i,j)$ is the total solar energy reaching the surface, kWh/m²; $\eta_{surf}(i,j)$ is the efficiency factor representing the fraction of extraterrestrial solar irradiance that successfully reaches the surface. This efficiency typically ranges between 0 and 1, with a value closer to 1 indicating minimal losses.

The surface efficiency factor, $\eta_{surf}(i,j)$, varies spatially and temporally due to location-specific and time-dependent factors. Spatially, it is influenced by atmospheric conditions like pollution, dust, or aerosols, which reduce transmittance, and altitude, which may lower

atmospheric losses. Local shading from buildings, trees, or terrain, as well as microclimatic variations like frequent cloud cover, also impact efficiency. Temporally, $\eta_{surf}(i,j)$ is affected by dynamic cloud cover, changes in solar angle causing variable atmospheric losses, and seasonal or daily shifts in shading patterns, such as longer shadows in winter or during early morning and late afternoon.

Integration with the energy output equation, the total energy $E(i)$ generated at location i is given by Eq. 3.7.

$$E(i) = \eta_{PV} \times A(i) \times E_{sol} \tag{3.7}$$

Substituting $E_{sol}(i,j)$ from Eq. 3.6 the new equation (Eq. 3.8) becomes

$$E(i) = \eta_{PV} \times A(i) \times E_{sol} \times \left(\sum_{j=t_s}^{t_e} (SI(i,j) \times \eta_{surf}(i,j) \times \Delta t)\right) \tag{3.8}$$

3.3.4 Achievable solar PV energy potential

In Eq. 3.8 the total energy generated by a PV system, the parameters were considered under ideal conditions. However, in actual practice, the energy generated is influenced by additional real-world factors, such as shading, inverter efficiency, tilt orientation, and module temperature.

To account for these influences, the equation is modified to include correction factors. The impact of temperature is accounted for using the Power Temperature Coefficient (PTC), which represents the percentage change in the output of a PV module for every degree Celsius deviation from the standard operating temperature of 25°C. Incorporating these factors, the modified equation becomes [2-5]:

$$E(i) = \eta \times A(i) \times E_{sol} \times (1 - L_{shading}) \times \eta_{inv} \times F_{tilt} \times \left(1 + \frac{PTC \times (T_{module} - 25℃)}{100}\right) \tag{3.9}$$

where $L_{shading}$ represents the percentage of energy loss due to shading; F_{tilt} adjusts the effective irradiance based on panel angle; η_{inv} represents the inverter efficiency; PTC is the temperature coefficient of power, %/°C; T_{module} is the module temperature, °C.

$$T_{module} = T_{ambient} + \left(\frac{NOCT - 20}{800}\right) \tag{3.10}$$

$NOCT$ being the Nominal Operating Cell Temperature, $\left(1+\frac{PTC\times(T_{module}-25℃)}{100}\right)$ adjusts the power output based on the deviation of the module temperature from the standard 25°C.

The correction factor can be represented as Performance Ratio (PR)

$$PR=(1-L_{shading})\times F_{tilt}\times\left(1+\frac{PTC\times(T_{module}-25℃)}{100}\right) \quad (3.11)$$

The performance ratio can also be represented as:

$$PR=\frac{Actual\ Output\ Energy}{Theoretical\ Maximum\ Energy\ Output\ at\ STC} \quad (3.12)$$

The performance ratio is a measure of the overall efficiency of a solar PV system, including all losses such as temperature effects, inverter losses, shading, dirt on panels, and other factors. It is expressed as a percentage of the theoretical maximum efficiency. Typical Value: PR typically ranges from (0.50 to 0.90, default value = 0.75) for well-maintained systems. The performance ratio gives a holistic view of how well the system is performing under actual conditions compared to its theoretical maximum output.

The solar potential $SP(i,j)$, which represents the usable energy generated by a PV system after accounting for system characteristics, is estimated using Eq. 3.13.

$$SP(i,j)=\eta_{PV}\times A(i)\times\left(\sum_{j=t_s}^{t_e}(SI(i,j)\times\eta_{surf}(i,j)\times\Delta t)\right)\times PR \quad (3.13)$$

Substituting $E_{sol}(i,j)$:

$$SP(i,j)=\eta_{PV}\times A(i)\times E_{sol}\times PR \quad (3.14)$$

The fill factor is a parameter that describes the quality of the solar PV cell [6, 7]. It is defined as the ratio of the maximum power point (P_{max}) to the product of the open-circuit voltage (V_{oc}) and the short-circuit current (I_{sc}) of the cell and estimated using Eq. 3.15.

$$FF=\frac{P_{max}}{V_{oc}\times I_{sc}} \quad (3.15)$$

The fill factor is typically in the range of 0.7 to 0.85 for silicon-based solar cells [6, 7]. While the fill factor is crucial at the individual solar cell or module level, it is usually already accounted for when determining the efficiency of the PV modules. The fill factor is generally

not needed in the system-level potential equation because it is already included in the calculation of the panel efficiency (η_{PV}) that we use in the equation. The efficiency of commercial solar panels inherently accounts for the fill factor.

3.4 Application of the spatial-temporal model framework for solar PV energy assessment

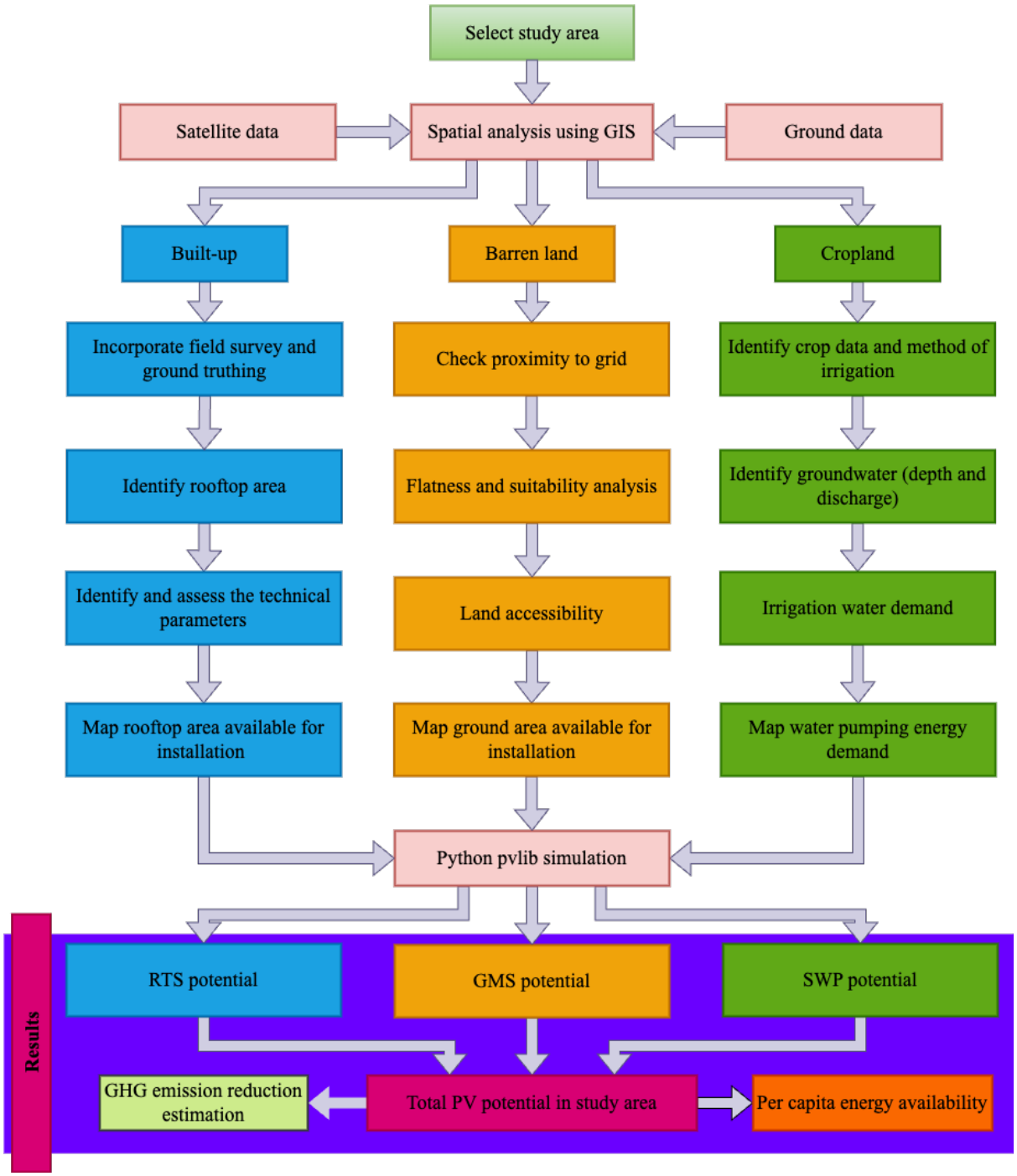

Fig. 3.2: PV potential assessment framework for RTS, GMS, and SWP systems

The spatial-temporal model framework for solar PV energy assessment, illustrated in **Fig 3.2**, integrates multiple data sources and analytical steps to evaluate the solar PV potential of a given study area. The framework begins with selecting the study area and employing Geographic Information System (GIS)-based spatial analysis of satellite and ground data. Key land types such as barren land, cropland, and built-up areas are identified and analyzed for PV installation. The model incorporates field surveys and technical assessments to map potential rooftop, ground and crop areas for solar installations. Using Python-based PVLib simulation, the model calculates the potential for PV systems. The results include estimations of total PV potential, greenhouse gas (GHG) emission reductions, and per capita energy availability within the study area.

3.4.1 Selection of study area

The selection of the study area aimed to encompass geographic diversity concerning key aspects of the study, specifically the potential for solar energy generation from RTS, GMS, and SWP, ensuring that the findings are broadly applicable. Based on a preliminary survey, a 10 km² area surrounding Tezpur University was chosen taking into consideration the varied land use patterns, and the presence of agricultural and institutional infrastructure in the area. This mix allows for a comprehensive feasibility analysis of rooftop solar potential, barren land solar capacity, and solar irrigation feasibility. The study area is depicted in **Fig. 3.3**.

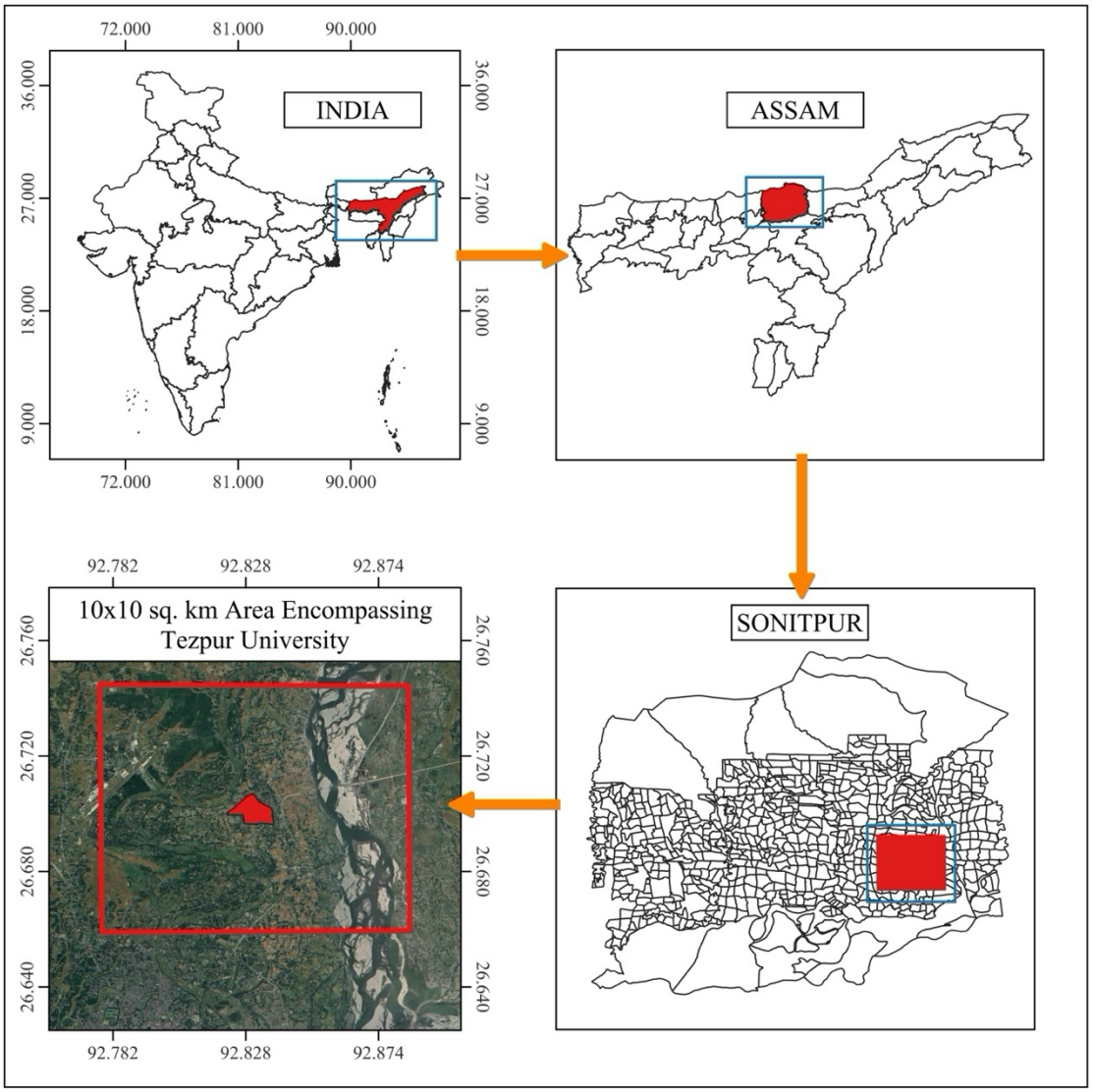

Fig 3.3: Location map of the selected study area

Additionally, **Fig. 3.4** presents the layout map of villages in the study area, including village names and boundaries, providing a clearer understanding of the local context for solar energy assessment. Furthermore, **Fig. 3.5** illustrates the distribution of the number of households across villages, offering insight into the demographic distribution and its relevance to solar energy deployment strategies. These figures collectively provide a comprehensive overview of the geographic, demographic, and infrastructural aspects of the study area, crucial for accurate solar energy potential assessment.

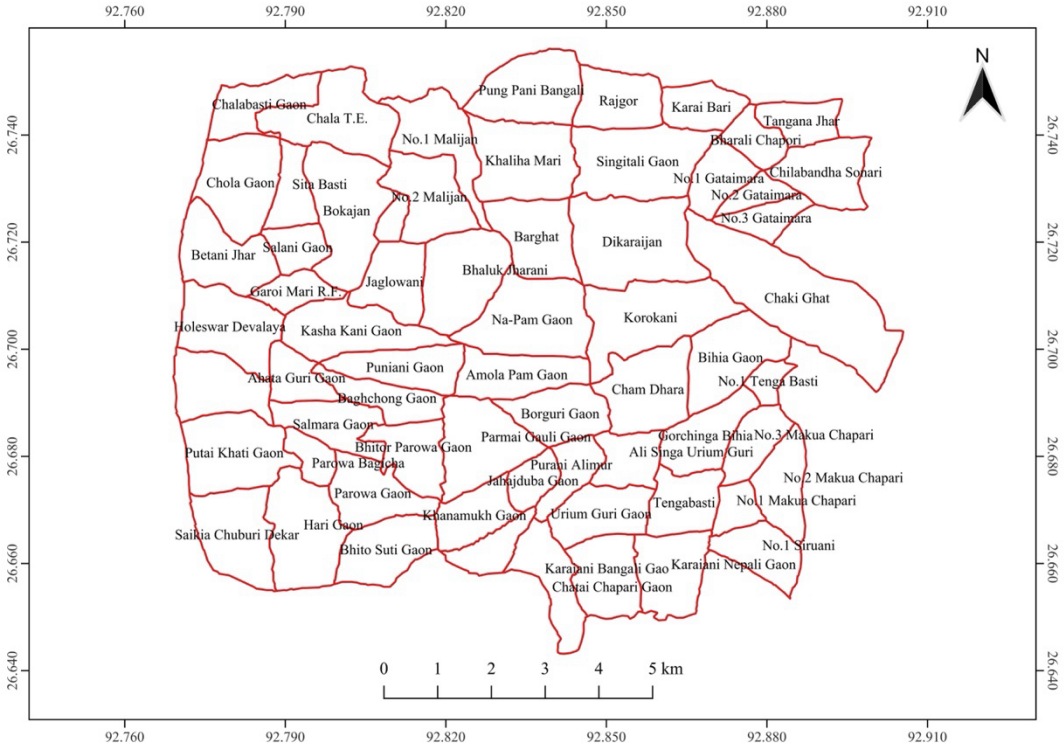

Fig 3.4: Layout map of villages in the study area with names and boundaries

The presence of large rooftops, both at Tezpur University and in residential areas, provides ample space for evaluating solar PV installations on buildings. The area has some stretches of unused and barren land that can be assessed for large-scale solar installations. This aligns with the objectives of mapping and evaluating barren land solar potential in rural regions.

Agriculture is a dominant activity in the villages around Tezpur University, with major crops like rice, mustard, and seasonal vegetables. Field visits revealed that major agricultural lands in the study area rely on irrigation systems powered by diesel and grid electricity-operated pumps. Detailed crop data is provided in **Appendix 3A** to offer further insights into the region's agricultural practices. These practices are heavily dependent on water, and diesel and grid-powered pumps often drive irrigation. Solar photovoltaic water pumps (SWPs) are expected to replace these systems, providing a more sustainable and cost-effective solution. The study area is suitable for implementing and studying solar irrigation systems, as it includes both rain-fed and irrigated agricultural lands. This offers an opportunity to evaluate how solar energy can be integrated into rural agricultural practices, helping farmers save on energy costs while reducing carbon emissions. **Table 3.1** summarizes the village demographics and the number of households surveyed.

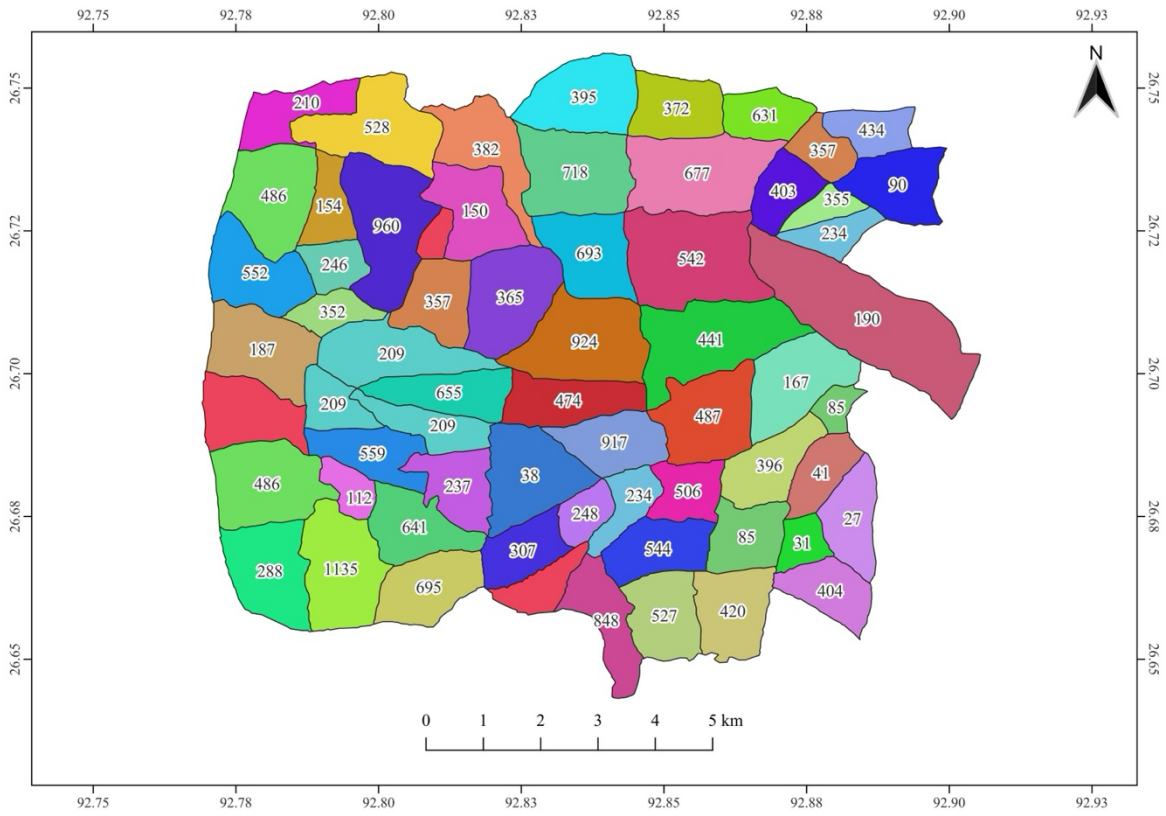

Fig 3.5: Distribution of the number of households across villages

Table 3.1: Village demographics and household survey data [8]

No. of Villages	No. of Households	No. of Households surveyed	Total Population
61	24,606	1,793	1,21,703

The detailed village data, including additional specifics and breakdowns, is provided in **Appendix 3B.**

3.4.2 Selection of solar PV system types

The study considers the following three types of solar PV systems as mentioned earlier, which are commonly deployed in rural areas for assessment of solar energy potential.

a) Rooftop solar (RTS): Designed for residential and commercial rooftops, RTS systems harness solar energy at the point of consumption, reducing transmission losses.
b) Ground-mounted solar (GMS): GMS installation, typically utility-scale, are deployed on open land and cater to relatively larger energy demands.
c) Solar photovoltaic water pump (SWP): Targeted at off-grid rural areas, SWP systems address critical needs such as irrigation and potable water supply.

3.4.3 Assessment and mapping of available space for solar PV installation

Assessment of area requirements for PV systems

The area required for the installation of a PV system is a critical parameter in determining its feasibility, particularly to ensure optimal utilisation of available space. Guidelines from the National Renewable Energy Laboratory (NREL) suggest that a 1 kW system, under standard conditions, typically requires approximately 100 square feet (9.3 square meters) of space [9]. Similarly, the Solar Energy Industries Association (SEIA) indicates that the space requirements for a 1 kW solar PV system range from 90 to 120 square feet (8.4 to 11.1 square meters), depending on the module's efficiency and installation conditions [10]. These estimations align with engineering standards, where approximately 10 square meters per kW is a reliable benchmark for designing PV systems [11].

This area estimation is influenced by several factors, including the efficiency of commercially available solar panels, the need for spacing between panels to reduce shading, and maintenance requirements. Additionally, the optimal tilt and orientation of the panels must be factored in to maximise sunlight exposure throughout the day [12]. These considerations ensure that system designs are technically feasible, economically viable, and adaptable to site-specific conditions while accounting for efficiency losses and maintenance needs.

Installation capacity calculation

The installation capacity $P_{install}$ in kW based on the available area (A) is then calculated using Eq. 3.16:

$$P_{install} = \frac{A}{A_{req}} \tag{3.16}$$

where $P_{install}$ is the installation capacity in kW; A is the available area for PV installation in m²; A_{req} is the area required to install 1 kW of PV capacity, which depends on the panel type and its efficiency.

The value changes depending on the panel efficiency. Higher efficiency panels will produce the same power in a smaller area compared to lower efficiency panels. The area requirement

per kW can be estimated based on the efficiency of the PV modules. The general relationship between area and power output is:

The value of A_{req} varies depending on the efficiency of the PV modules. Higher efficiency panels generate the same power output in a smaller area compared to lower efficiency panels. The area requirement per kW (A_{req}) can be estimated based on the efficiency (η_{PV}) of the PV modules using Eq. 3.17:

$$A_{req} = \frac{1}{\eta_{PV}} \tag{3.17}$$

Where η_{PV} represents the efficiency of the PV modules, which depends on the technology type and real-world conditions. **Table 3.2** below provides a comparison of different PV module technologies, detailing their efficiency ranges, area requirements per kW, and notable features. This serves as a reference for selecting the most appropriate technology, considering factors such as efficiency, available area, cost, and performance characteristics.

Table 3.2: PV technology types with efficiency, area requirements, and key features [13-15]

Technology Type	Efficiency Range (%)	Area Required per kW (m²/kW)	Typical features
Monocrystalline Silicon	18 – 22	5.56 – 4.55	High efficiency, performs well in low-light conditions. Typically, higher cost.
Polycrystalline (Multicrystalline) Silicon	15 – 20	6.67 – 5.00	Moderate efficiency, lower cost compared to monocrystalline. Not as efficient in low-light as monocrystalline.
Thin-Film (e.g., Cadmium Telluride or CIGS)	10 – 12	10.00 – 8.33	Lower efficiency, lightweight, flexible, and ideal for large installations. Typically, lower cost, good performance in diffused light.
Bifacial Modules (capture light from both sides)	19 – 24	5.26 – 4.17	Captures sunlight from both front and rear, leading to increased energy production. Requires reflective surfaces for optimal performance.

3.4.4 Application of geospatial tools

This study employed a range of advanced remote sensing and GIS tools to ensure precise mapping and analysis of available areas for solar PV installation, tailored to various system types. These tools were selected for their specific strengths in handling spatial data, land classification tasks, and integration with field observations.

GIS tools for spatial analysis

ArcGIS 10 was used to analyze and map available areas [16] for different solar PV system types, including rooftop solar (RTS), ground-mounted solar (GMS), and solar water pump (SWP) installations. Its high-resolution spatial visualization capabilities and layered analysis enabled detailed mapping of land-use patterns and identification of suitable locations. ArcGIS also facilitated the integration of field data, ensuring ground-truthing and validation of spatial analyses. The Sentinel Application Platform (SNAP) was central to Land Use Land Cover (LULC) classification [17], which identified critical land cover classes such as built-up clusters, barren/fallow land, and rice cropland. These classes informed the assessment of available space for each PV system type. SNAP's advanced capabilities in atmospheric correction and high-resolution image processing enhanced the accuracy of classification results, ensuring reliable identification of potential solar installation sites. QGIS played a crucial role in layout preparation and flexible data management [18]. Its extensive plugin ecosystem supported the creation of detailed maps for presentation and analysis, while its user-friendly interface allowed for efficient handling of attribute data and visualization of results.

This integration of GIS tools; ArcGIS for detailed spatial analysis, SNAP for efficient classification, Google Maps for high-resolution verification, and QGIS for layout preparation resulted in a robust and comprehensive approach to identifying areas suitable for PV installations.

Sentinel-2A imagery for LULC classification

The foundational data source for LULC classification was high-resolution multispectral imagery from the Sentinel-2A satellite, part of the European Space Agency's (ESA) Copernicus Programme [19]. The spectral and spatial detail of this imagery enabled precise identification of critical land cover types for solar PV planning. Key land cover classes included: (i) Built-up clusters for assessing rooftop solar (RTS) potential, (ii) Barren/fallow land for evaluating ground-mounted solar (GMS) feasibility and, (iii) Croplands for solar irrigation and water pumping applications (SWP).

To ensure accuracy, Sentinel-2A imagery underwent a series of rigorous pre-processing steps. Atmospheric correction was applied to remove distortions caused by atmospheric interference, followed by orthorectification and georeferencing to the Universal Transverse Mercator

(UTM) reference system (zone 46N). Additionally, spectral bands were resampled to a 10-meter spatial resolution using bilinear up-sampling and mean down-sampling techniques, ensuring consistent data quality across the dataset.

Classification techniques

Two supervised classification techniques were applied to the LULC data to identify areas available for solar PV installation:

a) Random Forest Classifier (RFC) [20]: A robust ensemble learning method used to manage the spectral complexity of Sentinel-2A imagery. RFC's ability to handle high-dimensional data and mitigate overfitting was particularly effective in distinguishing LULC types relevant to solar PV planning.

b) Maximum Likelihood Classifier (MLC) [21]: A probabilistic method assuming a Gaussian distribution of input data. MLC was used to delineate specific features like barren land and croplands, providing a straightforward yet reliable classification method.

A comparative analysis of the two methods evaluated their performance using accuracy metrics, such as user's accuracy, producer's accuracy, and overall classification accuracy. The results ensured reliable identification of available areas for solar PV installations.

3.4.4.1 RTS potential assessment

The identification of built-up areas, which are critical for rooftop solar installations, was initially performed through GIS-based Land Use and Land Cover (LULC) classification. The classification provided an overview of the built-up clusters within the selected villages, forming the basis for assessing RTS potential. However, to refine the analysis and enhance the accuracy of the estimates, detailed field surveys were conducted alongside the GIS analysis. This integration of spatial data and field observations ensured the identification of specific characteristics of rooftops, such as their structural suitability for solar panel installations and their shadow-free areas.

A random sampling method [22] was employed to estimate the total rooftop solar potential across the 61 villages. This method ensured that the collected data were representative of the larger population and minimized biases in the selection process. The population for the study comprised all residential buildings within the villages identified through LULC classification.

The administrative boundaries, geospatial socio-economic datasets, and information from the Village Information System (VIS) based on the 2001 Census of India were also incorporated to ensure the accuracy of the population definition.

To determine the sample size, a random selection of households was performed for each village, with the sample size ranging from 5% to 20% of the total households, depending on the village size. This approach maintained a statistically significant sample size that was manageable within the constraints of field data collection. The number of households to be sampled in each village, n_v, was calculated as:

$$n_v = \frac{N_v \times P}{100} \tag{3.18}$$

where N_v represents the total number of households in the village and P is the percentage of households sampled. The selection process was conducted using a random number generator applied to a complete list of households in each village, ensuring that every household had an equal probability of being included in the sample.

For each selected household, the field survey collected data on rooftop type (flat or sloped), building type (residential or commercial), rooftop area (in square meters), shadow-free areas (determined by identifying obstructions such as trees or nearby buildings), south-facing orientation (crucial for maximizing solar exposure in the Northern Hemisphere), tilt angle (roof angle with respect to the ground), and structural capacity to support solar panels. These parameters were essential for determining the suitability of rooftops for PV installations and their overall potential.

The collected data were extrapolated to the entire population of households in each village to estimate the total rooftop solar potential. The total rooftop area for each village, A_{total}, was calculated using:

$$A_{total} = \frac{A_s \times N_v}{n_v} \tag{3.19}$$

where, A_{total} is the estimated total rooftop area for the village and A_s is the average rooftop area from the sampled households. The same extrapolation method was used to calculate shadow-free areas and other relevant factors influencing solar potential. These calculations

allowed for a comprehensive estimate of the total rooftop solar potential across the 61 villages. By using random sampling and extrapolation techniques, this method provides a reliable and statistically sound estimation of the rooftop solar potential across the selected region.

3.4.4.2 GMS potential assessment

The assessment of Ground-Mounted Solar (GMS) potential involved identifying suitable barren and fallow land using GIS-based Land Use and Land Cover (LULC) classification. Sentinel-2A imagery with a 10-meter spatial resolution was used to perform supervised classification, distinguishing barren land from other land use categories such as built-up areas, water bodies, and agricultural land. The barren land category, essential for solar PV installation, was identified based on its unique spectral signature.

Field verification using GPS data ensured the accuracy of the classification. However, due to the limitations of the imagery's spatial resolution, barren land was grouped with grass-covered fallow areas and other indistinct features such as village playgrounds, classifying them collectively under the grassland/fallow land category. This step minimized misclassification while maintaining practical relevance for solar energy assessments.

3.4.4.3 SWP potential assessment

The assessment of solar water pump (SWP) potential began with the determination of cropland areas requiring irrigation. On-screen digitization of rice croplands was conducted using QGIS, incorporating data from the Land Use Land Cover (LULC) classification and high-resolution visualization from Google Earth. This process provided an accurate determination of cropland areas, forming the basis for estimating the volume of water required for irrigation.

From the digitized cropland area, the daily volume of water required (V, measured in m^3/day) was estimated based on agricultural water demand for rice cultivation. The next step involved calculating the hydraulic power required ($P_{hydraulic}$) to lift water, expressed as [23]:

$$P_{hydraulic} = \frac{\rho \times g \times V \times H}{t_{pump}} \tag{3.20}$$

In this equation, ρ represents the density of water, which is taken as 1000 kg/m^3, while g is the gravitational acceleration, equal to 9.81 m/s^2. The volume of water required per day is denoted by V, and the total head (H) represents the total lift height in meters, which includes the static

lift, friction losses, and any additional pressure requirements. The term t_{pump} specifies the daily operating hours of the pump.

Using the hydraulic power, the daily energy required for water pumping (E_{pump}, in kWh/day) was then calculated as:

$$E_{pump} = \frac{\rho \times g \times V \times H}{\eta_{pump} \times \eta_{motor} \times \eta_{inverter} \times 1000} \quad (3.21)$$

Here, η_{pump} is the efficiency of the pump. Similarly, η_{motor} represents the motor efficiency, $\eta_{inverter}$ refers to the inverter efficiency, which is typically around 90% or 0.9. The constant 1000 is used to convert watts (W) to kilowatts (kW).

The energy demand was then used to calculate the required PV power capacity (P_{PV}) using the formula:

$$P_{PV} = \frac{E_{pump}}{HSP \times F_{derating}} \quad (3.22)$$

In this equation, HSP represents the average daily peak sun hours at the location, measured in hours per day, while $F_{derating}$ accounts for various system losses, such as those caused by dust, temperature, and wiring inefficiencies. The derating factor typically ranges between 0.75 and 0.85.

The total number of solar panels (N) required to meet the pumping power demand was then determined using:

$$N = \frac{P_{PV}}{P_{panel}} \quad (3.23)$$

In this equation, P_{panel} refers to the rated power output of each solar panel, measured in kilowatts.

For systems using alternating current (AC) pumps, the inverter capacity ($P_{inverter}$) was calculated to ensure efficient operation while including a safety margin of 25% above the pump's peak power demand. The inverter capacity was calculated as:

$$P_{inverter} = P_{pump} \times 1.25 \quad (3.24)$$

Here, P_{pump} represents the actual power rating of the pump, measured in kW. Additionally, cables should be designed to ensure that they could handle the current with minimal voltage drop, typically less than 3% over the distance.

The total SWP potential for each location was computed by summing up the contributions from the identified croplands.

3.4.4.4 Combined solar potential assessment

To evaluate the overall solar energy potential at a given location, the contributions from the three systems were integrated into a unified framework. The total solar potential at location i was calculated using the following equation:

$$SP(i) = SP_{RTS}(i) + SP_{GMS}(i) + SP_{SWP}(i) \quad (3.25)$$

where, $SP(i)$ represents the total solar potential of the i location, combining the contributions from RTS, GMS and SWP. $SP_{RTS}(i)$ denotes the potential from RTS, $SP_{GMS}(i)$ represents the potential from GMS, $SP_{SWP}(i)$ refers to the potential from SWP at i-th location.

3.4.5 Simulation of PV energy potential using PVLib-Python

Simulation plays a critical role in assessing the performance of photovoltaic (PV) systems by providing detailed insights into energy output under varying environmental conditions. By leveraging computational tools, this study employs Python 3 [24] and Visual Studio Code (VS Code) to simulate the behavior of PV systems, incorporating site-specific parameters such as solar irradiance, module efficiency, and ambient temperature. The simulation process integrates advanced modeling techniques to predict PV system performance with precision and reliability, ensuring an accurate evaluation of energy generation potential.

Use of PVLib-Python library

The pvlib-python library was selected for its versatility in simulating PV system performance under various environmental conditions [25, 26]. This library supports detailed modeling of PV systems by accounting for geographic location, meteorological variables, and PV module characteristics. By enabling robust calculations of direct current (DC) and alternating current (AC) power output, pvlib-python offers an accurate estimation of energy generation potential.

The primary objective of the simulation is to evaluate the energy output of PV systems by incorporating factors such as solar irradiance, ambient temperature, and wind speed.

The simulations were conducted using Python 3 within the Visual Studio Code (VS Code) environment. VS Code was chosen for its integrated terminal, debugging tools, and extensions that enhance Python development. Its features, including IntelliSense, Git integration, and customizable interface, made the simulation process efficient and streamlined, ensuring accurate execution and analysis of the workflow.

3.4.6 Methodology for simulation

The workflow for simulating PV system performance using pvlib-python involves several sequential steps [27], as illustrated in **Fig. 3.6**. These steps include defining the geographic location, preparing weather data, specifying PV system parameters, constructing a model chain, executing the simulation, and analyzing the results. The methodology is detailed below:

a) Geographic location definition: The geographic location of the PV installation was defined by specifying the latitude, longitude, and time zone of the site. This information is critical for calculating solar angles, solar position, and the local availability of solar resources, which directly influence energy generation.

b) Weather data preparation: Weather data, including global horizontal irradiance (GHI), ambient temperature, and wind speed, was used to simulate environmental conditions. These parameters were sourced from meteorological databases or field measurements to ensure realistic input for the simulation. Weather data was prepared and formatted to align with pvlib-python's requirements.

c) PV system parameter specification: The parameters of the PV system were defined, including the nominal power of the PV modules, the inverter’s AC power capacity, tilt angle, azimuth, and other system properties. This step was critical for modeling the system’s energy production potential under specific environmental conditions.

Fig 3.6: PVlib simulation flowchart: Steps for photovoltaic energy system modeling

d) Model Chain Construction: The pvlib-python library was used to construct a ModelChain, which integrates system parameters, geographic location, and weather data to calculate the energy output of the PV system. The library provides specific models for DC and AC power calculations (e.g., 'pvwatts') to ensure consistency and simplicity. The ModelChain enabled dynamic simulation of the interaction between the environment and the PV system.

e) Simulation Execution: The simulation was executed using the run_model method provided by pvlib-python. This method calculated hourly or sub-hourly DC and AC power outputs for the simulation period. The output included estimated DC power, AC power, and total energy generated.

f) Result Analysis and Visualization: The temporal variations in energy output were analyzed using visualization techniques. The results provided insights into system performance over time, enabling the identification of patterns and trends in energy generation. Visualization tools, such as matplotlib, were used to create graphs and plots for detailed analysis.

Python script development and implementation

To streamline the simulation process, a Python script was developed to integrate all the aforementioned steps into a cohesive workflow. The script included definitions for location, weather data preparation, system parameter specification, simulation execution, and visualization of results. This design ensured that the workflow was reproducible, adaptable, and user-friendly.

The script relied on the pvlib-python library for accurate energy calculations and incorporated additional dependencies such as pandas for data manipulation and matplotlib for visualization. Users were advised to execute the script using Python 3 within the VS Code environment. The integrated tools in VS Code, including its debugging capabilities and dependency management, enhanced the usability and efficiency of the simulation workflow.

Reproducibility and flexibility

The developed Python script offers a practical example for analyzing photovoltaic system performance. By consolidating all steps into a single, cohesive script, the approach provides a flexible framework that allows users to tailor inputs and parameters to suit specific project

requirements. The methodology ensures reproducibility across different scenarios, enabling its application in diverse geographic locations and system configurations.

The script also serves as a flexible tool for researchers and practitioners, facilitating the analysis of PV system performance under varying environmental conditions. Detailed guidance on executing the script is provided in **Appendix 3C**.

3.4.7 Estimation of per capita energy availability (PCEA)

Per capita electricity consumption is a critical metric for evaluating energy access and its impact on quality of life, particularly in rural regions where energy deficits are prevalent [28, 29]. This section focuses on estimating the potential per capita energy availability (PCEA) derived from rooftop solar (RTS), ground-mounted solar (GMS), and solar water pump (SWP) systems across 61 villages in rural Assam. By integrating the estimated energy potential from these systems with population data, this analysis provides a quantitative measure of the additional electricity availability per individual, highlighting the transformative potential of solar energy deployment in bridging rural energy gaps.

Contribution of RTS systems

RTS systems, characterized by their decentralized nature, offer a targeted solution for enhancing household-level energy access. The deployment of RTS systems ensures that energy production is localized, making it especially impactful in areas where centralized energy distribution is limited. By evaluating the collective impact of RTS installations, this study illustrates how solar energy can elevate per capita energy availability to levels that align with national and global benchmarks. Furthermore, RTS systems provide the flexibility to scale energy generation in tandem with local energy demands, contributing to sustainable energy solutions at the household level [30].

Contribution of GMS systems

GMS systems are designed for large-scale energy production, addressing village-wide energy needs through their scalability and higher production potential. These systems are well-suited for collective energy solutions, ensuring equitable access across the community. By utilizing barren and fallow lands for installation, GMS systems not only maximize energy output but also contribute to regional energy independence. Their ability to generate substantial energy

makes them a crucial component in the overall strategy to enhance rural energy access and bridge the urban-rural energy divide [31].

Contribution of SWP systems

SWP systems primarily address agricultural energy needs by reducing dependence on conventional energy sources for irrigation and water pumping. While their primary utility lies in supporting agricultural activities, SWP systems often produce surplus energy that can be redirected for secondary purposes. This surplus energy can be integrated into local energy grids, enabling broader utilization and enhancing overall energy availability in rural areas. By incorporating the energy potential from SWP systems into the PCEA calculation, this study ensures a holistic representation of the contributions of solar energy to rural energy access, particularly in regions where agriculture is the dominant livelihood [32].

By combining the energy potentials of RTS, GMS, and SWP systems with population data, this approach offers a comprehensive perspective on the socio-economic benefits of solar energy deployment. The results demonstrate how solar energy can bridge energy gaps, enhance living standards, and align rural communities with global energy access goals. The integration of these systems into the rural energy framework not only addresses immediate energy needs but also fosters sustainable development, driving progress in line with the United Nations Sustainable Development Goals (SDGs).

The per capita energy availability for RTS, GMS, and SWP systems is calculated using the following equation:

$$PCEA\ (kWh/year) = \frac{Total\ Energy\ Potential\ (kWh/year)}{Population} \quad (3.26)$$

where, Total Energy Potential (kWh/year) = Energy Potential from RTS + Energy Potential from GMS + Energy Potential from SWP.

3.5 Data sources

The investigation relies on various data sources and parameters, as summarised in **Table 3.3**. For field surveys, the detailed questionnaire is provided in **Appendix 3D**.

Table 3.3: Data sources and parameters considered for the study [8, 33]

Sl. No.	Group	Parameters	Data Sources
1	Demographic and Village Information	Population, number of households, occupation, income	Census of India, Survey of India
2	Geographic Information System (GIS)	Satellite images, shapefiles, raster data	National Remote Sensing Centre, DIVA GIS, North Eastern Spatial Data Repository (NeSDR)
3	Solar Resource and Weather Information	Solar irradiance, temperature, wind speed	NASA Prediction of Worldwide Energy Resources, National Renewable Energy Laboratory (NREL), Global Solar Atlas, Centre for Wind Energy Technology (C-WET), Visualization of Earth Observation Data and Archival System (ISRO)
4	RTS Assessment	Rooftop area, tilt angle, south-facing orientation, structural feasibility	GIS analysis and field survey
6	GMS Assessment	Land availability, land slope, shading	GIS analysis and ground truthing
7	SWP Assessment	Cropland, irrigation patterns, water demand, SWP feasibility	GIS analysis, field Survey, State Agriculture Department, Package of Practices for Agricultural crops of Assam
8	Transportation and EV Charging	Road network, accessibility, EV charging station locations	GIS analysis, NeSDR
9	Environmental Assessment	GHG emission reduction potential, Lifecycle emission assessment	IPCC Emission Factors, Central Electricity Authority (CEA) of India

3.5.1 Remote sensing and GIS data

Satellite image

The satellite data used in this study were acquired from Sentinel-2A, a high-resolution multispectral imaging mission under the ESA's Copernicus Programme [45]. Sentinel-2A\u2019s capabilities, including a 10-meter spatial resolution and frequent revisit cycles, were instrumental in capturing temporal and spatial variations across the study area. Details of the Sentinel-2A imagery, including spectral band characteristics and acquisition parameters,

are summarized in **Table 3.4**. These data supported the study's LULC classification efforts, offering a robust foundation for spatial analysis.

Table 3.4: Characteristics of the sentinel 2A data used in this study

Parameter	Detail
Spatial resolution	10 × 10 m
	60 × 60 m
Spectral band-central wavelength (μm)	Band 1 (Coastal) 0.443 μm
	Band 2 (Blue) 0.490 μm
	Band 3 (Green) 0.560 μm
	Band 4 (Red) 0.665 μm
	Band 5 (Red edge) 0.740 μm
	Band 6 (Red edge) 0.783 μm
	Band 8 (NIR) 0.842 μm
	Band 8A (NIR) 0.865 μm
	Band 9 (Water) 0.940 μm
	Band 10 (SWIR) 1.375 μm
	Band 11 (SWIR) 1.610 μm
	Band 12 (SWIR) 2.190 μm
Swath	290 km
Cloud cover	0%
Date of acquisition	December 22, 2020
No. of scene used for present study	1

Tools such as Google Earth and handheld GPS devices were employed to validate the classification results [46]. Google Earth's high-resolution imagery was employed to visualise and verify road networks, infrastructure, and other spatial features, ensuring consistency between classified maps and on-ground realities. GPS devices provided precise latitude and longitude coordinates for selected locations, which were crucial for ground truthing. This process significantly enhanced the reliability of the LULC classification by cross-referencing satellite-derived data with field observations.

Shapefiles

Shapefiles, representing administrative boundaries and spatial data layers, were integral to the study. These shapefiles, sourced from reliable databases such as the Survey of India (SOI) [33], DIVA-GIS [35], and the North Eastern Spatial Data Repository (NeSDR) [36], were refined

and aligned with the UTM projection system to standardize spatial data across datasets. This alignment improved the accuracy of distance and area calculations, ensuring consistency in spatial analyses. Road network shapefiles, in particular, were verified by overlaying them with Sentinel-2A imagery and Google Earth data, ensuring their accuracy and relevance for solar infrastructure planning and electric vehicle (EV) charging integration.

Road network

The layout of the road network in the study area is depicted in **Fig. 3.7**, providing an essential framework for understanding accessibility and connectivity [36]. Two types of roads are present within the study area: kutchha roads (unpaved roads) and pucca roads (paved roads). The road network has been overlaid with the village boundary to provide a comprehensive understanding of its alignment with the spatial extent of the villages. The analysis reveals that the road network extends even into agricultural areas, including paddy fields, enabling detailed assessments of rural connectivity. This comprehensive mapping can be further utilized for advanced road network analyses, such as evaluating accessibility to key resources, planning transportation routes, or identifying optimal locations for infrastructure development. The eastern part of the map displays blank spaces, which correspond to riverine areas, naturally devoid of road infrastructure. On the western side, some areas appear to have missing road data, which corresponds to an airport area, where road infrastructure is limited or restricted. Despite these gaps, the mapped road network offers valuable insights into the transportation framework of the region, serving as a foundational tool for planning and development initiatives.

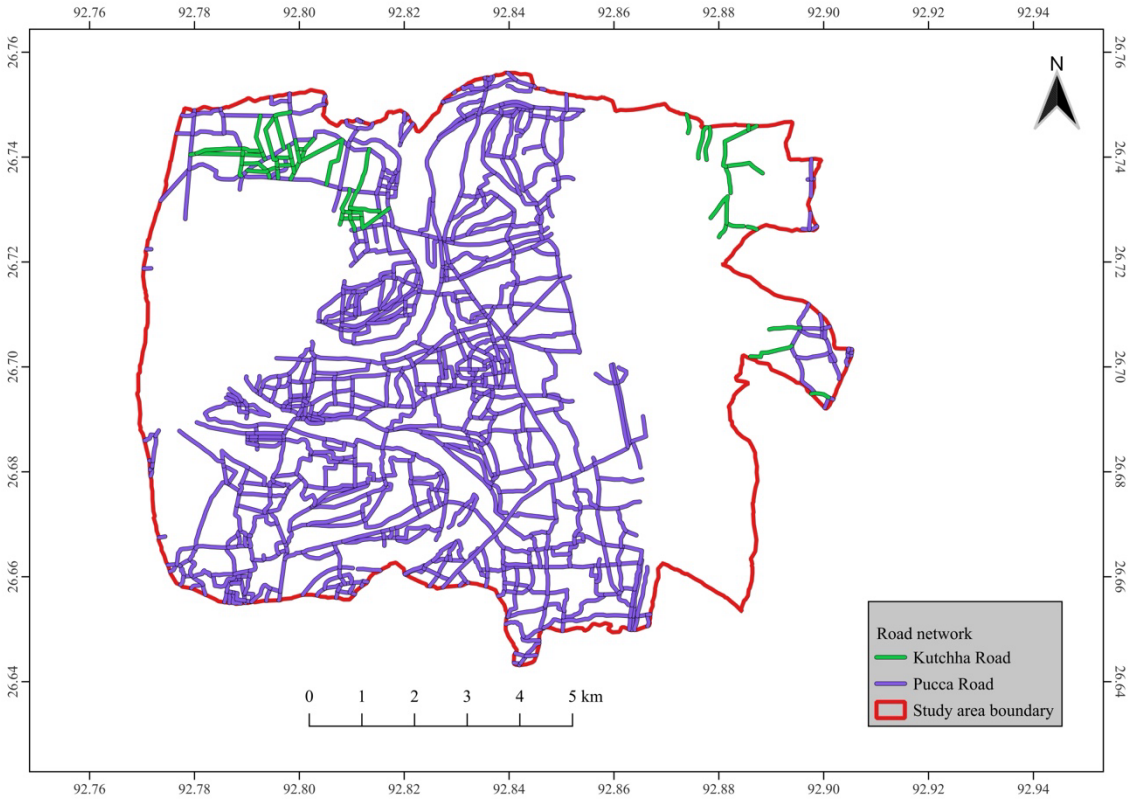

Fig 3.7: Road network of the study area

Field data and verification

A detailed field survey further validated the LULC classification results. A total of 42 locations, representing each identified LULC class for the selected study area, were strategically selected for field visits. At each site, GPS coordinates were recorded, and photographs were taken in all cardinal directions to capture a 360-degree view of the surrounding landscape. These field observations provided critical reference data for validating classification accuracy. The survey also documented rooftop characteristics, including type, condition, and shadow-free, south-facing sections, to assess solar installation feasibility. This comprehensive data collection ensured robust validation of satellite-derived classifications and informed the study's solar energy potential analysis. The classification accuracy was assessed using well-established metrics such as the confusion matrix, overall accuracy, and the kappa coefficient. These statistical tools provided a structured evaluation of classification performance, identifying areas for refinement and ensuring the reliability of the results. This rigorous methodology, combining advanced tools, manual digitization, and field validation, provided a solid

foundation for achieving the study's objectives of mapping land use and evaluating solar energy potential. [47, 48]

3.5.2 Solar insolation data

NASA data

The methodology adopted for estimation of the solar data is shown in **Fig 3.8** below. In this study two major approaches are considered to estimate the solar radiation, one is based on measured data from meteorological station and second method is derived from satellite data (NASA solar radiation data) [37, 40].

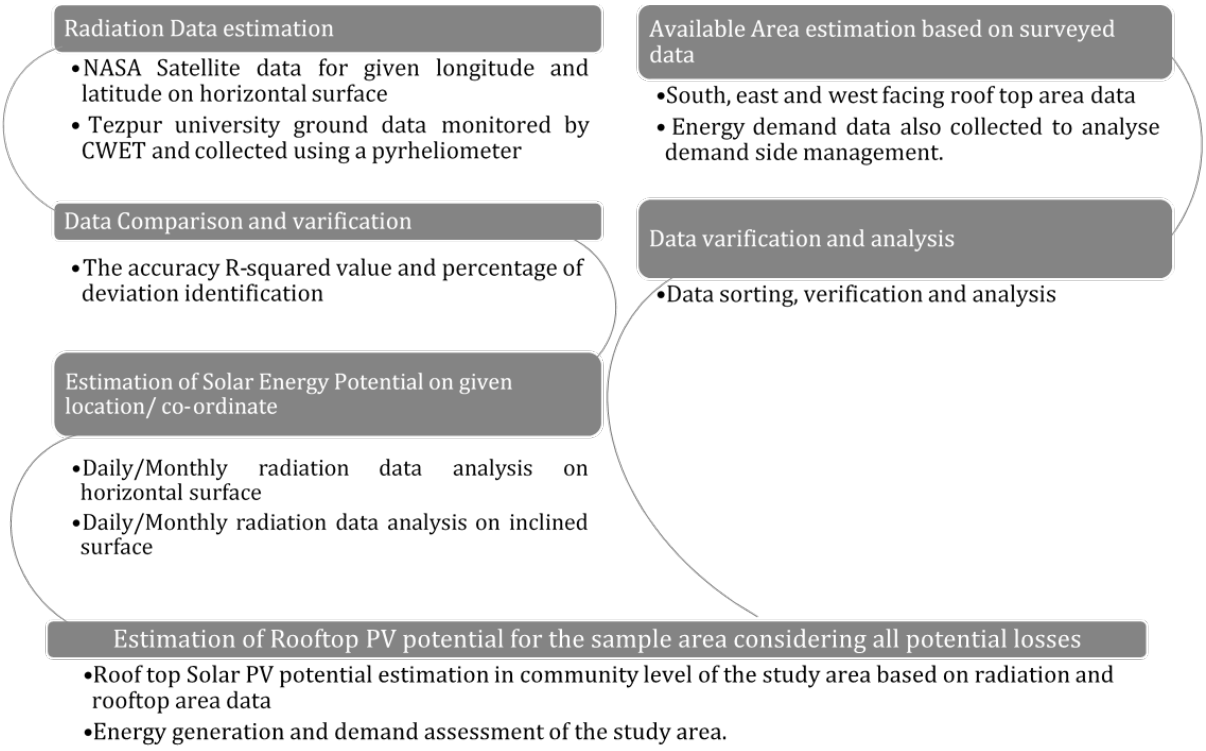

Fig 3.8: Methodology for solar data analysis

The meteorological station which is nearer to the study area is considered to be the most appropriate for verifying the estimated solar radiation. The NASA data are satellite-retrieved; its parameters are computed on a daily average basis using NASA/GEWEX surface radiation Budget model. The model considers the effect of cloud cover and local atmospheric conditions. Compared to BSRN (Baseline Surface Radiation Network) sites the NASA data showed high accuracy with Bias (less than 0.12) and RMSE (Root Mean Square Error) (less than 18%). BSRN sites are the most accurate approved ground sites.

To verify the NASA data accuracy, the data were verified with the Tezpur university ground data which is monitored by CWET (Centre for Wind Energy Technology) and collected using a pyrheliometer. The accuracy showed an R-squared value of 0.97 while the percentage of deviation was 9% as shown in **Fig 3.9** below.

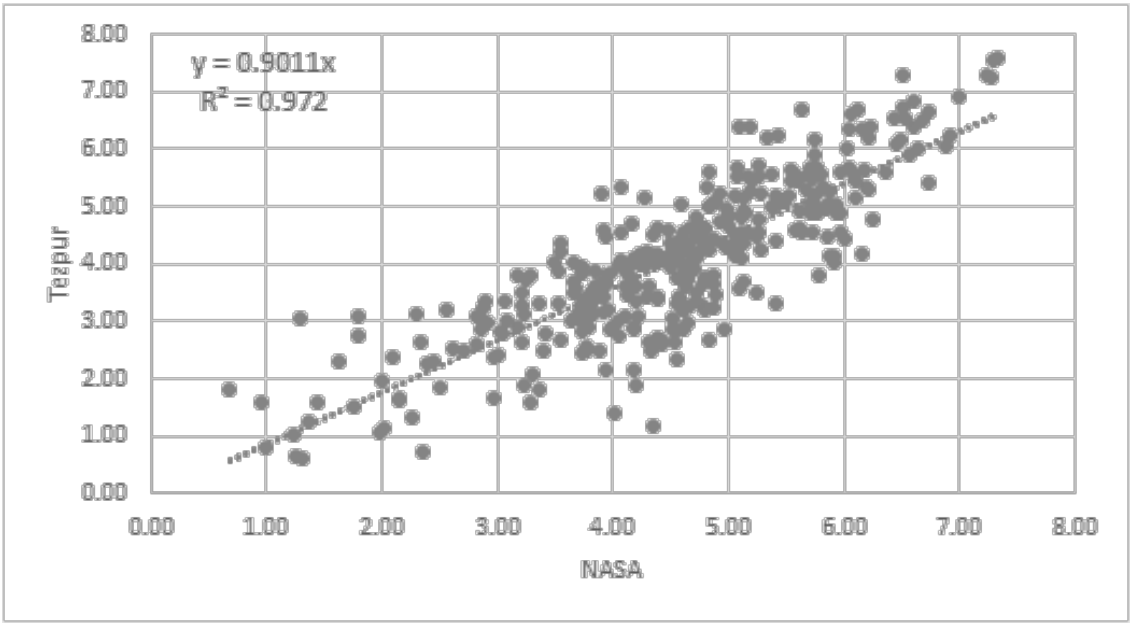

Fig. 3.9: Validation of NASA data with ground data for Tezpur

For optimum solar energy generation, it is required to calculate the radiation data on inclined surface at a tilt angle where solar PV modules will be mounted. The energy generation from a PV module depends not only on the energy contained in the sunlight, but also on the angle between the module and the sun. The energy density is maximum when the PV module is perpendicular to the sun. However, the angle between the sun and a collector area is continuously changing. Therefore, calculation of incident solar radiation on an inclined collector is an utmost requirement to estimate the maximum energy generation from the solar system.

Incident radiation on a tilted surface is calculated from solar radiation measured on horizontal surface or from satellite data.

The analysis aimed at estimating the energy generation potential for a south facing surface tilted at an angle of 30°. The analysis considered losses in different stages of the conversion process. Energy generation potential in a tilted surface in the study area for different days of a year was estimated.

Daily solar energy generation data has been estimated by using hourly solar radiation and ambient temperature data obtained from the NASA website (https://power.larc.nasa.gov/data-access-viewer/). The five-year average daily solar irradiance at a selected location in the study area is presented in **Fig. 3.10 (a).** In contrast, the five-year time series of daily irradiance is shown in **Fig. 3.10 (b)**.

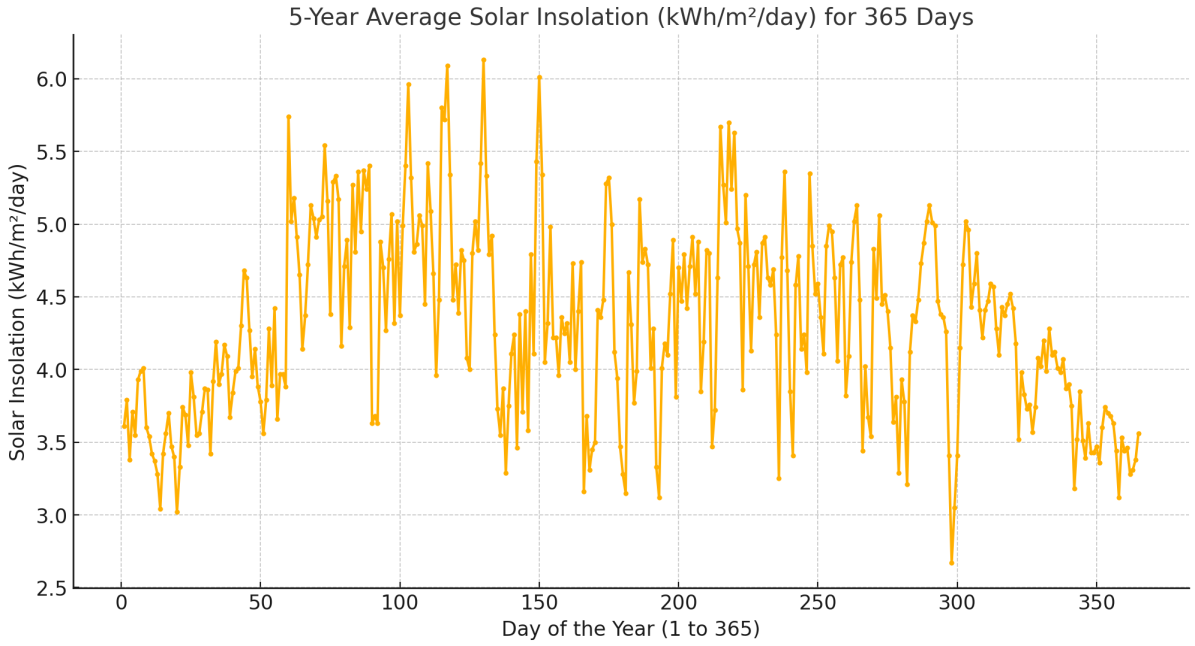

Fig 3.10 (a): Daily solar irradiance incident on a selected location in the study area [37]

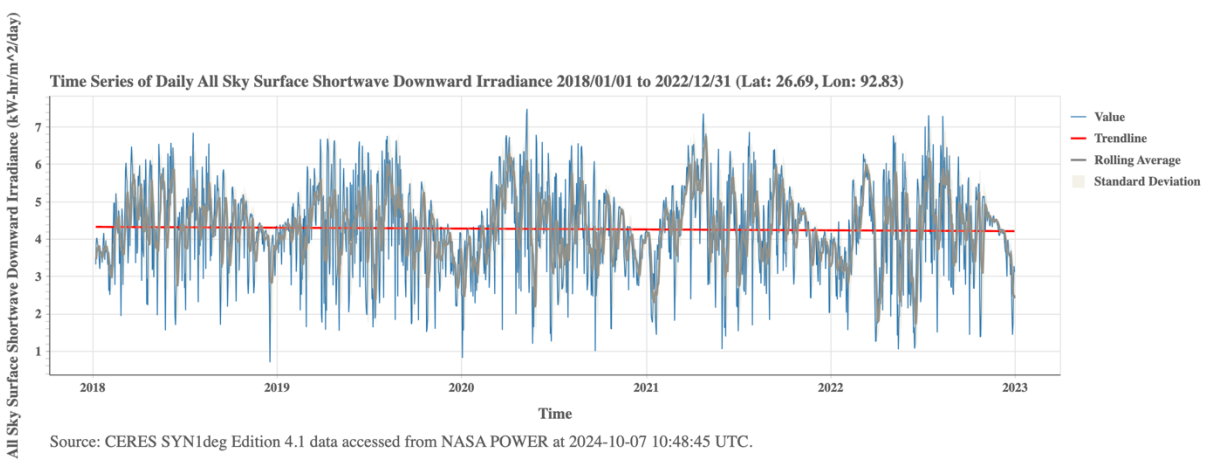

Fig 3.10 (b): Time series of daily all sky surface shortwave downward irradiance (kWh/m²/day) [37]

Global solar atlas data

Solar insolation data was systematically mapped at multiple geographic scales, starting from India, then Assam, Sonitpur District, and finally narrowing down to the 10 km² study area. Long-term average Global Horizontal Irradiance (GHI) data (1999–2018) has been used for this GIS map. The data was obtained from the Global Solar Atlas, developed by the World Bank Group and ESMAP, with data provided by Solargis [39]. The map represents spatial variation in average solar resource potential across the geographic scales analyzed. This step was undertaken to understand how solar insolation varies with geographical location. Across India, solar insolation varies significantly, ranging from 1 kWh/m² to 6.42 kWh/m², as shown in **Fig. 3.11(a)**. In Assam, this variation narrows to a range of 2.82 kWh/m² to 4.72 kWh/m², as depicted in **Fig. 3.11(b)**. In Sonitpur District, the range is further constrained to 3.8 kWh/m² to 4.5 kWh/m², as shown in **Fig. 3.11(c)**. Within the study area itself, solar insolation varies between 4.26 kWh/m² and 4.35 kWh/m², as illustrated in **Fig. 3.11(d)**.

The data highlights that as the geographical scale becomes smaller, the variation in solar insolation becomes narrower. This trend is evident in the 10 km² study area, where there is minimal variation in solar insolation. However, despite the limited variation, the study area receives a significant amount of solar insolation, making it suitable for photovoltaic systems. Relevant GIS maps depicting solar insolation variations across these geographic scales are provided in the figures, offering a visual representation of the data and supporting the analysis. This data underscores the potential of the study area for effective solar energy utilization and reinforces its viability for solar PV installations.

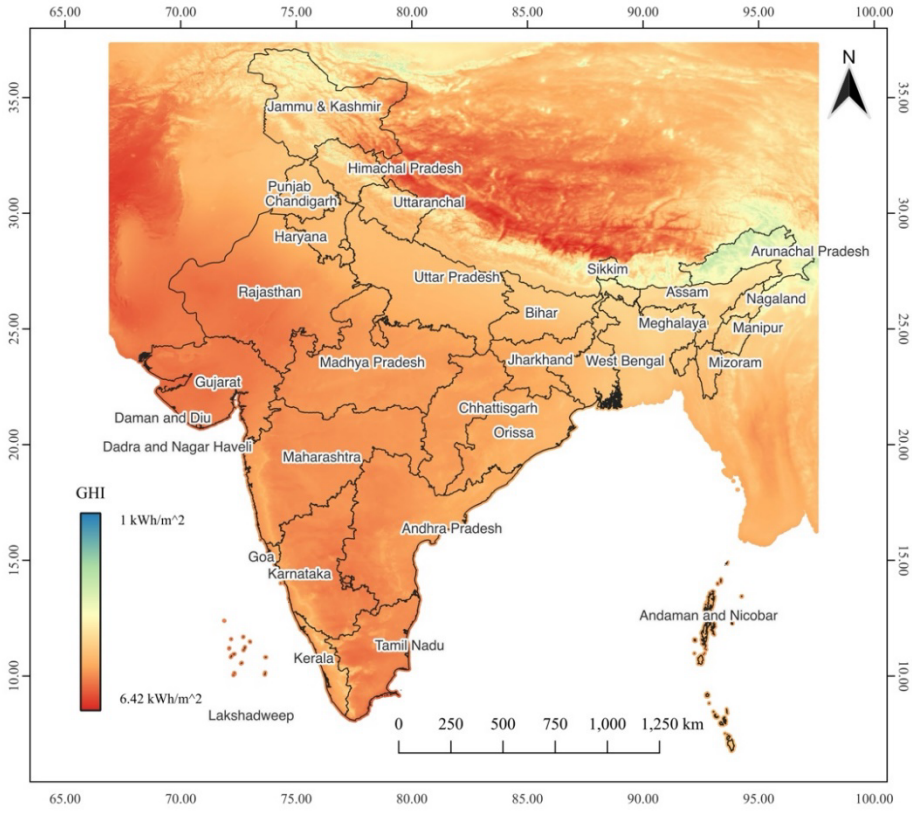

Fig 3.11 (a): Solar insolation map of India (1999–2018)

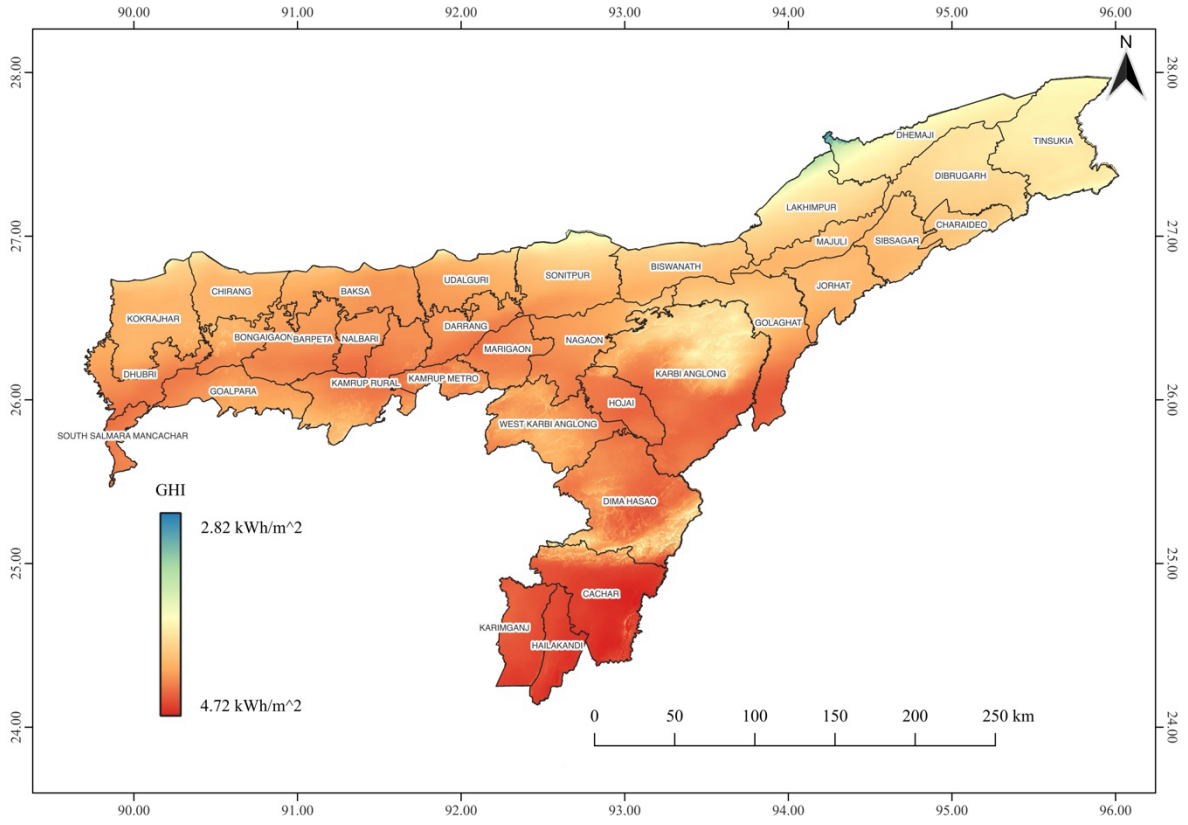

Fig 3.11 (b): Solar insolation map of Assam (1999–2018)

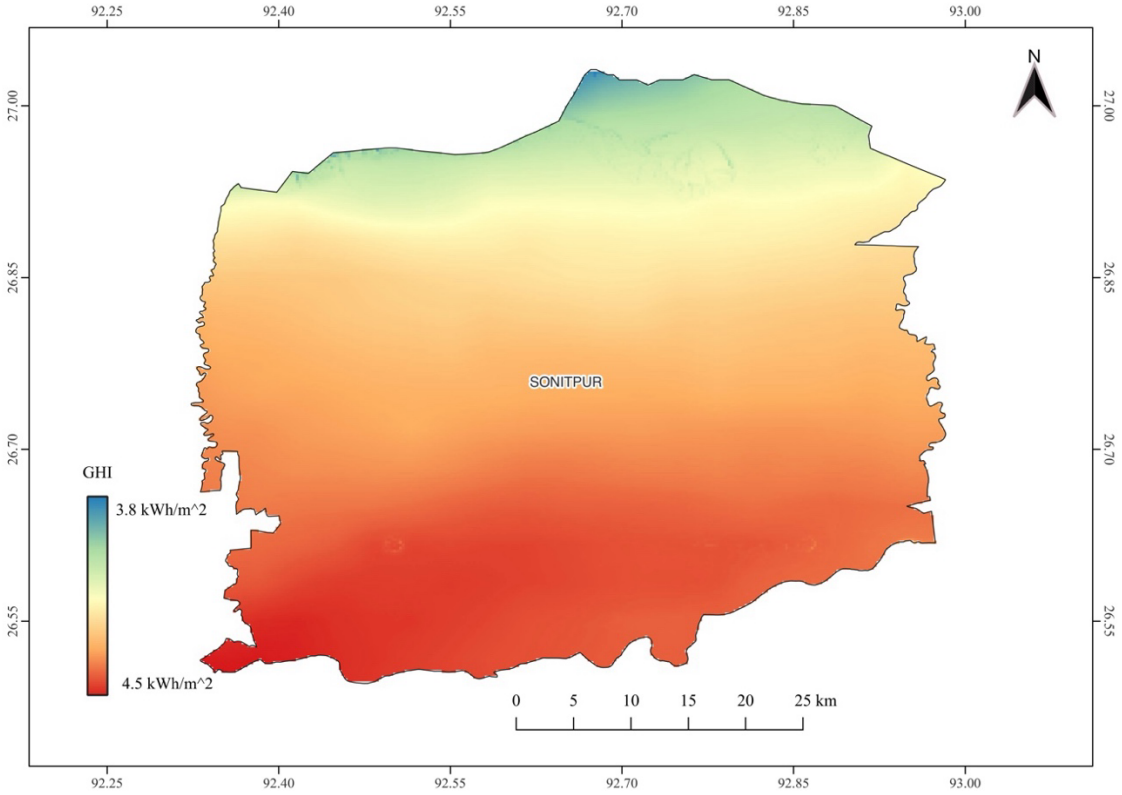

Fig 3.11 (c): Solar insolation map of Sonitpur district (1999–2018)

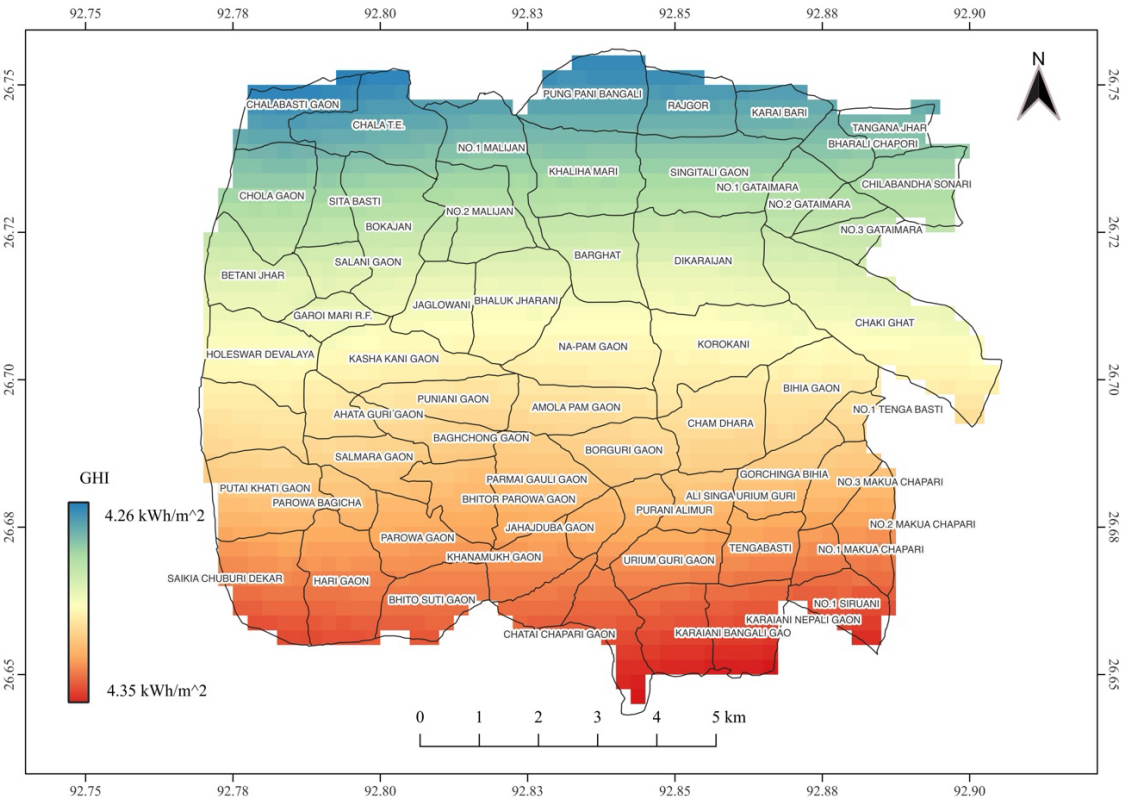

Fig 3.11 (d): Solar insolation map of the study area (10 km²) (1999–2018)

3.5.3 Temperature data

Temperature data is a critical input parameter in the assessment of solar PV potential, as the efficiency and performance of PV modules are significantly influenced by temperature variations. Both ambient temperature and module temperature are key considerations, and their accurate estimation is necessary for reliable solar energy modeling.

Ambient temperature *($T_{ambient}$)*, typically measured at 2 meters above ground level (T2M), is the external temperature surrounding the PV system. It plays a fundamental role in determining the operating temperature of the solar module. High ambient temperatures generally reduce the efficiency of PV modules due to their temperature-dependent characteristics. The temperature coefficient of the PV modules, which indicates the rate of power loss with rising temperature, is a critical factor for performance analysis.

The module temperature (T_{module}) is a function of ambient temperature, wind speed, and solar irradiance. Empirical models such as the Nominal Operating Cell Temperature (NOCT) model [49] or the Faiman model are widely used to estimate module temperature under real-world conditions [50].

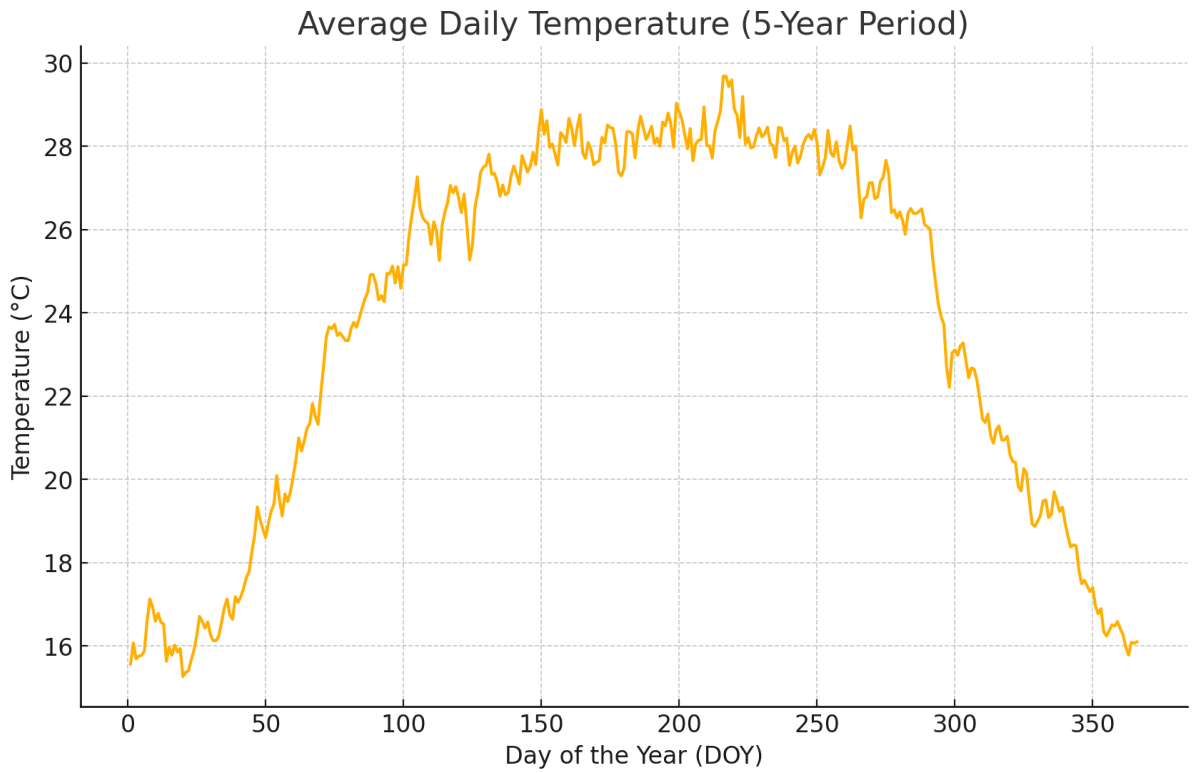

Fig 3.12 (a): Five-year daily average of ambient temperature (T2M) [37]

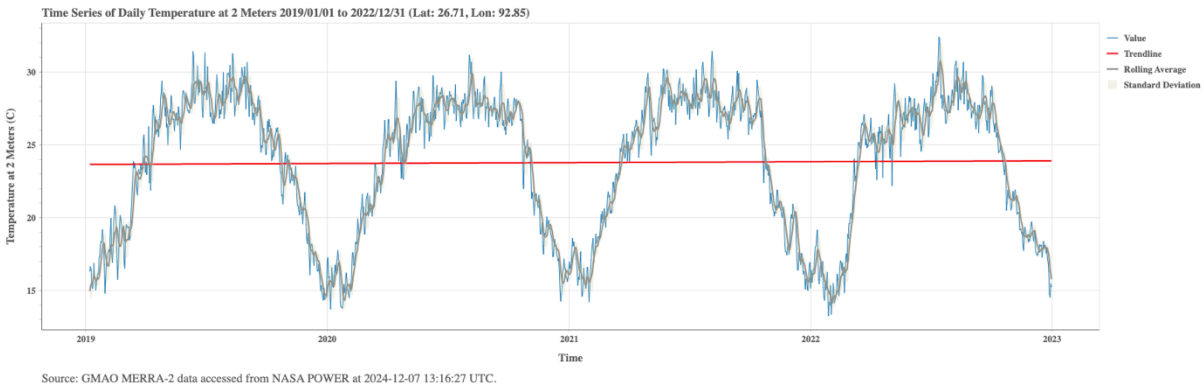

Fig 3.12 (b): Five-year time series of ambient temperature (T2M) [37]

The 5-year daily average **Fig 3.12 (a)** and 5-year time series **Fig 3.12 (b)** of ambient temperature (T2M) are critical for understanding seasonal and long-term temperature trends, which directly influence the performance of photovoltaic (PV) systems. Seasonal variations highlight periods of high ambient temperatures, such as summer, where PV efficiency decreases due to thermal losses, while cooler months may enhance performance. The time series data provides insights into long-term temperature stability, helping to assess the potential impact of climate trends on module performance. Accurate T2M data improves module temperature estimation, ensuring reliable predictions of power output and performance ratio (PR). This analysis is essential for system design, module selection, and mitigation strategies, particularly in regions with persistent high temperatures, thereby enhancing the accuracy of solar potential estimation in rural Assam.

3.5.4 Wind speed data

Wind speed is an essential parameter for modelling the performance of PV systems, particularly for estimating module temperature and assessing mechanical stability. The NASA POWER dataset provides wind speed data at 10 meters above ground level (WS10M) [37], including the average, maximum, minimum, and range of wind speed. The average wind speed is used to model the convective cooling effect on PV modules, which reduces their operating temperature and mitigates efficiency losses. The maximum wind speed is significant for structural design to evaluate wind load impacts on PV systems, while the minimum wind speed highlights calm conditions where convective cooling is negligible, leading to peak module temperatures. The wind speed range indicates variability in wind conditions, helping assess fluctuations in cooling effects over time. Empirical models, such as the Faiman model,

integrate wind speed to estimate module temperature accurately, ensuring robust performance predictions under varying environmental conditions [51].

The Faiman model integrates wind speed (v) as follows:

$$T_{module} = T_{ambient} + \frac{G_{POA}}{U_0 + U_1.v} \tag{3.27}$$

The module temperature (T_{module}) is determined by a combination of environmental and system-specific factors, where it is influenced by the ambient temperature ($T_{ambient}$), the plane-of-array irradiance (G_{POA}) measured in (W/m²), and the wind speed (v), which is typically recorded at a height of 10 meters and may require adjustment to match the module height. Additionally, empirical heat loss coefficients (U_0 and U_1) account for thermal dissipation mechanisms, incorporating both convection and radiative heat transfer processes that impact the module's thermal balance. These factors collectively contribute to the thermal behaviour of PV modules under various operational and environmental conditions.

For this study, the average wind speed (WS10M) is used to estimate module temperature using Python PVLib models (e.g., Faiman or NOCT models). The maximum wind speed will be analyzed for structural design considerations, while the range and variability of wind speed will be examined to identify periods of limited cooling or extreme conditions. This analysis ensures accurate temperature modelling and robust PV system design, enhancing the overall solar potential estimation for rural Assam.

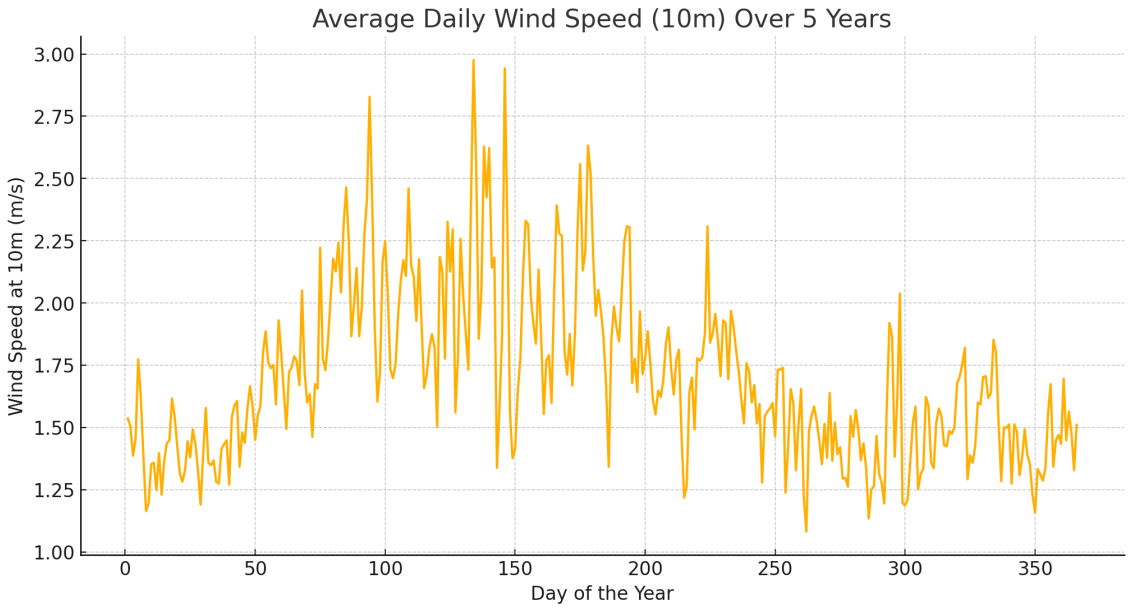

Fig 3.13 (a): Five-year daily average of wind speed at 10 m (WS10M) [37]

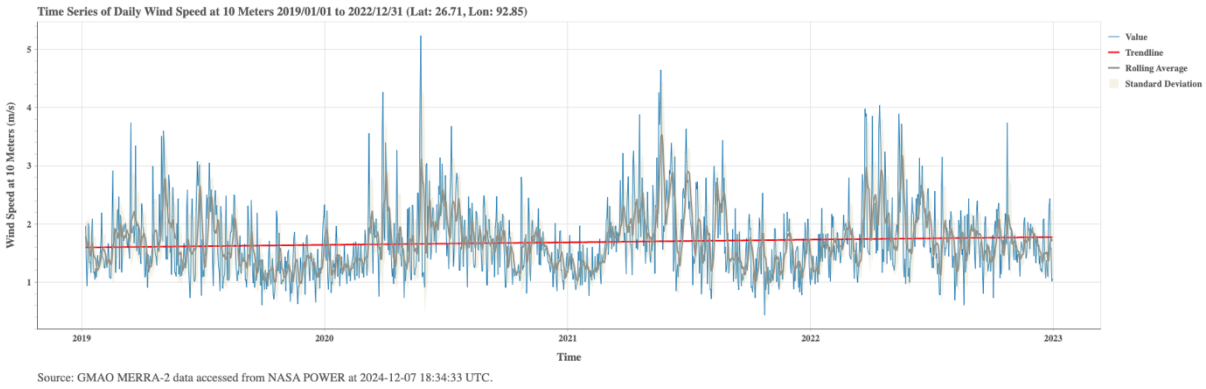

Fig 3.13 (b): Five-year time series of wind speed at 10 m (WS10M) [37]

The analysis of 5-year daily average wind speed **Fig. 3.13 (a)** and its 5-year time series **Fig. 3.13 (b)** provides details into the influence of wind speed on PV system performance. The daily average highlights typical wind conditions that contribute to convective cooling, which is particularly critical in regions with high ambient temperatures, such as rural Assam. The time series analysis captures the variability of wind speed over the years, including extreme events, which aids in understanding wind load impacts on PV system structures. Together, these analyses ensure accurate module temperature modeling, performance optimization, and the design of mechanically stable PV systems, enhancing the reliability of solar potential estimation in the study area.

3.6 Results and Discussions

3.6.1 Assessment of available area for solar PV installation

Land use land cover classification

The preliminary results of the LULC classification are presented in **Fig. 14 (a)** for the Random Forest Classifier (RFC) method, **Fig. 14 (b)** for the Maximum Likelihood Classifier (MLC) method, and **Fig. 14 (c)** for on-screen digitization of rice croplands. These analyses identified three key land cover classes critical for solar photovoltaic (PV) installations: built-up clusters for assessing rooftop solar (RTS) potential, barren/fallow land for evaluating ground-mounted solar (GMS) feasibility, and rice croplands for solar irrigation and water pumping applications (SWP). In addition to these, other LULC classes such as forests, water bodies, and grasslands were identified but excluded from consideration for PV installations due to their unsuitability. The LULC classification provided precise spatial distribution data, with details of the identified

classes outlined in **Table 3.5**. By combining results from the RFC, MLC, and on-screen digitization methods, the analysis ensured accuracy and reliability, particularly in delineating agricultural areas like rice croplands. This comprehensive assessment of land use forms the foundation for estimating the energy generation potential of RTS, GMS, and SWP systems, as detailed in subsequent sections.

Table 3.5: Land use land cover (LULC) classes, classification criteria, and descriptions

LULC Classes	Classification Criteria and Descriptions
Water bodies	Major river (*Jia Bhalari*), minor river (*Mora Bharali*) and small water bodies such as wetland, ponds are classified under the same class 'water bodies'.
Sand	The satellite image was acquired on December 22, 2021. During this winter period *Jia Bhalari* river dried up and sandbars are also visible in the satellite image. To distinguish the sand bars from built-up/settlement areas, a separate class 'sand' is created.
Forest-Plantation forest	The study area includes two tea gardens, a forested area and also rural home garden plantation. Although such different vegetation patterns can be visually distinguished in the satellite image, it is difficult to precisely train the classification algorithm to differentiate the vegetation as different classes. Therefore, the tea gardens, forested areas and rural home gardens are mapped as a single class 'forest/plantation'. On-screen or manual method of classification is also done separately to distinguish the tea gardens from the forested area. However rural home gardens could not be mapped separately because they are closed mixed with rural built-up areas so not possible to map accurately using Sentinel-2A image (10 m resolution).
Built up-Settlement	Rural and urban houses, industries, institutions are mapped as a single class 'built-up/settlement'.
Airport tarmac	The study area covers a small airport, the airport tarmac is mapped separately. This was also done to avoid false classification of the airport tarmac as a water body.
Rice cropland	Winter rice cultivation is the major agricultural activity in the study area. Rice is planted during June-July and harvested in November-December. After harvesting, the rice fields remain as current fallow land till next cropping season. As mentioned earlier, the acquired image belongs to the month of December (22 December, 2020), when rice harvesting is already completed in the study region. Therefore, rice growing areas were mapped as 'rice cropland'. The rice growing areas were also manually digitized as individual polygons using the satellite image. The comparison of area under digital and manual classification was done to assess the classification accuracy.
Winter cropland	Winter vegetables such as cabbage, cauliflower, brinjal, potato are also grown in the study area, but in small amounts. Therefore, winter crop growing areas were

	mapped as 'winter cropland'. Land use shared by different winter vegetables could not be mapped separately.
Wetland-Wetland rice	Some parts of the river *Mora Bharali* is converted to artificial wetland for fishing and wetland rice cultivation. Those areas were mapped as wetland/wetland rice. The differentiation between wetland and wetland rice areas could not be made because wetland rice areas are not permanent. Wetland rice covers a small part of the river. Depending on depth and water content of the river, the wetland rice areas change from one season to another.
Barren land-Fallow land	There are no distinct grasslands in the study area as one can observe in a protected forest like a national park. However, there are grass-covered playgrounds in villages, in school and in community areas. Similarly, there is also fallow land (grass-covered in the study area. It is difficult to identify those areas separately using a 10 m image. Therefore, they are mapped together as 'grassland/fallow land'.

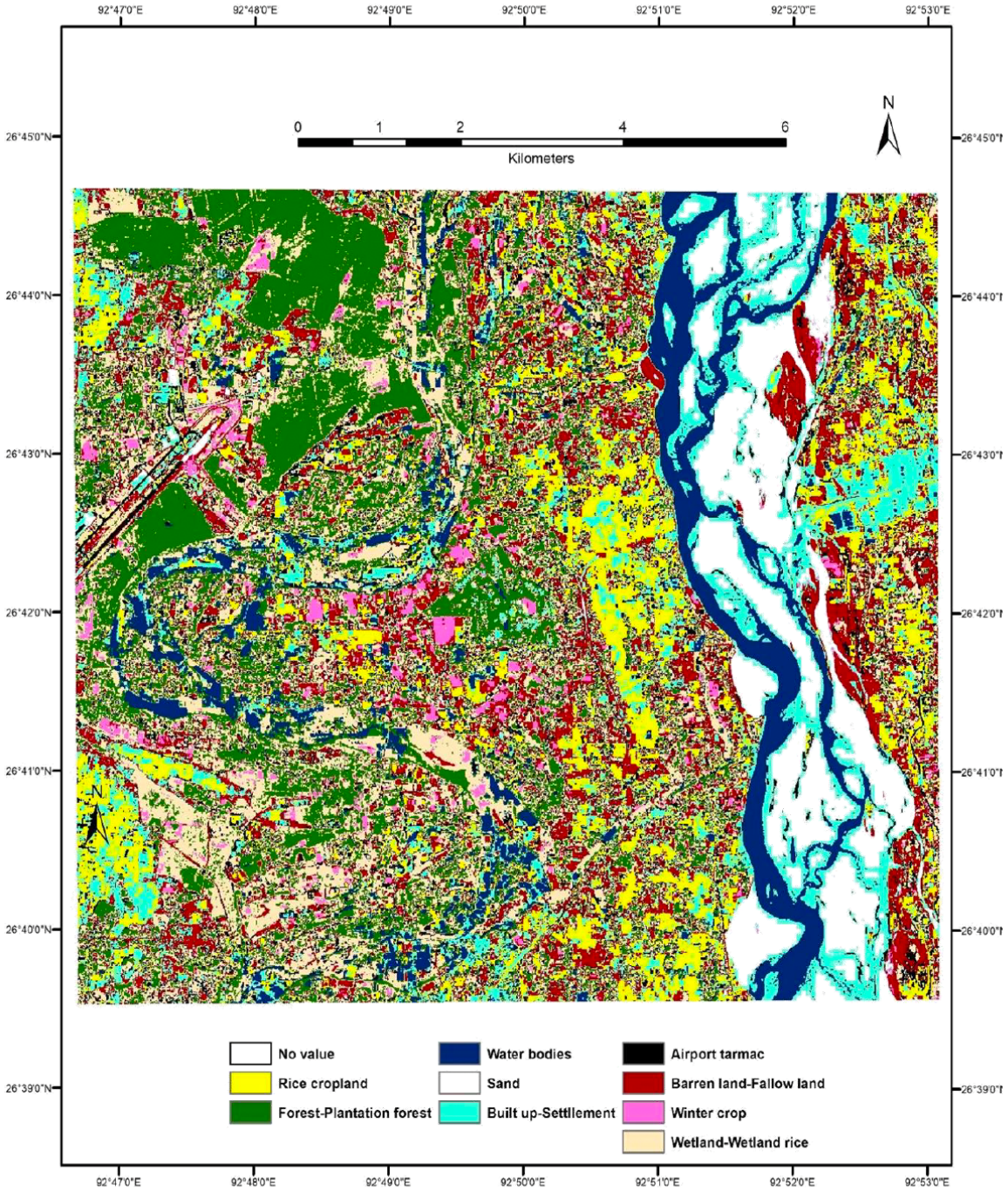

Fig 3.14 (a): Identifying ground mounted options based on RFC method

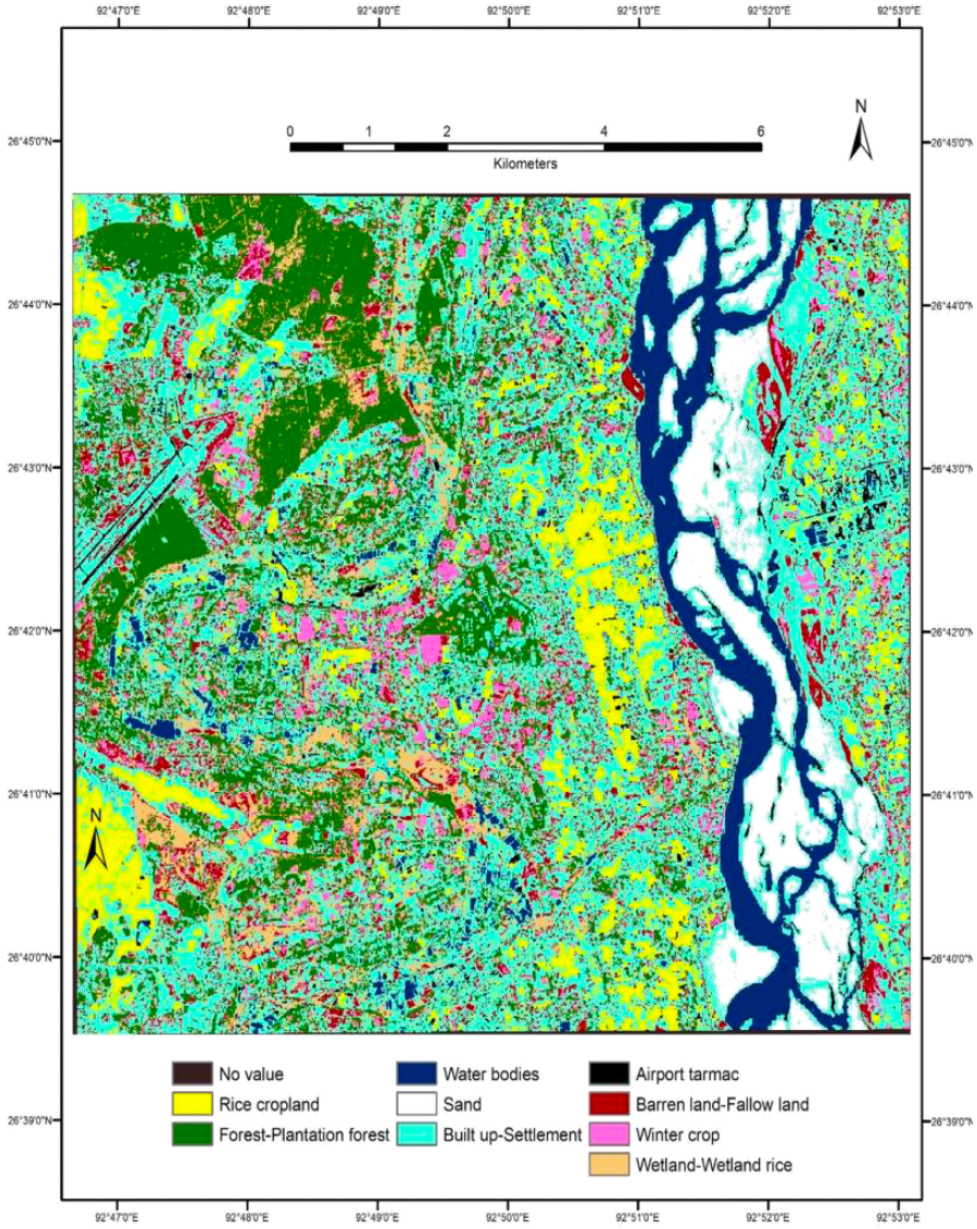

Fig 3.14 (b): Identifying built-up area for RTS options based on MLC

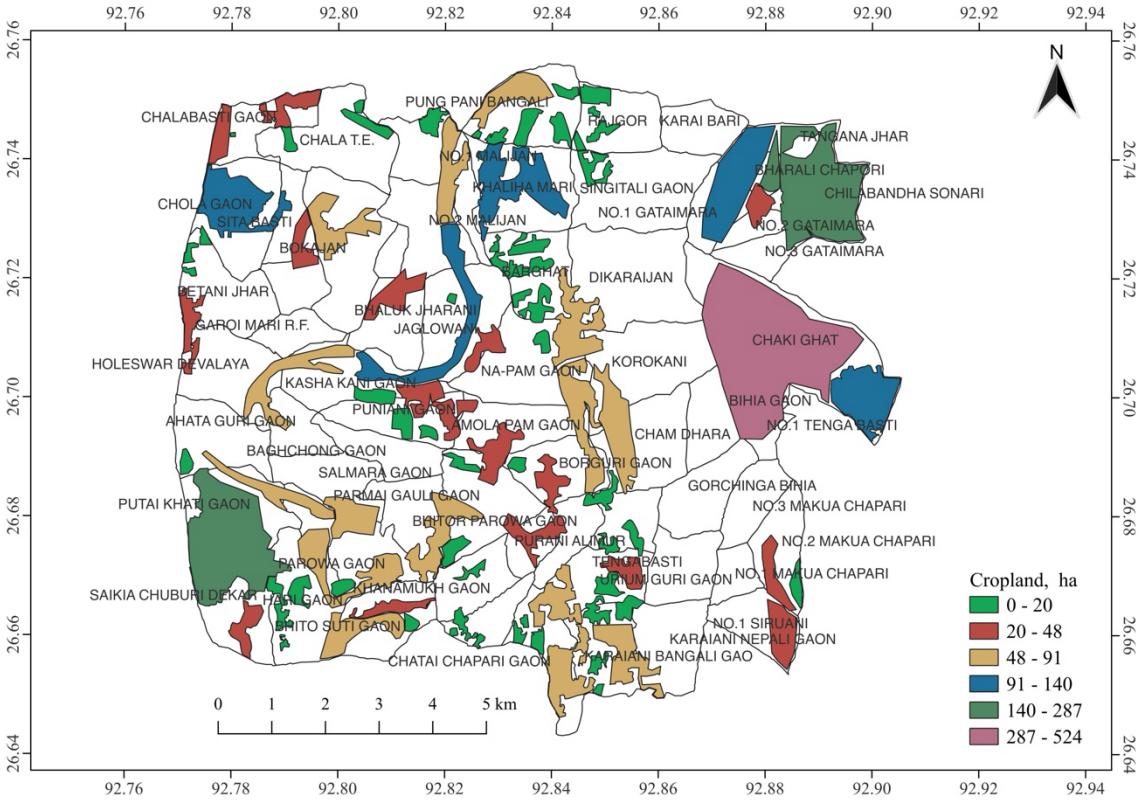

Fig 3.14 (c): Distribution of cropland in the study area (on-screen digitization)

Assessment of available area for RTS installation

The household-wise area available for RTS ranges from 27 m² to 65 m², with an average of 47 m² per household. Smaller roof areas, such as 27 m², may limit the feasibility of installing larger photovoltaic systems, constraining energy generation capacity, whereas larger roof areas, such as 65 m², offer greater potential for energy generation, enabling households to meet their energy needs and even contribute surplus energy to the grid.

At the village level, the available area varies from 1,277 m² to 45,315 m², with an average of 18,967 m² per village. Villages with extensive rooftop areas, such as 45,315 m², provide significant opportunities for large-scale solar PV adoption. In contrast, villages with limited rooftop areas, such as 1,277 m², may require supplementary solutions, including ground-mounted systems or shared community solar installations.

The total rooftop area available for the study area amounts to 1,157,013 m², while the roof area per hectare across villages ranges from 11 m²/ha to 346 m²/ha, with an average of 114 m²/ha. Villages with higher rooftop area densities, such as 346 m²/ha, indicate clustered opportunities

for efficient solar energy planning, whereas those with lower densities, such as 11 m²/ha, may face challenges in achieving significant rooftop solar deployment. **Fig 3.15 (a)** illustrates the rooftop area available on a village-wise basis, providing a clear visualization of the spatial distribution and variations across the study area.

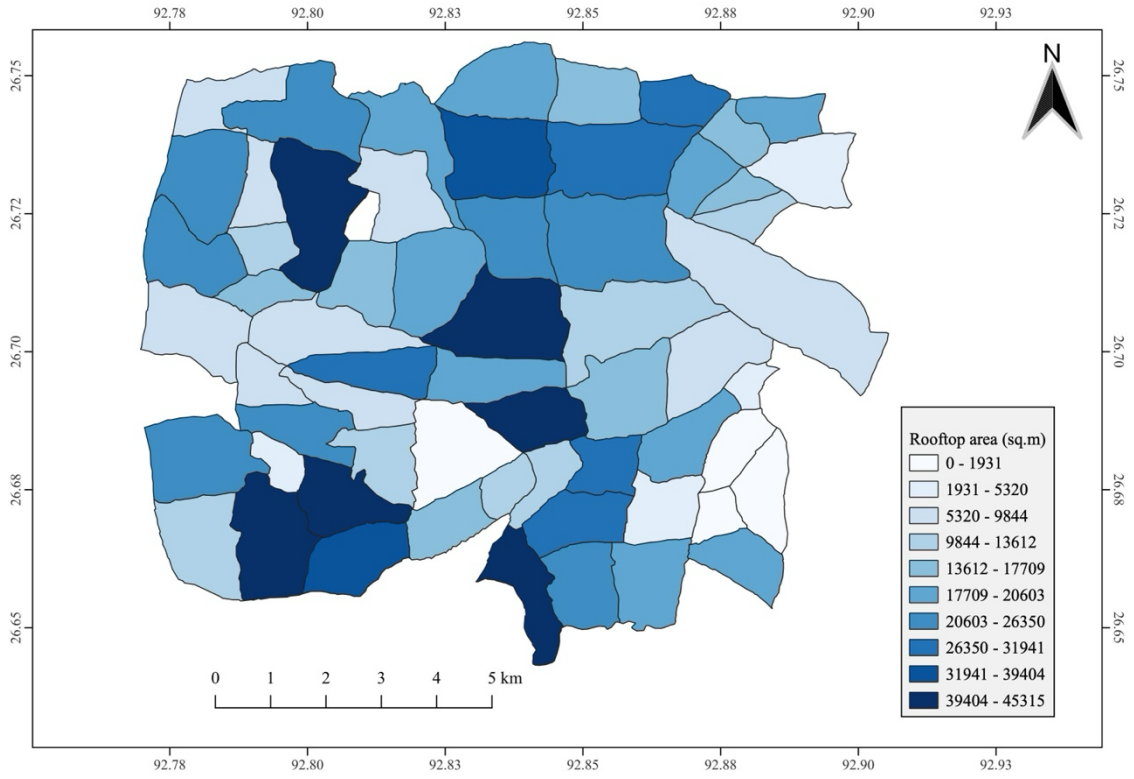

Fig 3.15 (a): Map representing area available for installation of RTS in the study area

Assessment of available area for GMS installation

The area available for Ground-Mounted Solar (GMS) installations at the village level ranges from 4,341 m² to 271,413 m², with an average of 105,036 m² per village. The analysis is conducted at the village scale due to the absence of household-level data on the distribution of barren or fallow land that is suitable for GMS installations. Villages with larger available areas, such as 271,413 m², represent ideal candidates for large-scale solar energy projects, enabling significant contributions to regional renewable energy targets. Conversely, villages with smaller available areas, such as 4,341 m², may require strategic prioritization or alternative solar energy solutions.

The total ground area available for GMS installations across the study area amounts to 6,407,182 m², underscoring the substantial potential for widespread solar PV deployment. The variation in available ground area per hectare further highlights spatial disparities, with values ranging from 38 m²/ha to 1,691 m²/ha and an average of 620 m²/ha for the study area. Villages with higher densities, such as those with 1,691 m²/ha, indicate concentrated opportunities for efficient land utilization and energy planning. In contrast, villages with lower densities, such as those with 38 m²/ha, may face challenges in achieving impactful solar energy deployment due to dispersed land availability. This analysis reflects the critical role of barren or fallow land in contributing to the feasibility and scalability of ground-mounted solar projects. By leveraging such land resources effectively, GMS installations can significantly enhance the region's renewable energy capacity while avoiding competition with productive agricultural or urban land uses. **Fig 3.15 (b)** illustrates the village-wise distribution of GMS area availability, providing a visual representation of the spatial variation and potential opportunities for ground-mounted solar installations.

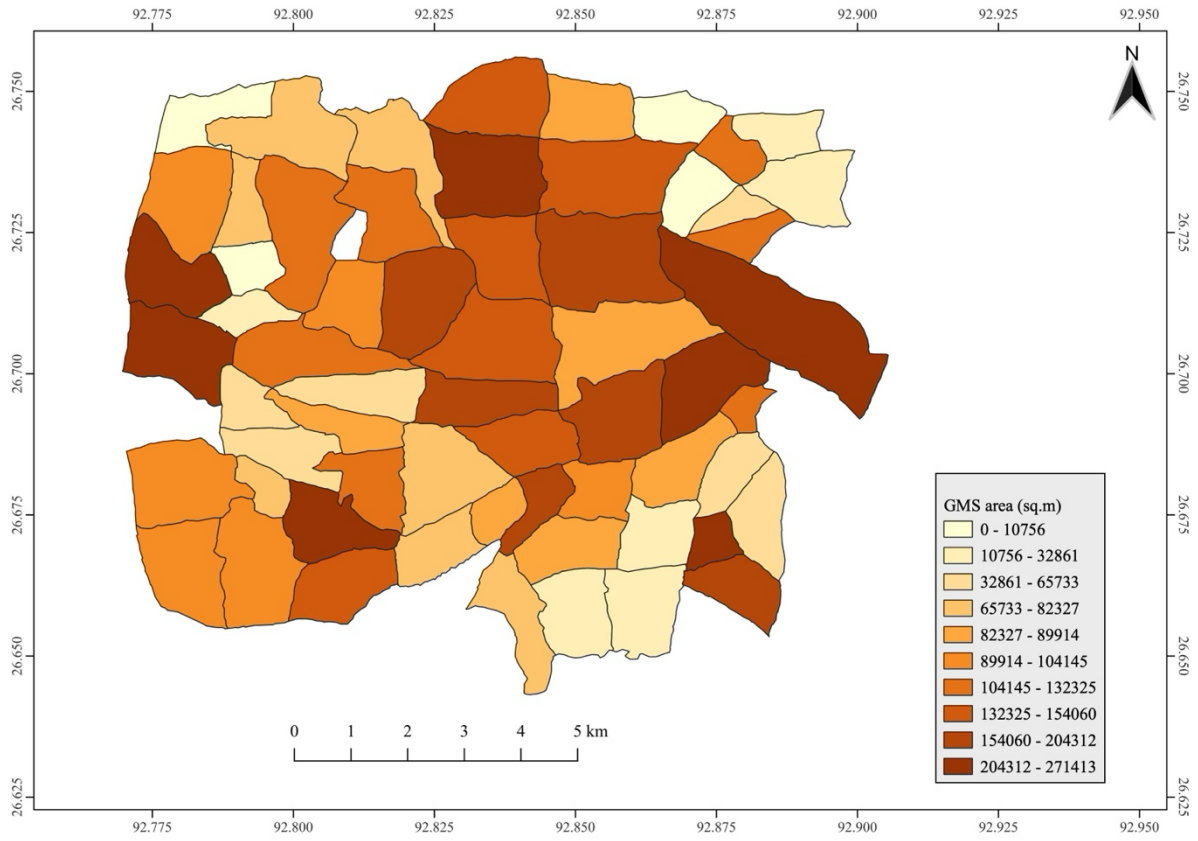

Fig 3.15 (b): Map representing area available for installation of GMS in the study area

Assessment of available crop area for SWP systems

The area available for Solar Water Pumping (SWP) systems at the village level ranges from 90 m² to 4,616,460 m², with an average of 546,682 m² per village. The analysis is conducted at the village scale as detailed household-level data on the distribution of crop area is unavailable. Villages with larger available crop areas, such as 4,616,460 m², demonstrate significant potential for SWP system deployment, enabling efficient irrigation of large agricultural fields. Conversely, villages with smaller crop areas, such as 90 m², may have limited capacity for SWP installations, potentially constraining their use to small-scale agricultural operations or specialized crop irrigation.

The total crop area available for SWP systems across the study area amounts to 33,347,620 m², reflecting the substantial potential for integrating solar water pumping systems into the region's agricultural landscape. This total highlights the critical role SWP systems can play in enhancing agricultural productivity while promoting renewable energy use. However, the availability of crop area per hectare within villages varies significantly, ranging from 1 m²/ha to 9,746 m²/ha, with an average of 2,737 m²/ha. Villages with higher crop area densities, such as 9,746 m²/ha, present concentrated opportunities for SWP deployment, offering efficient energy and water management. In contrast, villages with lower densities, such as 1 m²/ha, may face challenges in achieving significant SWP integration due to the sparse distribution of irrigable land. This variability in crop area availability reflects the diverse agricultural landscape of the study area, influenced by factors such as land-use patterns, soil conditions, and irrigation practices. While SWP systems are primarily constrained by water demand and irrigation requirements, their deployment provides an opportunity to reduce dependency on conventional energy sources and improve the sustainability of agricultural practices. Future considerations, such as integrating agrivoltaics, may further enhance the utility of available crop areas by combining agricultural production with solar energy generation. **Fig 3.15 (c)** illustrates the village-wise distribution of crop area availability for SWP systems, providing a visual representation of spatial variations and potential opportunities for solar water pumping installations across the study area.

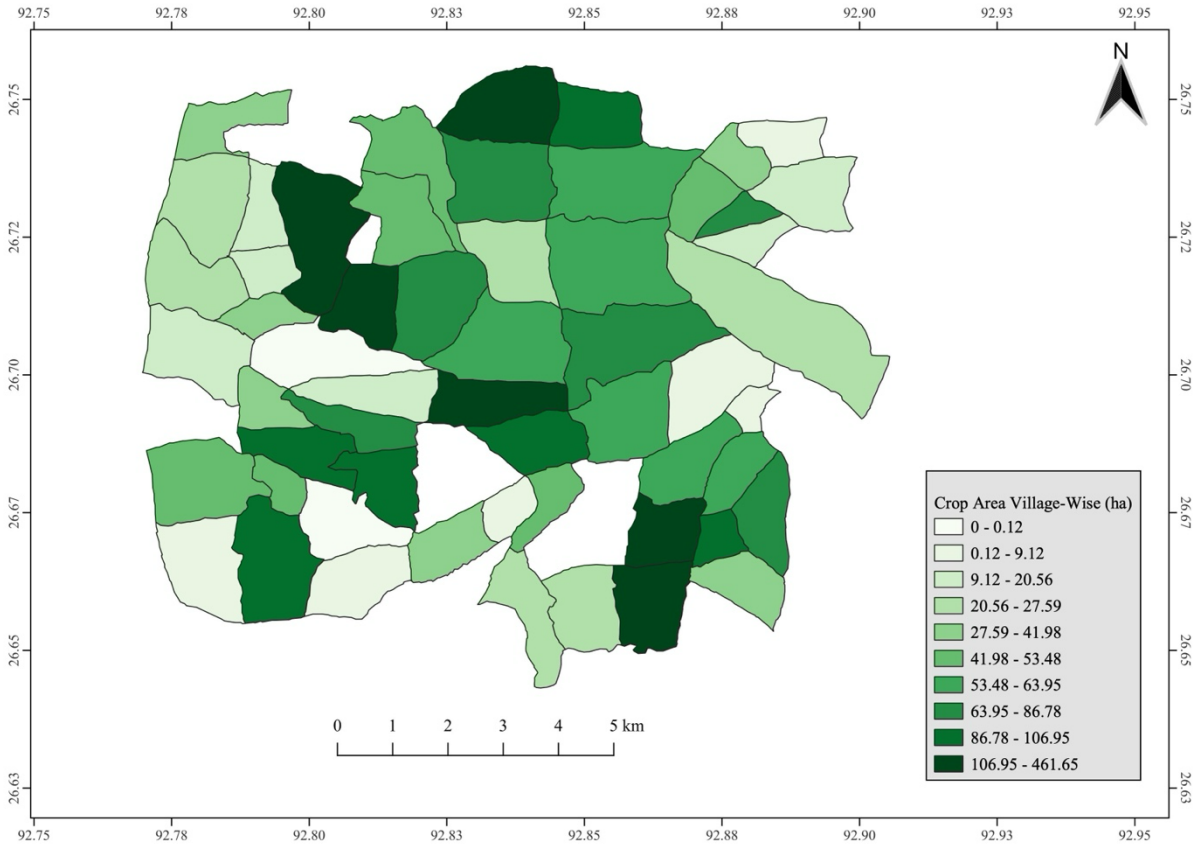

Fig 3.15 (c): Map representing cropland for installation of SWP in the study area

3.6.2 Assessment of solar PV system potential

Assessment of photovoltaic (PV) system output

Spatial and temporal maps of PV system output have been generated to represent energy production in kWh/kWp for both annual averages and monthly temporal variations from January to December. These assessments provide valuable insights into the performance of PV systems under varying climatic and seasonal conditions within the study area. By analyzing the annual average output, the overall efficiency and productivity of PV system installations can be assessed, while the monthly variations highlight the impact of seasonal changes on energy generation.

The spatial maps offer a visual representation of geographic variations in PV system output, identifying areas with higher or lower energy production potential. Meanwhile, the temporal maps help in understanding how the output fluctuates across different months, enabling better planning for energy storage and management systems.

The annual average map is provided in **Fig 3.16** and monthly temporal variations maps are provided in **Appendix 3E** figures **Fig A.1** to **Fig A.12**, illustrating both the spatial and temporal distribution of PV system output. These results underscore the viability of PV system installations in the study area and provide a comprehensive framework for optimizing solar energy utilization throughout the year.

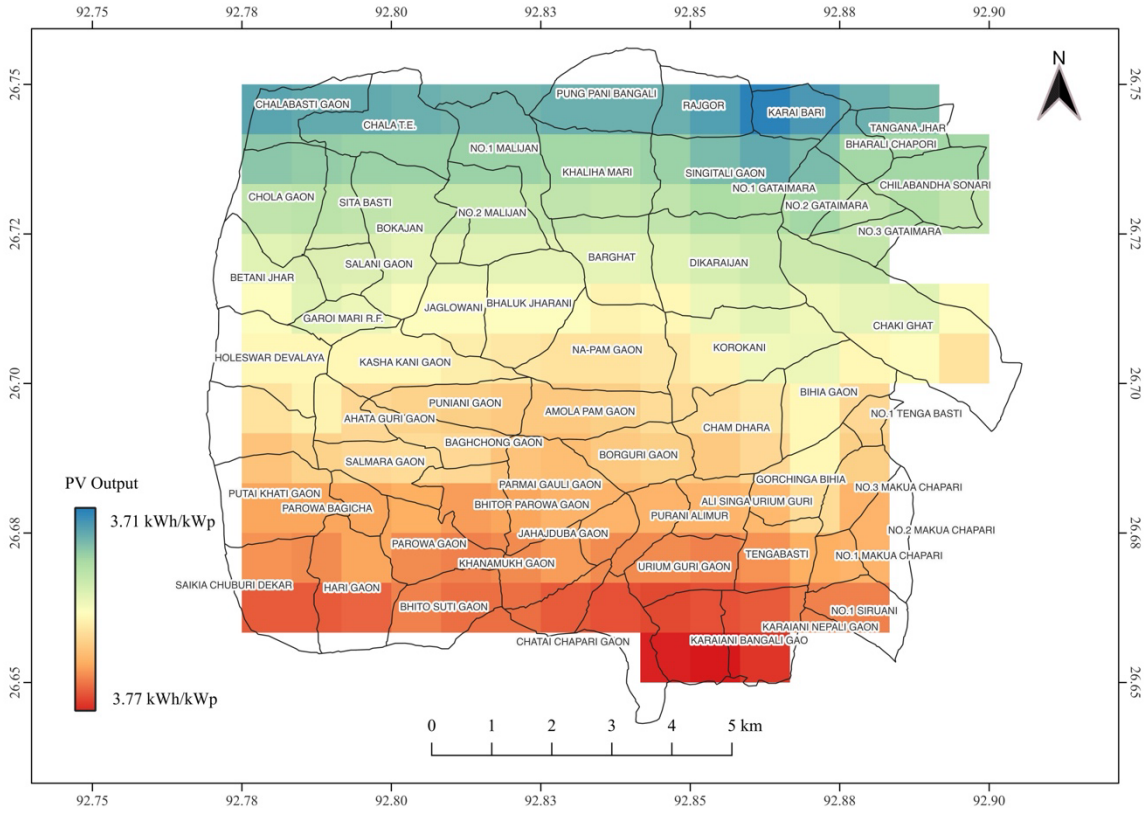

Fig 3.16: Annual average PV system output (kWh/kWp)

The PV system potential for each energy system RTS, GMS, and SWP has been determined both on a village-wise basis and for the entire study area. The aggregated results for the entire study area are summarized in **Table 3.6**, which includes the total energy generation potential and the per capita energy availability from each system. This table provides a comprehensive overview of the contribution of each system to the energy landscape of the study area.

Table 3.6: Total energy production and utilization metrics for different energy systems in the study area

Category	Installation Capacity (MW)	Annual Generation (GWh/y)	Per Capita (kWh/y)	Surplus Energy Available (GWh/y)

RTS	208	244.25	2,036	NA
GMS	1,153	1,352.62	11,275	NA
SWP	13	15.76	101	12.13
Total	1,374	1,612.63	13,412	12.13

3.6.2.1 RTS: Installation and generation capacity

The installation capacity for RTS systems at the household level ranges from a minimum of 5 kW to a maximum of 12 kW, with an average of 8 kW per household. At the village level, the installation capacity varies from 230 kW to 8,157 kW, with an average of 3,414 kW per village. The total RTS installation capacity for the study area is 208,262 kW, reflecting substantial potential for meeting local energy demands. Considering the mix of urban and rural demographics and the prevailing energy consumption patterns, this capacity has the potential to make households and villages largely energy self-sufficient, with surplus energy available for grid supply. This surplus presents an opportunity to enhance regional energy security and contribute to the overall renewable energy mix. **Fig 3.17 (a)** illustrates the village-wise spatial distribution of RTS installation capacity, providing insights into the spatial variability across the study area.

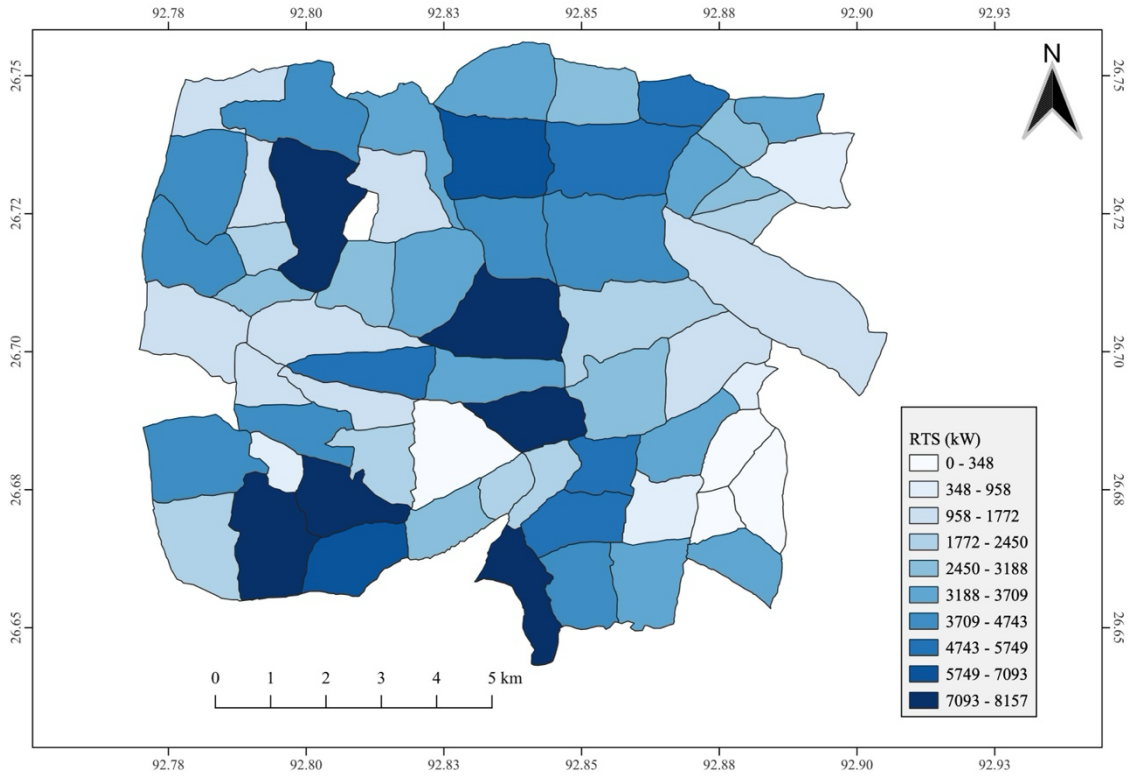

Fig 3.17 (a): Map of village-wise spatial distribution of RTS installation capacity

The generation capacity for RTS systems at the household level ranges from a minimum of 5,700 kWh/y to a maximum of 13,691 kWh/y, with an average of 9,940 kWh/year per household. At the village level, the generation capacity varies significantly, from 269,501 kWh/y to 9,566,470 kWh/y, with an average of 4,004,221 kWh/y per village. The total RTS generation capacity for the study area amounts to 244,257,462 kWh/y, demonstrating its ability to address energy demands while reducing reliance on conventional energy sources. **Fig 3.17 (b)** depicts the village-wise spatial distribution of RTS generation capacity, offering a clear visualization of potential hotspots for solar energy production.

The household-level installation and generation capacities highlight the suitability of RTS systems for diverse residential settings. Households with smaller capacities, such as 5 kW, may find it sufficient for basic energy needs, while those with larger capacities, such as 12 kW, can cater to higher consumption levels or even contribute excess energy to the grid. Similarly, villages with higher capacities, such as 8,157 kW in installation and 9,566,470 kWh/y in generation, represent key nodes for solar energy production and distribution. These villages could act as energy hubs, facilitating surplus energy transfer to surrounding areas.

The significant total capacity of 208,262 kW and annual generation of 244,257,462 kWh/y underscore the transformative potential of RTS systems in achieving energy self-sufficiency and sustainability for the study area. Furthermore, the analysis aligns with the region's mixed urban-rural demographic, where diverse energy demands can be effectively addressed through distributed generation. The availability of surplus energy also highlights opportunities for economic benefits through energy trading or grid integration, particularly in regions with well-developed grid infrastructure.

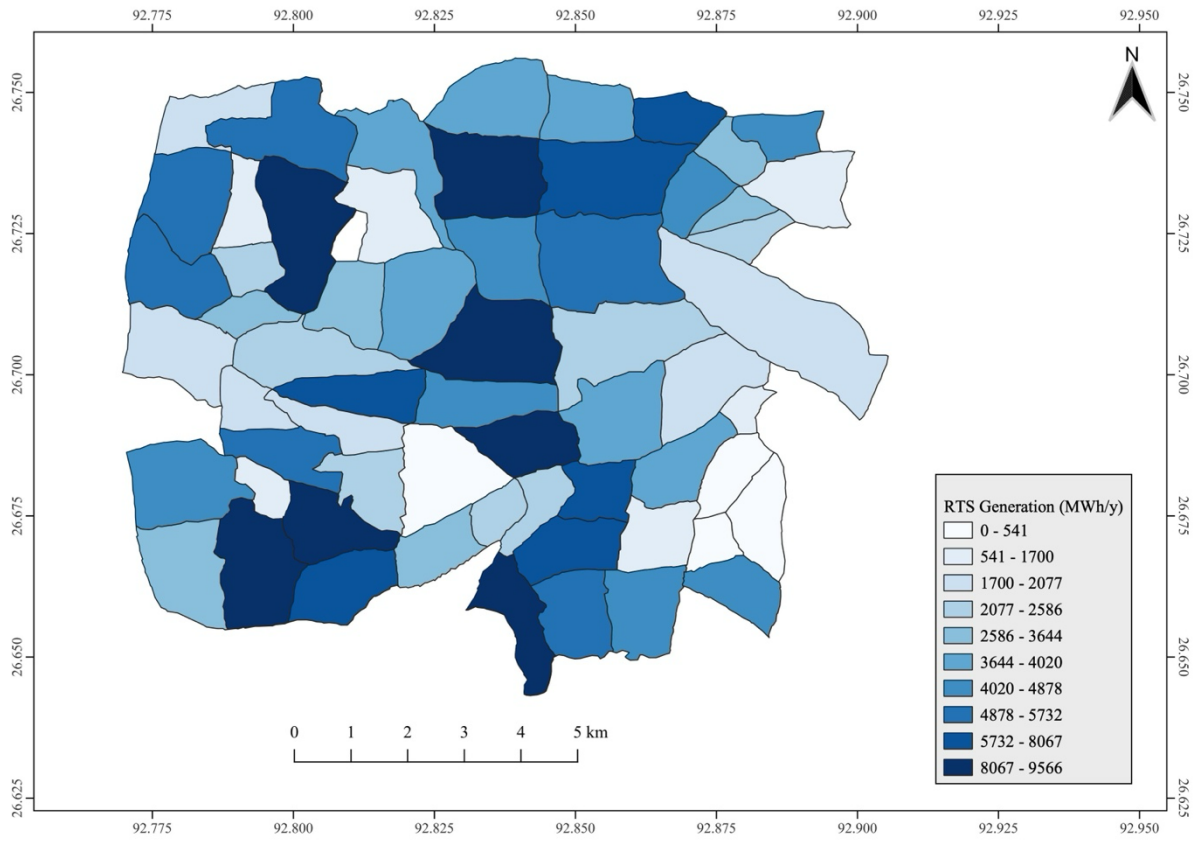

Fig 3.17 (b): Map of village-wise spatial distribution of RTS generation capacity

3.6.2.2 GMS: Installation and generation capacity

The installation capacity for GMS systems at the village level ranges from a minimum of 781 kW to a maximum of 48,854 kW, with an average of 18,906 kW per village. The total GMS installation capacity for the study area is 1,153,293 kW, reflecting its significant potential for large-scale solar energy production. Given the high capacity potential, GMS installations have the ability to meet local energy demands comprehensively while creating surplus energy for grid integration. This surplus capacity can enhance regional energy security and facilitate the transition toward renewable energy systems. **Fig 3.18 (a)** illustrates the village-wise spatial distribution of GMS installation capacity, providing insights into areas with significant potential for solar energy production.

The generation capacity for GMS systems varies significantly at the village level, ranging from a minimum of 916,484 kWh/y to a maximum of 57,297,979 kWh/y, with an average of 22,174,133 kWh/y per village. The total GMS generation capacity for the study area amounts to 1,352,622,119 kWh/y, demonstrating its ability to contribute substantially to the energy mix

and support regional sustainability goals. **Fig 3.18 (b)** depicts the village-wise spatial distribution of GMS generation capacity, offering a clear visualization of potential hotspots for energy production.

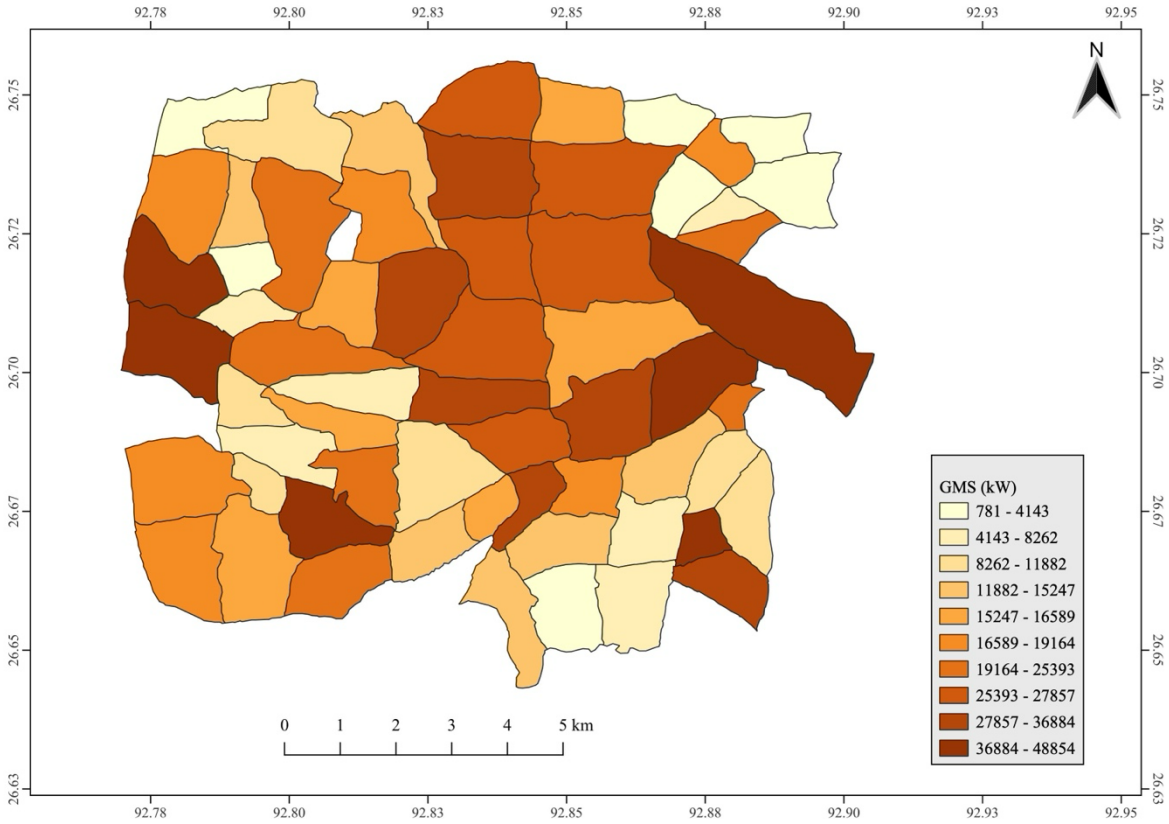

Fig 3.18 (a): Map of village-wise spatial distribution of GMS installation capacity

Due to the nature of GMS installations, the analysis is conducted at the village scale rather than the household level. Barren or fallow land suitable for GMS systems is distributed across the study area and has been attributed to the administrative boundaries of villages. This method reflects the challenges of directly associating land availability with individual households while ensuring a comprehensive understanding of the potential within the administrative framework.

The analysis of GMS installation and generation capacities underscores its critical role in addressing energy demands at a large scale. Villages with higher capacities, such as those exceeding 48,000 kW in installation or generating over 57 million kWh/y, represent key sites for extensive solar energy production. These high-capacity villages could serve as energy hubs, supplying surplus energy to adjacent regions through grid integration. Conversely, villages with lower capacities, such as 781 kW in installation or generating 916,484 kWh/y, can still

benefit from GMS systems by supplementing local energy needs and reducing dependence on conventional energy sources.

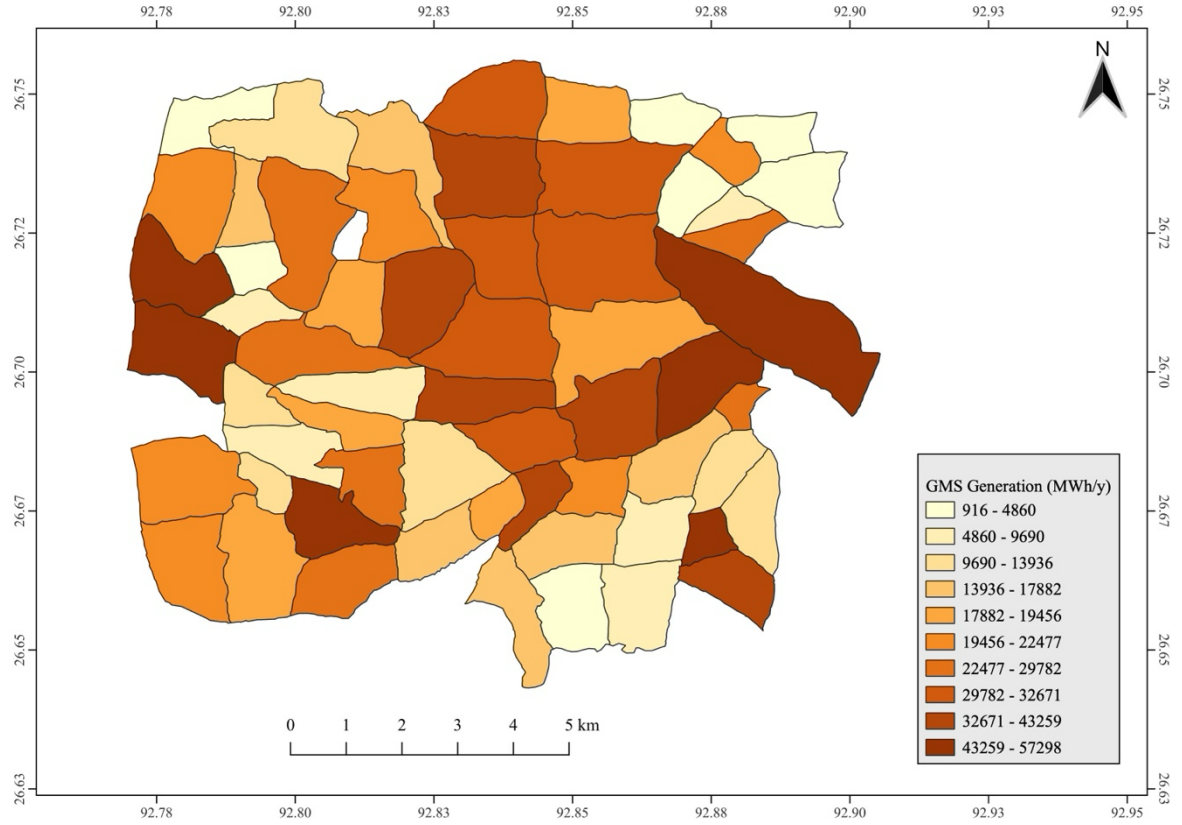

Fig 3.18 (b): Map of village-wise spatial distribution of GMS generation potential

The total capacity of 1,153,293 kW and generation of 1,352,622,119 kWh/y highlight the transformative potential of GMS systems in achieving regional energy self-sufficiency. By leveraging barren and fallow land for solar PV deployment, GMS installations avoid competition with agricultural or urban land uses, making them a sustainable and efficient solution for scaling renewable energy.

However, the reliance on aggregated village-level data introduces some limitations. Variations in land quality, accessibility, and competing land uses within villages may influence the feasibility and scalability of GMS installations. Addressing these challenges will require localized assessments and strategic planning to optimize land utilization and maximize energy generation. Furthermore, technical and economic support for grid infrastructure development will be essential to ensure the effective integration of surplus energy into the regional grid.

The GMS system's ability to meet energy demands while providing surplus energy underscores its pivotal role in transitioning toward a sustainable and decentralized energy future. The substantial capacity and generation potential offer an opportunity for large-scale contributions to renewable energy targets, fostering energy security and environmental sustainability in the study area.

3.6.2.3 SWP: Installation and generation capacity

For the SWP system, the water requirement of rice, the predominantly cultivated crop in the region and one with the highest water demands among crops is considered. This design ensures that the system is capable of meeting the peak water demand during the cropping season, addressing the primary irrigation needs of the area effectively.

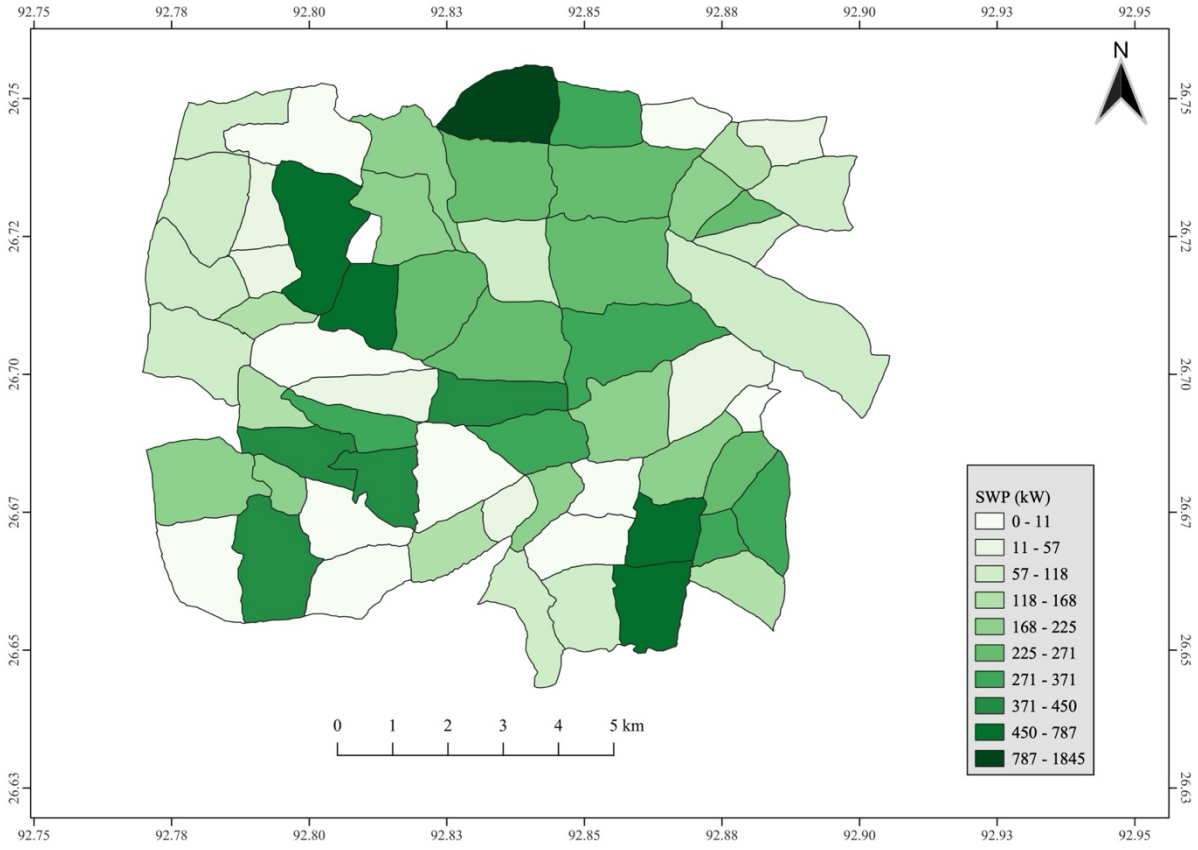

Fig 3.19 (a): Map of village-wise SWP installation capacity

While the RTS and GMS systems are designed to either feed energy into the grid or be consumed locally, the SWP system exhibits a unique characteristic: surplus energy generation during non-irrigation periods. This surplus, which can be effectively utilized for alternate

energy applications such as EV charging, is depicted in the corresponding figures. Notably, for some months, the surplus energy matches the total production, as irrigation scheduling indicates no irrigation requirements during these periods. This is a significant observation, emphasizing the seasonal nature of energy demand in agricultural applications.

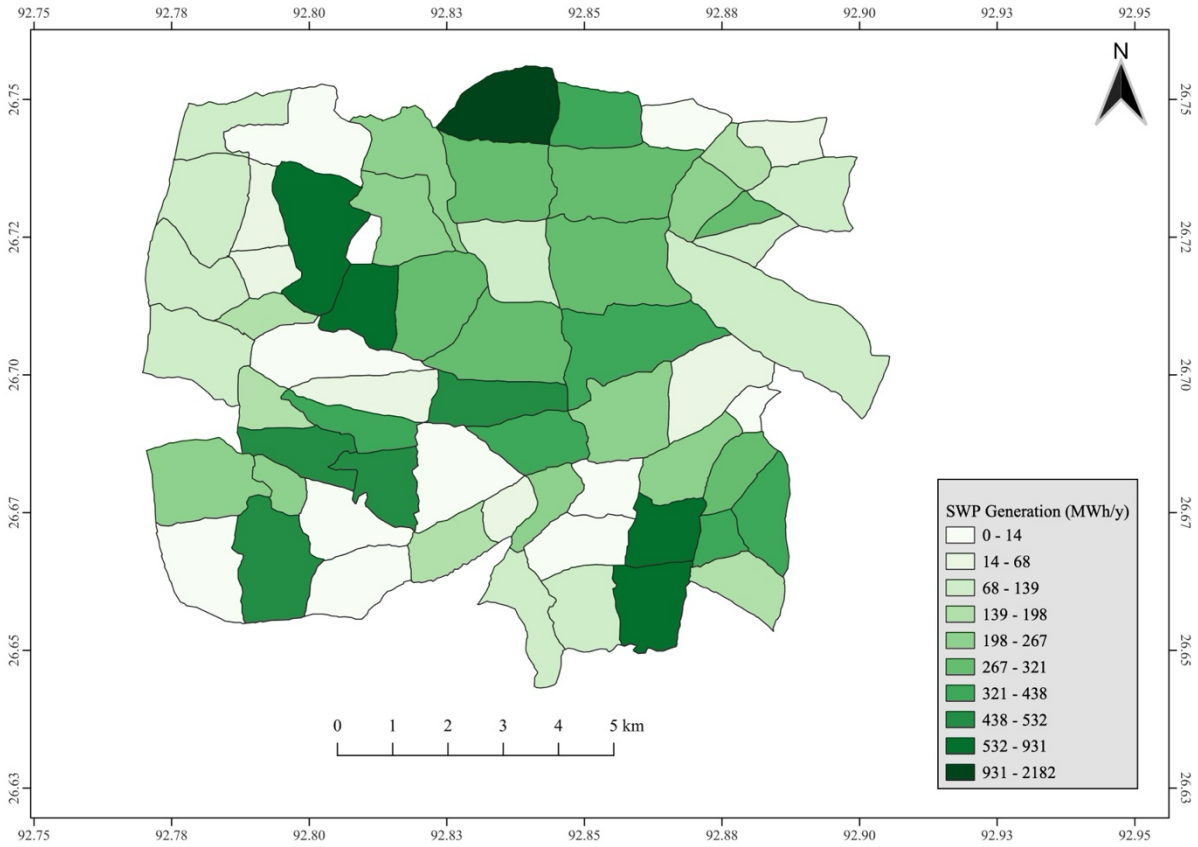

Fig 3.19 (b): Map of village-wise SWP generation potential

The analysis underscores the versatility and potential of each system in meeting both localized energy needs and broader sustainability goals. The surplus energy from SWP, in particular, presents an opportunity for innovative energy solutions in rural areas, while RTS and GMS contribute to strengthening the grid infrastructure. Together, these systems demonstrate the ability to transform the energy ecosystem of the study area into a more sustainable and resilient model.

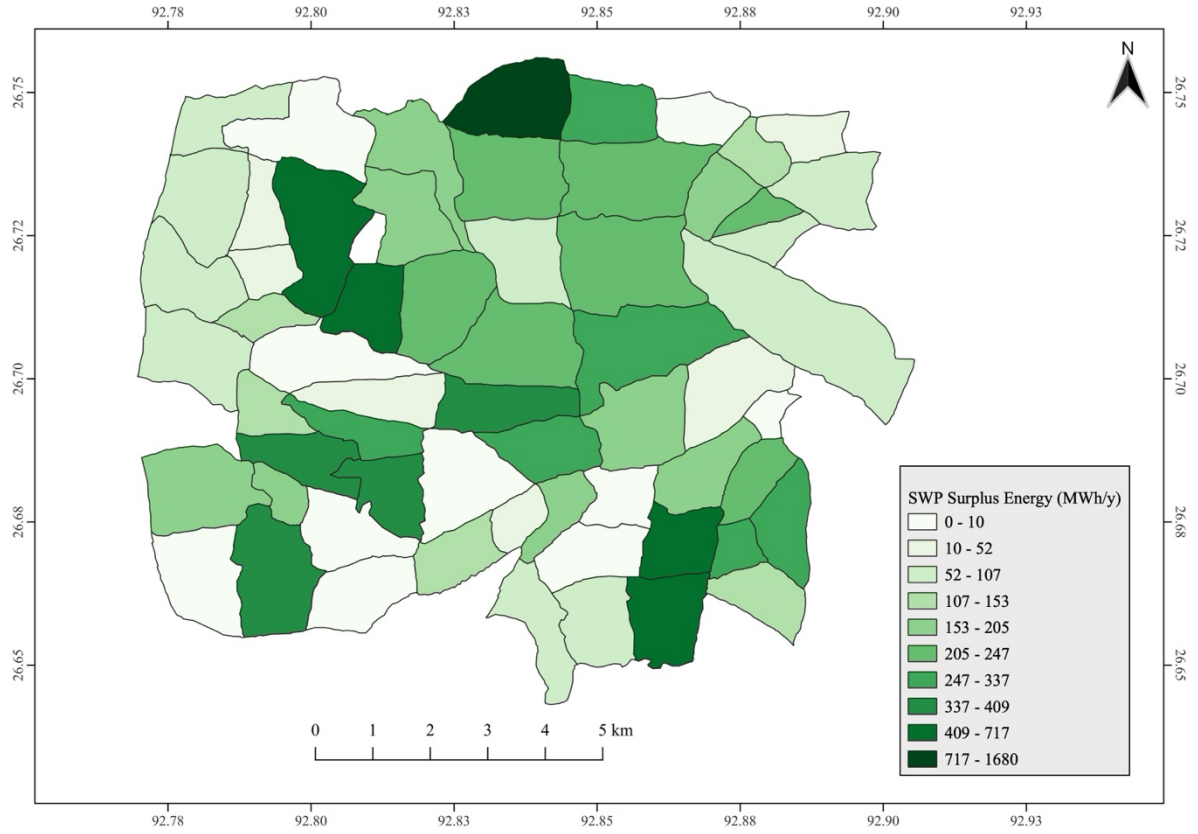

Fig 3.19 (c): Map of village-wise surplus energy from SWP systems

3.6.3 Temporal Variations in Generation Capacity: System-wise Assessment

The monthly energy generation potential for each solar PV system in the study area, including RTS, GMS, and SWP, from January to December, is depicted in **Fig 3.20 (a)** (RTS), **Fig 3.20 (b)** (GMS), and **Fig 3.20 (c)** (SWP). Additionally, **Fig 3.20 (d)** illustrates the monthly surplus energy available from SWP systems during non-operational periods. This temporal analysis provides critical insights for energy planning and management, enabling stakeholders to optimize resource allocation, ensure grid stability, and align energy supply with demand patterns.

The RTS systems, as depicted in **Fig 3.20 (a)**, exhibit a consistent generation pattern across the year, with slight variations influenced by seasonal changes in solar irradiance. The peak generation months typically align with periods of high solar insolation, such as the summer months, while slightly lower outputs are observed during the monsoon season due to cloud cover and rainfall. This predictable generation pattern supports stable energy supply for residential and commercial purposes. The temporal analysis aids in designing efficient energy storage systems to store excess energy during high-generation months and utilize it during

periods of lower output. Additionally, it facilitates grid integration planning by identifying peak surplus periods for energy export.

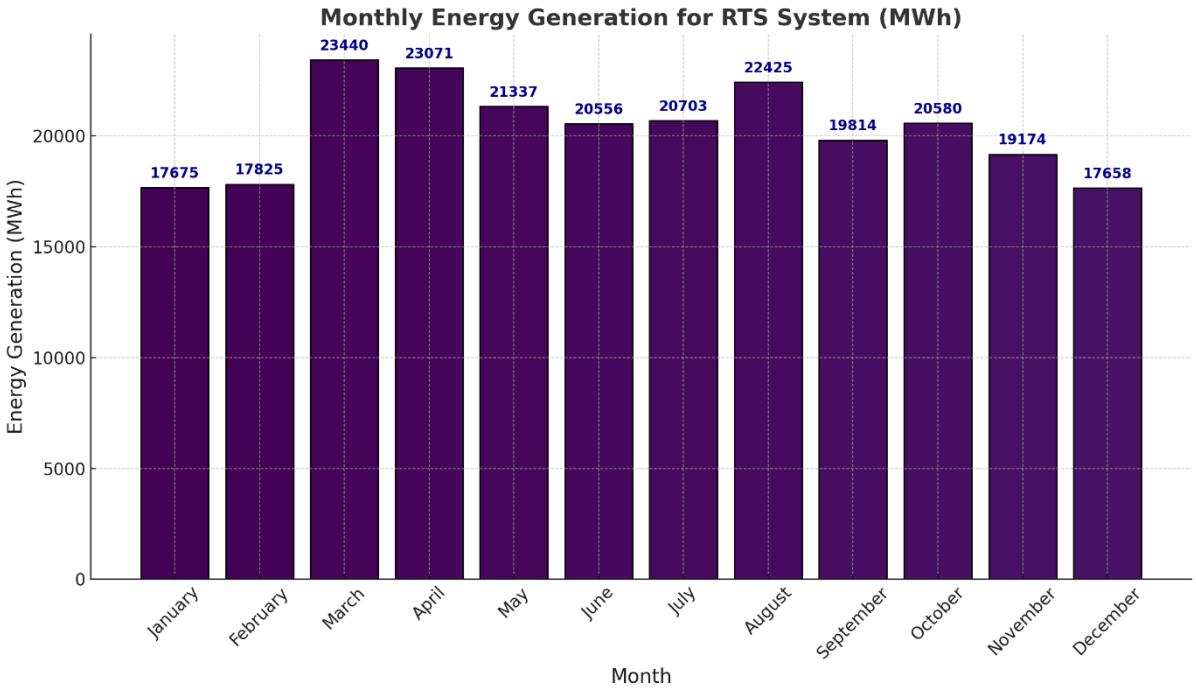

Fig 3.20 (a): Monthly energy generation for RTS system

For GMS systems, shown in **Fig 3.20 (b)**, the seasonal generation trends follow a similar pattern to RTS systems, with higher outputs during sunny months and reduced performance during monsoon periods. However, the scale of GMS installations allows for substantial energy generation even during suboptimal conditions. This makes GMS systems a reliable backbone for meeting large-scale energy demands. Temporal analysis of GMS generation capacity helps in planning grid infrastructure, such as transmission and distribution systems, to handle seasonal variations and surplus energy efficiently. It also supports policy frameworks for encouraging solar farms to supply energy during peak demand periods, enhancing regional energy stability.

The energy generation from SWP systems, presented in **Fig 3.20 (c)**, demonstrates strong seasonality driven by agricultural cycles and water demand patterns. Peak generation coincides with irrigation seasons, while energy output is underutilized during non-irrigation periods. This temporal alignment with agricultural needs ensures reliable energy availability for farmers during critical cropping months. However, during non-operational periods, surplus energy is generated, as shown in **Fig 3.20 (d)**, highlighting the potential for alternative energy utilization.

This surplus energy could be redirected for secondary applications, such as powering rural electrification projects, supporting local microgrids, or charging electric vehicles, thereby maximizing the utility of SWP systems.

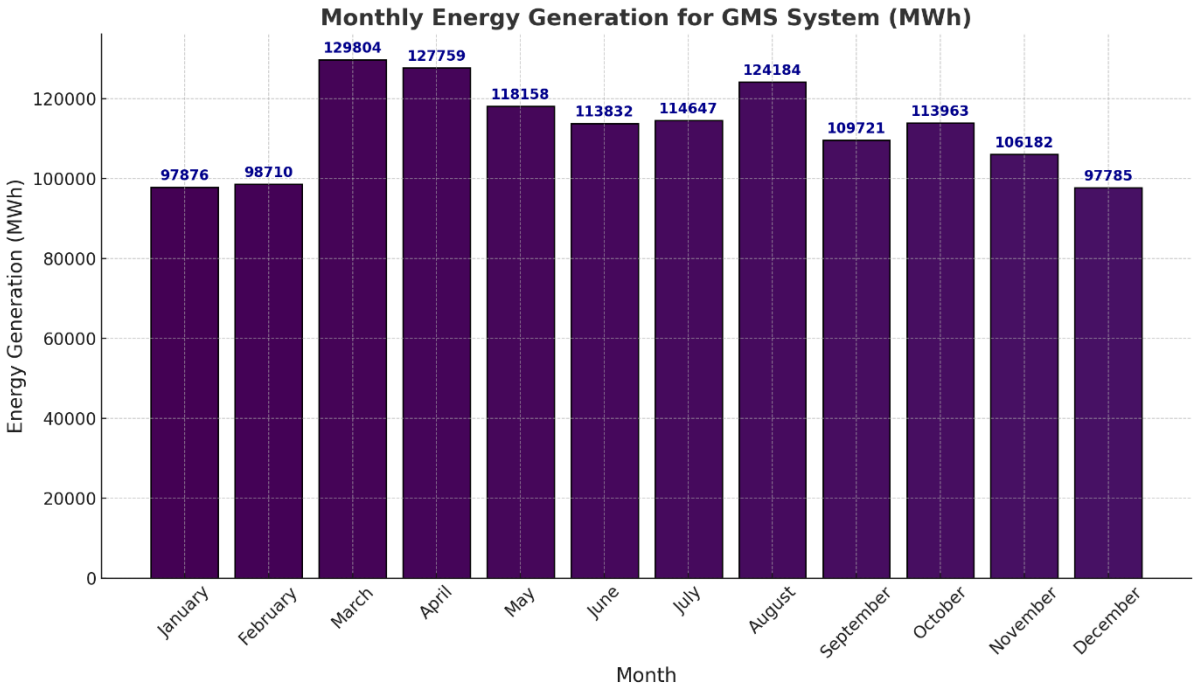

Fig 3.20 (b): Monthly energy generation for GMS system

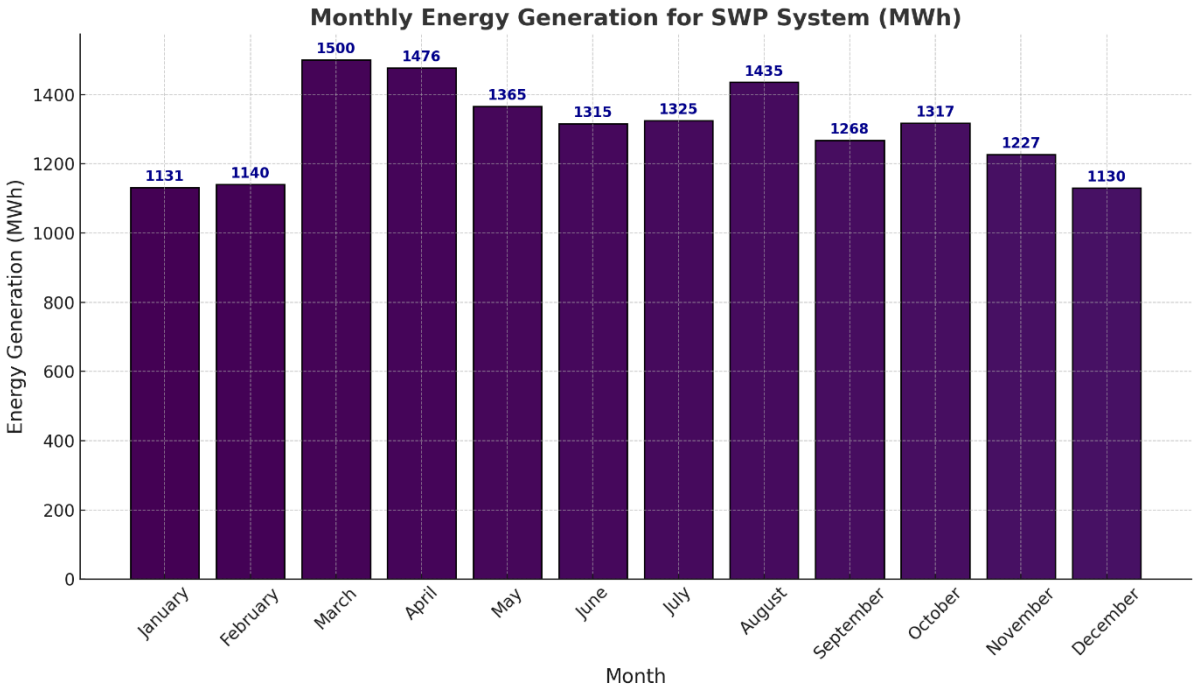

Fig 3.20 (c): Monthly energy generation for SWP system

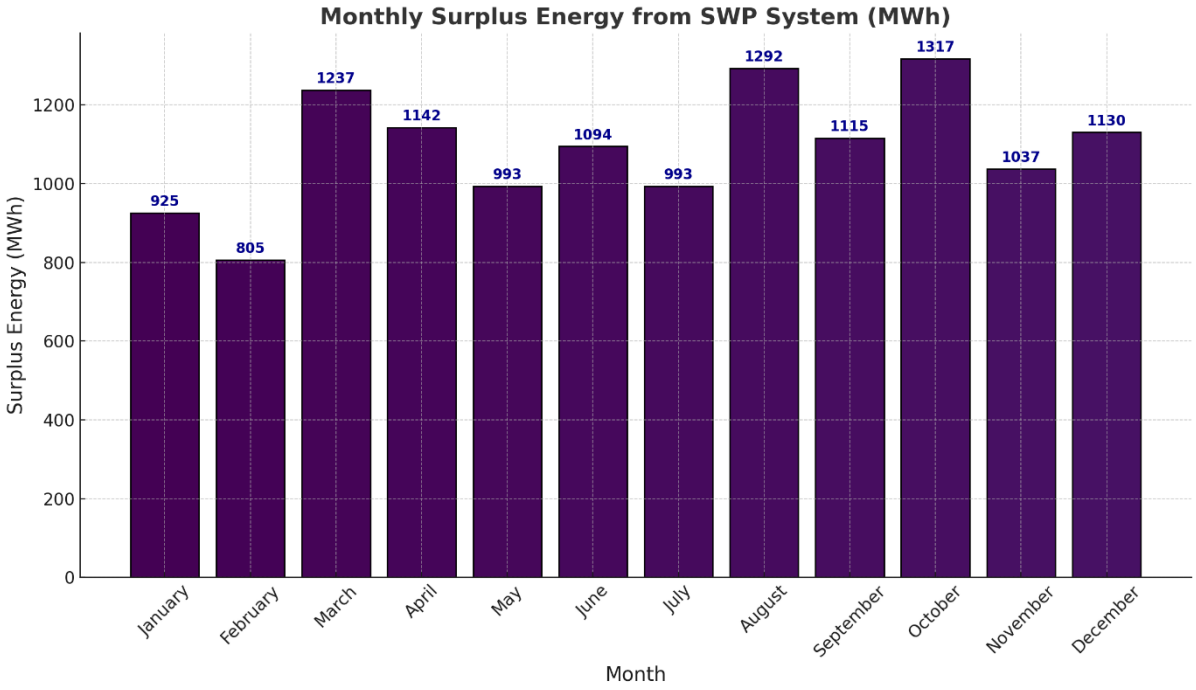

Fig 3.20 (d): Monthly surplus energy from SWP system

3.6.3.1 Implications of diurnal and seasonal variability in solar PV generation

The generation potential of solar PV systems is inherently variable due to natural fluctuations in solar irradiance, which follow clear diurnal (daily) and seasonal patterns. While the preceding subsections present system-wise assessments of temporal variations, it is important to interpret how such variability influences solar PV-based energy availability, consumption planning, and the integration of end-use applications such as EV charging.

Solar PV systems only generate electricity during daylight hours, with zero generation occurring during nighttime. Within each day, irradiance levels and power output rise from sunrise to midday and decline toward sunset. This intra-day variability was analytically captured through hourly irradiance data retrieved from the NASA POWER Data Access Viewer. Monthly and annual generation profiles presented earlier in this chapter were derived by aggregating this hourly data, ensuring a robust temporal representation of potential energy yields.

Seasonal variations are also prominent. During summer months, longer daylight hours and higher irradiance intensities result in increased PV output, whereas winter months experience shorter day lengths and often reduced insolation. These fluctuations have direct implications

for energy reliability, particularly in rural regions where the energy demand pattern may not align with solar availability.

To address this generation-consumption mismatch, two technical strategies are commonly adopted:

- Grid-tied operation: Connecting solar PV systems to the local grid allows for net metering or energy exchange. Surplus energy generated during sunny hours can be fed into the grid, while energy demand during non-generating hours (e.g., night-time or cloudy days) can be met by drawing electricity from the grid. This enables the continuity of power supply despite generation variability.
- Energy storage solutions: Incorporating battery energy storage systems (BESS) allows excess solar electricity generated during the day to be stored and used during the night or periods of low irradiance. This not only enhances energy availability but also supports critical end uses such as EV charging or irrigation scheduling.

Furthermore, these temporal insights play a critical role in the planning of EV charging infrastructure. Aligning EV charging hours with peak solar generation windows, or alternatively buffering with stored energy, can mitigate the risks of supply intermittency. Demand-side management strategies, such as incentivized daytime charging or smart scheduling, can further improve the system's performance.

3.6.3.2 Energy planning and management implications

The temporal analysis of generation capacity for RTS, GMS, and SWP systems provides a foundation for effective energy planning and management:

a) RTS Systems: Enable residential and commercial users to plan energy usage, optimize self-consumption, and reduce reliance on the grid during high-generation months. Surplus energy can be fed into the grid or stored using battery systems.
b) GMS Systems: Support large-scale energy supply for industrial and commercial needs. Temporal insights help in synchronizing generation with demand patterns, ensuring efficient transmission and minimizing grid congestion.

c) SWP Systems: Address energy-water nexus challenges by aligning generation with irrigation needs. Surplus energy during non-operational months offers opportunities for secondary applications, enhancing the economic and operational viability of SWP systems.

This system-wise temporal analysis of generation capacity underscores the importance of integrating renewable energy systems into regional planning frameworks. It also highlights the need for advanced energy management systems and supportive policies to maximize the utility of solar PV systems across diverse applications.

3.6.4 Estimation of per capita energy availability (PCEA)

India's per capita electricity consumption is approximately 1,255 kWh per year (2022), significantly lower than the global average of 3,500 kWh per year. This disparity highlights the challenges of equitable energy access in a rapidly developing economy. In 2022, the per capita power consumption in Assam was 346 kilowatt hours (kWh). This was an increase from the previous year when it was around 313 kWh, which is still very low compared to the national. In the study area encompassing 61 villages, per capita electricity availability varies significantly based on the type of energy system deployed. For example, renewable technologies like rooftop solar (RTS) provide a per capita availability of 2,036 kWh/year, which is above the national average but still falls short compared to developed nations. Grid-based systems (GMS) offer a much higher per capita availability of 11,275 kWh/year, approaching consumption levels of countries like Germany (7,000 kWh/year) and even nearing that of the United States (12,000 kWh/year). Conversely, small-scale solar water pumping systems (SWP) contribute a modest 101 kWh/year per capita, closer to levels observed in less developed regions such as Niger (147 kWh/year) [24-27].

These findings demonstrate the potential of grid and distributed solar systems in bridging the energy access gap in rural India. Leveraging resources such as solar energy can significantly enhance electricity availability while ensuring sustainability. The wide range of per capita electricity availabilities among different systems highlights the need for targeted strategies to optimize energy generation and distribution. By addressing these disparities, it is possible to move closer to achieving equitable energy access and supporting the broader goals of socioeconomic development.

3.6.5 Surplus energy from SWP and planning for EV charging infrastructure

In the study area, SWP systems are primarily operational during irrigation periods, leaving significant surplus energy during non-irrigation times. This surplus energy, amounting to approximately 12.136 GWh/year, presents a valuable opportunity to support emerging energy demands, such as charging electric vehicles (EVs). Utilizing surplus energy for EV charging can optimize the use of renewable energy resources while contributing to the development of sustainable transport infrastructure in rural areas.

To implement this strategy, the spatial distribution of agricultural lands within the study area was analyzed to identify potential sites for SWP installations. Agricultural land clusters were mapped and overlaid with the existing road network to assess accessibility for EV users. For each identified cluster, centroids were determined as central locations for deploying EV charging stations, ensuring optimal accessibility and minimizing infrastructure costs. These centroids serve as potential hubs where surplus energy from nearby SWP systems can be efficiently redirected for EV charging. The layout map illustrating the identified agricultural clusters, road network, and proposed EV charging station centroids is provided in **Fig. 3.21**.

This integrated approach not only enhances the utilization of renewable energy but also aligns with national goals to promote EV adoption and reduce reliance on fossil fuels. By strategically placing EV charging infrastructure near agricultural clusters, the study area can address dual challenges: providing sustainable energy solutions for transportation and optimizing the use of SWP systems. Furthermore, such initiatives can contribute to rural economic development by improving accessibility and connectivity while fostering a transition toward a low-carbon future.

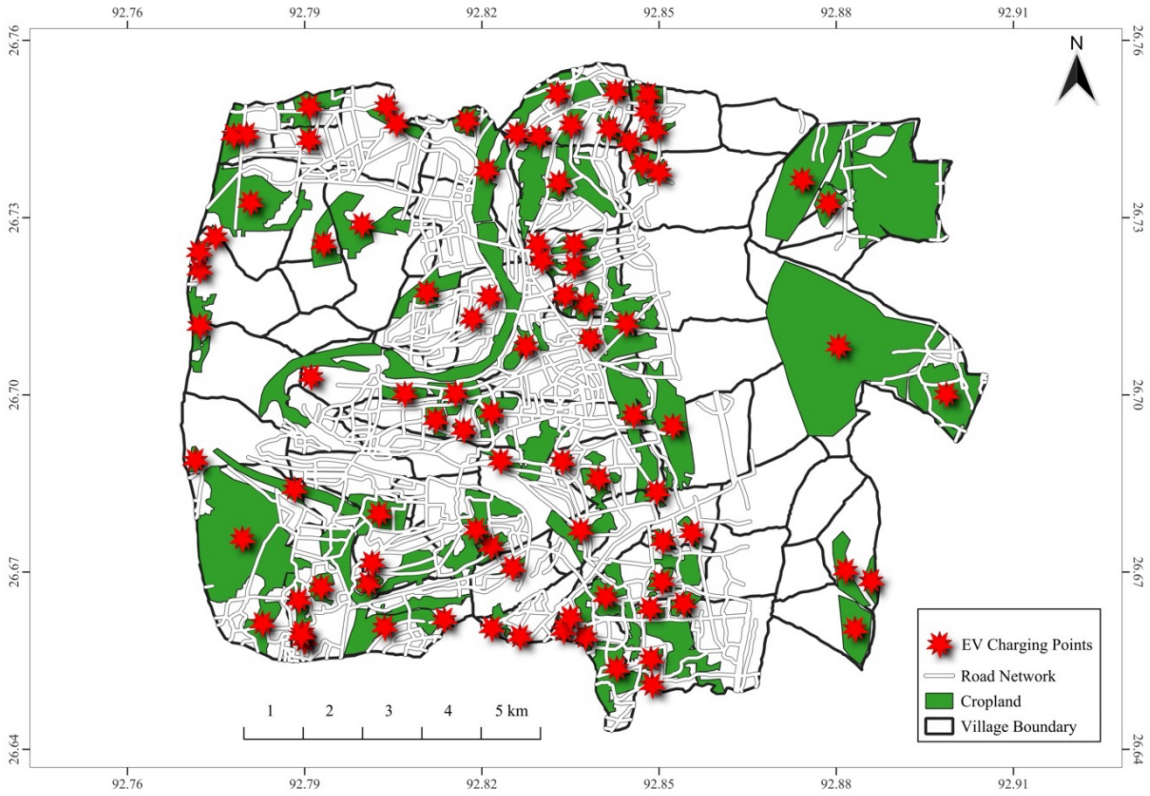

Fig 3.21: Layout map of proposed EV charging infrastructure utilizing surplus energy from SWP systems

3.6.6 Key assumptions and limitations

The assessment of solar PV potential in the study area is based on several assumptions. First, the calculations for installation capacity and energy generation assume uniform efficiency for RTS, GMS, and SWP systems across the study area. Site-specific variations in efficiency, such as those caused by shading, panel orientation, and maintenance practices, are not explicitly considered. Additionally, the availability of rooftop, barren, fallow, and crop areas for solar PV installations is assumed to be unrestricted, with no conflicts arising from competing land uses. The analysis further assumes full utilization of the identified areas, without accounting for technical, social, or legal barriers that may limit their deployment. For SWP systems, the potential capacity is determined based on static water demand for agricultural crops, assuming that current irrigation practices and crop patterns will remain unchanged in the near future.

Despite its comprehensive scope, the study has several limitations. The potential of agrivoltaic systems, which integrate agricultural and energy production, is not assessed in this study, limiting the scope of land-use optimization. Dynamic land-use changes, such as urbanization

or infrastructure development, are not considered, which may affect the availability of land for GMS or crop areas for SWP in the future. Furthermore, the study does not account for potential environmental impacts, such as biodiversity loss, or social factors, such as land ownership conflicts, which could influence the feasibility of solar PV installations.

Economic viability is another unaddressed aspect, as this study does not include detailed cost-benefit analyses or financial feasibility assessments for large-scale solar deployment. However, these aspects are addressed comprehensively in subsequent **Chapter 4** and **Chapter 5**, which focus on techno-economic feasibility assessments and business models for scaling solar photovoltaic systems. Lastly, the analysis relies on aggregated data at the village level for GMS and SWP, which may not capture localized variations or constraints, potentially leading to overestimations or underestimations.

Future studies should address these limitations by incorporating agrivoltaics, modeling land-use dynamics, and conducting detailed economic, environmental, and social analyses. Integrating stakeholder feedback and adopting participatory planning approaches will further enhance the feasibility and acceptance of solar PV projects. These efforts will provide a more holistic assessment, ensuring the sustainability and effectiveness of renewable energy solutions in the study area.

3.6.7 Summary

The total combined installation capacity for solar photovoltaic systems in the study area is 1,374 MW, with an annual generation capacity of 1,612.63 GWh/year. This corresponds to a potential per capita energy availability of 13,412 kWh/year, highlighting the significant renewable energy potential of the region. Individually, the capacities from RTS, GMS, and SWP systems are 208 MW, 1,153 MW, and 13 MW, respectively, with GMS demonstrating the highest contribution to the total capacity in the study area. Among the three systems, GMS exhibits the highest area availability, making it the most significant contributor to the overall capacity. This is attributed to the availability of extensive barren or fallow land, which can support large-scale installations. RTS, on the other hand, is limited by the household rooftop areas, which vary significantly across villages. SWP, although associated with relatively large crop areas, has a limited installation capacity due to its dependency on water demand for agricultural crops.

The concept of Agrivoltaics, which integrates agricultural activities with photovoltaic energy generation, emerges as a promising solution for optimizing land use. While this study does not include agrivoltaics, it represents a potential area for future exploration, particularly in regions where competing demands for land resources exist. Future assessments can help determine its feasibility and scalability in the study area.

Competing use of land area and future perspectives

The availability of land for solar installations is increasingly influenced by competing demands, such as agriculture, infrastructure development, and conservation efforts. Effective planning and management are essential to balance these demands while maximizing renewable energy potential. Strategic prioritization of areas for GMS, RTS, and SWP systems should consider not only technical feasibility but also socio-economic and environmental impacts. For example, integrating agrivoltaics could mitigate land-use competition while enhancing agricultural productivity and energy generation.

The findings from Part A establish a comprehensive understanding of the potential capacity and energy generation from RTS, GMS, and SWP systems. While the focus so far has been on assessing spatial and technical feasibility, it is equally important to evaluate the environmental impacts of these systems. **Part B: Lifecycle GHG Emission Estimation** will address this critical dimension by quantifying the greenhouse gas emissions associated with the lifecycle of solar photovoltaic systems, providing deeper insights into their sustainability and alignment with net-zero energy goals.

References

[1] Solanki, C.S. *Solar photovoltaics: fundamentals, technologies and applications*. Phi learning pvt. Ltd, 2015.

[2] Singh, G.K. Solar power generation by PV (photovoltaic) technology: A review. *Energy*, 53:1-13, 2013.

[3] Saurenergy. Saur Energy International. Retrieved on 16 March, 2022, from https://www.saurenergy.com/solar-energy-blog/here-is-how-you-can-calculate-the-annual-solar-energy-output-of-a-photovoltaic-system#:~:text=Globally%20a%20formula%20E%20%3D%20A,output%20of%20a%20photovoltaic%20system, 2016.

[4] Van Sark, W.G.J.H.M., Reich, N.H., Müller, B., Armbruster, A., Kiefer, K., and Reise, C. Review of PV performance ratio development. In *World renewable energy congress*, page 4795-4800, Denver CO, USA, 2012.

[5] Dierauf, T., Growitz, A., Kurtz, S., Cruz, J.L.B., Riley, E., and Hansen, C. *Weather-corrected performance ratio* (No. NREL/TP-5200-57991). National Renewable Energy Lab.(NREL), Golden, CO (United States), 2013.

[6] Green, M.A. Solar cell fill factors: General graph and empirical expressions. *Solid-State Electronics*, 24(8):788-789, 1981.

[7] Greulich, J., Glatthaar, M. and Rein, S. Fill factor analysis of solar cells' current–voltage curves. *Progress in Photovoltaics: Research and Applications*, 18(7):511-515, 2010.

[8] Census of India, Government of India. Census 2021 reports. Retrieved on 25 February, 2024, from https://censusindia.gov.in, 2023.

[9] National Renewable Energy Laboratory (NREL) (2023). Guidelines for space requirements for solar PV systems. Retrieved on 10 February, 2024, from https://www.nrel.gov.

[10] Solar Energy Industries Association (SEIA) (2023). Space requirements for solar photovoltaic installations. Retrieved on 12 February, 2024, from https://www.seia.org.

[11] Solar Engineering and Installation Guidelines (2023). Standards for solar PV system design and space requirements. Retrieved on 15 February, 2024, from https://www.solarinstallationguidelines.org.

[12] Zhong, Q., and Tong, D. Spatial layout optimization for solar photovoltaic (PV) panel installation. *Renewable energy*, 150:1-11, 2020.

[13] Romero-Fiances, I., Muñoz-Cerón, E., Espinoza-Paredes, R., Nofuentes, G., and De la Casa, J. Analysis of the performance of various pv module technologies in Peru. *Energies*, 12(1):186, 2019.

[14] Notton, G., Lazarov, V. and Stoyanov, L. Optimal sizing of a grid-connected PV system for various PV module technologies and inclinations, inverter efficiency characteristics and locations. *Renewable Energy*, 35(2):541-554, 2010.

[15] Rahman, M.M., Hasanuzzaman, M., and Rahim, N.A. Effects of various parameters on PV-module power and efficiency. *Energy Conversion and Management*, 103:348-358, 2015.

[16] Scott, L.M., and Janikas, M.V. Spatial statistics in ArcGIS. In *Handbook of applied spatial analysis: Software tools, methods and applications*, 27-41, Berlin, Heidelberg: Springer Berlin Heidelberg, 2009.

[17] Zuhlke, M., Fomferra, N., Brockmann, C., Peters, M., Veci, L., Malik, J., and Regner, P. SNAP (sentinel application platform) and the ESA sentinel 3 toolbox. In *Sentinel-3 for Science Workshop*, 734:21, 2015.

[18] Kurt Menke, G.I.S.P., Smith Jr, R., Pirelli, L., and John Van Hoesen, G.I.S.P. *Mastering QGIS*. Packt Publishing Ltd, 2016.

[19] Cavur, M., Duzgun, H.S., Kemec, S., and Demirkan, D.C. Land use and land cover classification of Sentinel 2-A: St Petersburg case study. *The International Archives of the Photogrammetry, Remote Sensing and Spatial Information Sciences*, 42:13-16, 2019.

[20] Pal, M. Random forest classifier for remote sensing classification. *International journal of remote sensing*, 26(1):217-222, 2005.

[21] Shivakumar, B.R., and Rajashekararadhya, S.V. Investigation on land cover mapping capability of maximum likelihood classifier: a case study on North Canara, India. *Procedia computer science*, 143:579-586, 2018.

[22] Etikan, I., & Bala, K. Sampling and sampling methods. *Biometrics & Biostatistics International Journal*, 5(6):00149, 2017.

[23] Tuzson, J. *Centrifugal pump design*. John Wiley & Son, 2000.

[24] Hunt, J. *Advanced guide to Python 3 programming*, 35-42. Berlin: Springer, 2019.

[25] Anderson, K.S., Hansen, C.W., Holmgren, W.F., Jensen, A.R., Mikofski, M.A., and Driesse, A. pvlib python: 2023 project update. *Journal of Open Source Software*, 8(92):5994, 2023.

[26] Gurupira, T., and Rix, A.J. October. Photovoltaic System Modelling using PVLib-Python. In Southern African Solar Energy Conference (SASEC), pages 1-6, Stellenbosch, South Africa, 2016.

[27] Holmgren, W.F., Hansen, C.W. and Mikofski, M.A. pvlib python: A python package for modeling solar energy systems. *Journal of Open Source Software*, 3(29):884, 2018.

[28] Jackson, R.B., Ahlström, A., Hugelius, G., Wang, C., Porporato, A., Ramaswami, A., Roy, J., and Yin, J. Human well-being and per capita energy use. *Ecosphere*, 13(4):3978, 2022.

[29] Simionescu, M., Bilan, Y., Krajňáková, E., Streimikiene, D. and Gędek, S. Renewable energy in the electricity sector and GDP per capita in the European Union. *Energies*, 12(13):2520, 2019.

[30] Wiginton, L.K., Nguyen, H.T. and Pearce, J.M. Quantifying rooftop solar photovoltaic potential for regional renewable energy policy. *Computers, Environment and Urban Systems*, 34(4):345-357, 2010.

[31] Sahu, B. K. A study on global solar PV energy developments and policies with special focus on the top ten solar PV power producing countries. *Renewable and Sustainable Energy Reviews*, 43:621-634, 2015.

[32] Meah, K., Ula, S. and Barrett, S. Solar photovoltaic water pumping—opportunities and challenges. *Renewable and Sustainable Energy Reviews*, 12(4):1162-1175, 2008.

[33] Survey of India, Government of India (2023). Topographic maps and village information. Retrieved on 25 February, 2024, from https://surveyofindia.gov.in.

[34] National Remote Sensing Centre (NRSC), Indian Space Research Organisation (ISRO) (2023). Satellite imagery and spatial data. Retrieved on 25 February, 2024, from https://nrsc.gov.in.

[35] DIVA GIS (2023). Free GIS data for mapping and analysis. Retrieved on 25 February, 2024, from https://diva-gis.org.

[36] North Eastern Spatial Data Repository (NeSDR) (2023). Spatial data for the northeastern region of India. Retrieved on 25 February, 2024, from https://nesdr.gov.in.

[37] NASA Prediction of Worldwide Energy Resources (2023). Solar and weather data resources. Retrieved on 25 February, 2024, from https://power.larc.nasa.gov.

[38] National Renewable Energy Laboratory (NREL) (2023). Solar radiation and weather data. Retrieved on 25 February, 2024, from https://nrel.gov.

[39] Global Solar Atlas, World Bank Group and ESMAP. Solar resource maps and data for photovoltaic systems. Data provided by Solargis. Retrieved on 18 February, 2024, from https://globalsolaratlas.info, 2023.

[40] Centre for Wind Energy Technology (C-WET) (2018). Renewable energy resources and wind data. Retrieved on 25 February, 2018, from https://cwet.res.in.

[41] ISRO (2023). Visualization of Earth Observation Data and Archival System (VEDAS). Retrieved on 25 February, 2024, from https://vedas.sac.gov.in.

[42] State Agriculture Department, Assam (2023). Package of practices for agricultural crops. Retrieved on 25 February, 2024, from https://diragri.assam.gov.in/portlet-innerpage/package-of-practices.

[43] IPCC (2023). Guidelines for national greenhouse gas inventories. Retrieved on 25 February, 2024, from https://ipcc.ch.

[44] Central Electricity Authority (CEA), Government of India (2023). CO_2 baseline database. Retrieved on 25 February, 2024, from https://cea.nic.in.

[45] European Space Agency (ESA) (2019). Sentinel-2A: High-resolution satellite imagery for Earth observation. Retrieved on 22 December, 2020, from https://sentinel.esa.int/web/sentinel/home.

[46] Google Earth. High-resolution satellite imagery and mapping platform. Retrieved on 21 March, 2024, from https://earth.google.com, 2024.

[47] Rwanga, S.S., and Ndambuki, J.M. Accuracy assessment of land use/land cover classification using remote sensing and GIS. *International Journal of Geosciences*, 8(04):611, 2017.

[48] Foody, G.M. Explaining the unsuitability of the kappa coefficient in the assessment and comparison of the accuracy of thematic maps obtained by image classification. *Remote sensing of environment*, 239:111630, 2020.

[49] García, M.A., and Balenzategui, J.L. Estimation of photovoltaic module yearly temperature and performance based on nominal operation cell temperature calculations. *Renewable energy*, 29(12):1997-2010, 2004.

[50] Koehl, M., Heck, M., Wiesmeier, S., and Wirth, J. Modeling of the nominal operating cell temperature based on outdoor weathering. *Solar Energy Materials and Solar Cells*, 95(7):1638-1646, 2011.

[51] Barykina, E., and Hammer, A. Modeling of photovoltaic module temperature using Faiman model: Sensitivity analysis for different climates. *Solar Energy*, 146:401-416, 2017.

PART B: LIFECYCLE GHG EMISSION ESTIMATION

3.7 Introduction

Lifecycle GHG (Greenhouse Gas) emission estimation is a critical component in assessing the environmental sustainability of solar PV systems [1]. The estimation follows a chronological approach to comprehensively evaluate the emissions associated with PV systems from cradle to grave. The estimation involves quantifying emissions for each lifecycle phase, including manufacturing, transportation, installation, operation and maintenance, and end-of-life. These phases were chosen as they represent the most significant contributors to the overall carbon footprint of solar PV systems to identify areas for reducing environmental impact [2-6]. Following this, the GHG emission reduction achieved by replacing conventional grid-based electricity with solar PV systems is quantified. This comparison highlights the potential of PV systems to mitigate emissions compared to fossil-fuel-based energy sources [7, 8]. The study then proceeds to estimate the net GHG emissions by juxtaposing the emissions generated throughout the lifecycle of the PV systems with the emissions avoided due to their deployment. To systematically evaluate the environmental impact of PV systems, the study presents the parameters, equations, and assumptions necessary for calculating emission reductions over their lifespan. The scope covers all relevant phases for RTS, GMS, and SWP systems, ensuring a comprehensive framework for assessing the net environmental benefits of solar energy adoption.

3.8 Framework for lifecycle GHG emission estimation

The lifecycle GHG emission estimation follows a systematic framework based on the principles of Lifecycle Assessment (LCA), as standardized by the ISO 14040 and ISO 14044 guidelines [9]. The flowchart for the lifecycle GHG emission estimation framework is shown in **Fig 3.22**. This diagram visually represents the structured approach, depicting the interactions between various LCA phases and critical elements such as system boundaries, impact categories, and data inventory processes [10].

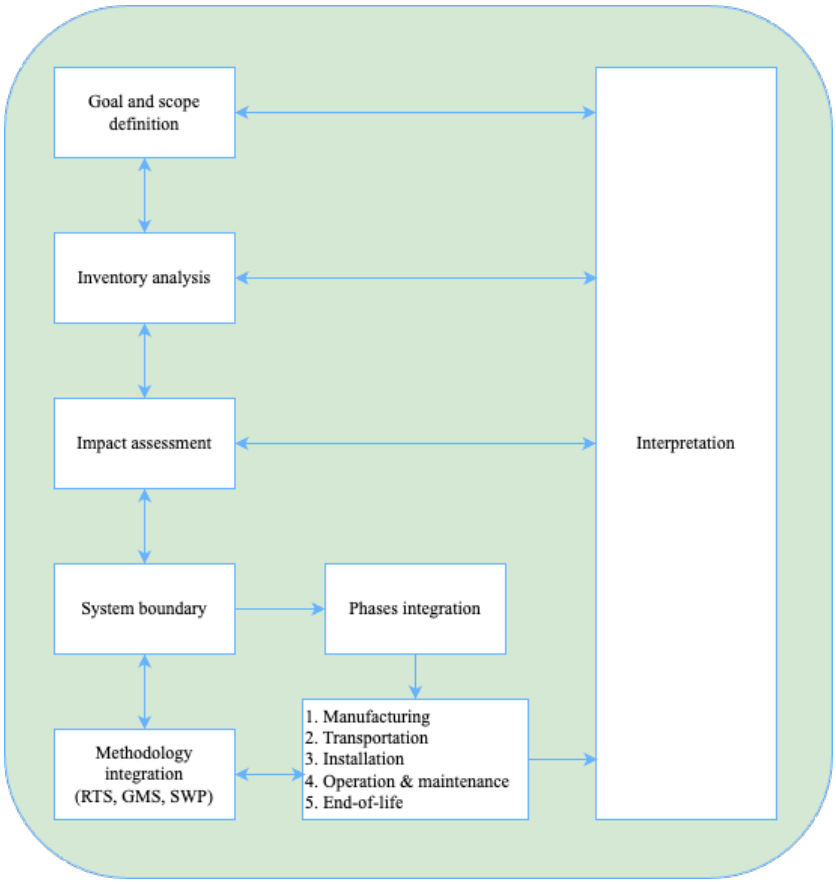

Fig 3.22: Framework for lifecycle GHG emission estimation

3.8.1 Goal and scope definition

The goal of this lifecycle GHG estimation is to assess the total emissions associated with the deployment of PV systems in rural Assam. The analysis follows a Gate-to-Gate approach [11], covering emissions within the phases. A functional unit is defined as the energy output of the system per kilowatt-hour (kWh) over its operational lifetime, serving as a reference point for comparison across different systems or scenarios [12]. This facilitates a standardized evaluation of emissions and performance across various configurations, ensuring alignment with industry benchmarks and sustainability goals. The impact category considered in the analysis is global warming potential (GWP), expressed in CO_2-equivalents (CO_2e), providing a comprehensive assessment across selected lifecycle stages.

3.8.2 System boundary selection

The system boundary defines which lifecycle stages and processes are considered in the estimation, with a focus on a Gate-to-Gate approach that encompasses manufacturing,

transportation, installation, operation, maintenance, and end-of-life disposal. This approach ensures a detailed assessment of emissions related to these stages while excluding upstream activities such as raw material extraction. The system boundary includes the stages for each of the systems, RTS, GMS, and SWP to provide a more precise evaluation of emissions associated with system deployment, thereby facilitating meaningful comparisons and aiding in the identification of process optimization opportunities.

3.9 Methodology for lifecycle GHG emission estimation

The lifecycle GHG emissions are estimated using Process-Based LCA, complemented by Input-Output (IO) Analysis where necessary, following an inventory-based approach in line with the GHG Protocol and IPCC guidelines. Two methods are considered for GHG emission estimation: Process-Based LCA, which provides a detailed process-level assessment using primary and secondary data, allowing specificity in emission sources and hotspots, making it suitable for small-to-medium scale assessments with reliable data sources; and Economic Input-Output LCA (EIO-LCA), which is based on national and sectoral economic data and is useful for broad estimations where detailed process data are unavailable. Process-based LCA is selected due to its higher accuracy and relevance in product-specific emissions, while IO-LCA serves as a complementary tool for assessing broader system-wide impacts.

3.9.1 Emission calculations for each phase

3.9.1.1 Manufacturing phase

The GHG emissions during the manufacturing phase of the PV system for each system k (RTS, GMS, SWP) are calculated using Equation (3.28), which accounts for emissions generated from the production of PV modules, batteries, and inverters. The total emissions, denoted as $GHG_{manufacture_k}$, are derived by summing the contributions of these three major components.

$$GHG_{manufacture_k} = P_{PV_k} \times EF_{PV} + B_{capacity_k} \times EF_{battery} + I_{capacity_k} \times EF_{inverter} \quad (3.28)$$

where, P_{PV_k} represents the total PV system capacity for each system k measured in kW, while EF_{PV} denotes the emission factor associated with PV production, expressed in kg CO_2/kW. Similarly, $B_{capacity_k}$ refers to the battery capacity for system k, where applicable, measured in kWh, and $EF_{battery}$ corresponds to the emission factor for battery production, quantified in kg

CO_2/kWh. Furthermore, $I_{capacity_k}$ indicates the inverter capacity for system k, measured in kW, while $EF_{inverter}$ represents the emission factor associated with inverter production, expressed in kg CO_2/kW.

3.9.1.2 Transportation phase

The GHG emissions associated with the transportation phase account for the emissions generated during the delivery of all system components from manufacturing facilities to the installation site. These emissions depend on the total weight of the transported components, the distance travelled, and the emission factor per unit distance and weight. The emissions for the transportation phase are calculated using the following equation:

$$GHG_{transport_k} = D_{transport} \times EF_{transport} \times W_{weight} \quad (3.29)$$

where, W_{weight} represents the total weight of all PV system components transported, including PV modules, inverters, and batteries, measured in kg; $D_{transport}$ denotes the total distance travelled for transportation from the manufacturing facility to the installation site, expressed in km; and $EF_{transport}$ refers to the emission factor associated with transportation, which quantifies the emissions produced per unit distance travelled per unit weight transported, measured in kg CO_2/km.

3.9.1.3. Installation phase

The GHG emissions associated with the installation phase of a PV system arise predominantly from the energy and material resources expended during the labour-intensive process of mounting, wiring, and commissioning the system components. These emissions are not attributed to the PV modules themselves, but rather to the human and mechanical efforts involved in physically assembling the infrastructure at the site.

In lifecycle assessment, this phase includes emissions from auxiliary activities such as the operation of lifting equipment, use of installation tools, temporary site infrastructure, and transportation of personnel. The GHG emissions associated can be estimated based on the installed system capacity and a corresponding emission factor per kilowatt of installed capacity. This approach is commonly used in literature and LCA databases where installation-related emissions are normalized by system size, incorporating typical energy consumption and labour

requirements per kW of installed PV. The emissions for the installation phase are calculated using the following equation:

$$GHG_{install_k} = P_{PV_k} \times EF_{install} \quad (3.30)$$

Where, $GHG_{install_k}$ represents the total GHG emissions during the installation phase (kg CO_2-eq); P_{PV_k} represents the total PV system capacity for each system k measured in kW and $EF_{install}$ is the emission factor for installation per unit capacity (kg CO_2/kW).

3.9.1.4 Operation and maintenance phase

The GHG emissions during the operation and maintenance (O&M) phase of the PV system primarily arise from routine maintenance activities conducted throughout the system's lifespan. These emissions are influenced by the frequency and intensity of maintenance operations and the system's operational lifetime. The total emissions for the O&M phase are calculated using the following equation:

$$GHG_{O\&M_k} = P_{PV_k} \times T_{life} \times EF_{maintenance} \quad (3.31)$$

where, P_{PV_k} represents the total PV system capacity for each system k measured in kW, T_{life} represents the total lifespan of the PV system, typically measured in years, and $EF_{maintenance}$ denotes the annual emissions resulting from maintenance activities, expressed in kg CO_2/kW/year. This equation provides an estimation of the cumulative emissions over the entire operational period of the system by taking into account the annual maintenance requirements and the expected duration of operation.

3.9.1.5 End-of-life phase

The GHG emissions associated with the end-of-life (EOL) phase of the PV system arise from the processes involved in the recycling and disposal of system components once they reach the end of their operational lifespan. These emissions are dependent on the quantities of materials being recycled and disposed of, along with their respective emission factors. The GHG emissions associated with the end-of-life phase of the PV system are calculated by considering both recycling and disposal pathways for major components, including PV modules and inverters. The total emissions are estimated using the following equation:

$$GHG_{end_k} = (W_{recycled} \times EF_{recycle}) + (W_{disposed} \times EF_{disposed}) \quad (3.32)$$

where, $W_{recycled}$ represents the total weight of PV system components that are recycled, measured in kg, and $W_{disposed}$ denotes the weight of components that are disposed of without recycling, also measured in kg. These quantities are calculated separately for PV modules and inverters and then summed. The parameter $EF_{recycle}$ refers to the emission factor associated with the recycling process, expressed in kg CO_2/kW, while $EF_{disposal}$ represents the emission factor for disposal processes, also measured in kg CO_2/kW.

Determining the weight of recycled and disposed components

To estimate the GHG emissions associated with the EOL phase of a PV system, it is essential to determine the weight of recycled and disposed components. This process involves several key steps, including estimating the total system weight, identifying recycling and disposal rates, and calculating the weight of materials subject to each process.

a) Estimation of total system weight

The total weight of the PV system encompasses various components such as PV modules, inverters, and batteries (if applicable). The weight of PV modules depends on the type and size of the system, with silicon-based panels typically weighing around 10-12 kg per square meter. Given that a 1 kW system requires an area of approximately 6-8 m², the total panel weight is estimated to be around 60-100 kg per kW, with an average of 80 kg per kW [13-15]. Inverters, which convert DC power to AC power, usually weigh between 10-50 kg depending on their capacity; for a 1 kW system, an average inverter weight of 10-15 kg can be assumed [16, 17]. Batteries, if incorporated into the system (viz., in solar water pumping or electric vehicle charging applications), weight approximately 7-10 kg per kWh, with a typical assumption of 7 kg per kWh for calculations [18, 19].

b) Determination of recycling and disposal rates

Recycling and disposal rates depend on the materials used in the components and the efficiency of recycling technologies available. PV modules, which primarily consist of recyclable materials such as glass, aluminium, and certain metals (viz., silicon and silver), have an estimated recycling rate of 85-90% for silicon-based modules [14]. Inverters, composed mainly

of metals and plastics, have an estimated recycling potential of 70-80% [20]. Lithium-ion batteries, commonly used in PV systems, have a recycling rate of around 50-60%, with the potential for improvement as recycling technologies advance [21, 22]. The disposal rate for each component is calculated as the complement of the recycling rate, representing the fraction of material that cannot be recycled and is instead directed to landfills or other waste management facilities.

$$Disposal\ rate = 1 - Recycling\ rate \tag{3.33}$$

c) Calculation of recycled and disposed component weights

Using the total system weight and the respective recycling and disposal rates, the weight of recycled and disposed materials for each component can be determined. For PV modules with a total weight of 80 kg, an 85% recycling rate results in 68 kg being recycled and 12 kg being disposed of. Inverters with a total weight of 12 kg and a 75% recycling rate result in 9 kg recycled and 3 kg disposed of. For batteries weighing 7 kg per kWh with a 55% recycling rate, approximately 3.85 kg will be recycled, while 3.15 kg will be disposed of.

d) General formula for component weight estimation

The weight of recycled and disposed materials for each system component can be estimated using the following general formulas:

$$W_{recycled} = W_{total} \times Recycling\ Rate \tag{3.34}$$

$$W_{disposed} = W_{total} \times (1 - Recycling\ Rate) \tag{3.35}$$

where W_{total} represents the total weight of the component (viz., PV modules, inverters, or batteries), and the recycling and disposal rates are specific to each component type. These formulas provide a standardised approach to quantifying the environmental impact of PV system decommissioning by assessing material recovery and waste generation.

3.9.2 Total lifecycle GHG emissions for each system

The total lifecycle GHG emissions for each system (RTS, GMS, and, SWP), denoted as GHG_{total_k}, represents the cumulative emissions resulting from various stages of the system's lifecycle. The total lifecycle GHG emissions for each system k can is represented as follows:

$$GHG_{total_k} = E_k \cdot X_k \tag{3.36}$$

where, $E_k = [GHG_{manufacture_k}, GHG_{transport_k}, GHG_{install_k}, GHG_{O\&M_k}, GHG_{end_k}]$ (a vector containing emissions from all lifecycle stages for strategy k), $X_k = [x_{manufacture_k}, x_{transport_k}, x_{install_k}, x_{O\&M_k}, x_{end_k}]$ (a vector of activity data or scaling factors for each lifecycle stage).

Thus, the total GHG emissions across all strategies can be expressed as:

$$GHG_{total} = \sum_{k \in \{RTS,GMS,SW\}} E_k \cdot X_k \tag{3.37}$$

3.10 GHG emission reductions estimation

GHG emission reductions are estimated by comparing the energy generated by solar PV systems with the baseline energy derived from conventional sources such as diesel-powered or grid-connected systems. This comparison allows for the quantification of the emissions avoided by transitioning to solar energy, thus highlighting the environmental benefits of adopting PV technology. The key parameters considered in this estimation include energy generation, system lifespan, and emission factors associated with conventional energy sources.

3.10.1 GHG emission reductions for each system

The emission reductions for solar PV systems are calculated separately for different system types, including RTS, GMS, SWP, and EV charging applications. Each system's reduction potential is evaluated based on its energy generation capacity and the emission factors of the displaced conventional energy sources. This assessment helps in determining the contribution of solar PV systems to overall carbon footprint reduction in the study region.

3.10.1.1 GHG emission reductions for RTS and GMS

For RTS and GMS, which are primarily grid-connected systems, the avoided emissions are calculated using the energy generated by the solar PV system over its operational lifetime. The emissions avoided by substituting grid electricity with solar power are determined using the following equations:

$$GHG_{reduction_{RTS}} = E_{solar_k} \times EF_{grid} \times T_{life} \quad (3.38)$$

$$GHG_{reduction_{GMS}} = E_{solar_k} \times EF_{grid} \times T_{life} \quad (3.39)$$

where, EF_{grid} represents the emission factor for grid electricity, which varies by country or region. For India, it is approximately 0.716 kg CO_2/kWh. E_{solar_k} denotes the daily energy generated by the solar PV system k, measured in kWh/day [23]. The parameter k represents the RTS and GMS systems under consideration.

3.10.1.2 GHG emission reductions for SWP

Solar Water Pumping (SWP) systems can replace conventional diesel or grid electricity-powered pumps, leading to significant GHG emission reductions. In the case of diesel replacement, the emission reductions are calculated based on the energy generated by the solar system, considering the emission factor of diesel-powered pumps. Similarly, for grid electricity substitution, the emissions avoided are determined by comparing the solar energy output to the emissions generated by grid electricity consumption. The equations used to estimate these reductions are as follows:

$$GHG_{reduction_{SWP,diesel}} = E_{solar_{SWP}} \times EF_{diesel} \times 365 \times T_{life} \quad (3.40)$$

$$GHG_{reduction_{SWP,grid}} = E_{solar_{SWP}} \times EF_{grid} \times 365 \times T_{life} \quad (3.41)$$

where, EF_{diesel} represents the emission factor for diesel, typically 2.68 kg CO_2/liter, which is widely accepted in India and globally for calculating emissions from diesel-powered pumps, particularly in rural agricultural settings [24].

3.10.2 Total GHG emission reductions

The total GHG emission reductions are derived by summing the emission reductions achieved by all solar PV systems considered in the study, including RTS, GMS, SWP, and EV charging. This provides a comprehensive estimate of the overall environmental benefits of solar energy deployment. The total emission reductions are computed using the following equation:

$$GHG_{reduction_{total}} = \sum_{k=1}^{n} GHG_k \quad (3.43)$$

where, k represents the specific GHG reduction source (RTS, GMS, SWP, EV), n is the total number of GHG reduction strategies (n = 4), GHG_k refers to each individual reduction contribution.

3.10.3 Net GHG emission reductions

The net GHG emission reductions for each system are determined by subtracting the total lifecycle emissions from the calculated GHG reductions, providing a realistic estimate of the environmental impact. This calculation takes into account emissions generated during the system's entire lifecycle, from manufacturing to disposal. The net emission reductions for an individual system and all systems combined are calculated using the following equations:

$$GHG_{net_k} = GHG_{reduction_k} - GHG_{total_k} \quad (3.43)$$

For all systems combined, the total net GHG emission reduction over the system's lifetime is:

$$GHG_{net_{total}} = GHG_{reduction_{total}} - GHG_{total} \quad (3.44)$$

3.11 Data sources, assumptions, and limitations

3.11.1 Data sources

The lifecycle GHG emission estimation for solar PV systems in rural Assam relies on both primary and secondary data sources. Primary data include the technical specifications of PV systems installed in the study area, providing insights into system configurations, energy outputs, and operational parameters. Secondary data are derived from peer-reviewed literature, databases such as Ecoinvent and GREET, and government reports. For example, the Central Electricity Authority (CEA) provides an emission factor for the Indian grid for FY 2022-23 at 0.716 tCO_2/MWh, which is utilized in the analysis. These data sources enable comprehensive modelling of emissions while ensuring the incorporation of region-specific factors.

Table 3.7: LCA phases and assumptions parameters for RTS, GMS, and SWP systems

Phase	Parameter	Value	Unit	Remarks
Manufacturing phase	PV emission factor	750	kg CO_2/kW	Mid-range value for polycrystalline modules in Indian conditions [25, 26].
	Inverter emission factor	75	kg CO_2/kW	Reflects mid-range emissions for inverter production [17, 20].
	Battery emission factor (if applicable)	175	kg CO_2/kWh	Accounts for lithium-ion battery emissions in SWP systems [27, 28].
	Pump emission factor	50	kg CO_2/kW	Manufacturing emissions for water pumps in SWP systems [29].
Transportation phase	Transport emission factor	0.2	kg CO_2/ton-km	Reflects suboptimal transport efficiency in rural Assam [30, 31].
	Transportation distance	500	km	Conservative estimate for transporting components to rural Assam.
	PV module weight	80	kg/kW	Standard weight for silicon-based PV panels [13-15].
	Inverter weight	12	kg/kW	Typical weight for inverters per kW of capacity [16, 17].
	Battery weight (if applicable)	7	kg/kWh	Standard weight for lithium-ion batteries in SPVWP systems [18, 19].
	Pump weight	20	kg/kW	Average weight for water pumps used in SWP systems [32].
Installation phase	Installation energy emission factor	0.05	kg CO_2/kW	Scales installation emissions proportionally to system capacity [33].
Operation & maintenance	Annual maintenance emission factor	0.5 for RTS and GMS, 1 for SWP	kg CO_2/kW/year	SWP has higher maintenance emissions due to water pump operations [34, 35].
	System lifespan	25	years	Typical lifespan for solar PV systems and components [36].
End-of-Life phase	PV module recycling rate	85	%	Assumes partial recycling of silicon PV panels [14].
	Inverter recycling Rate	75	%	Assumes moderate recycling potential for inverters [20].
	Battery recycling Rate (if applicable)	55	%	Reflects limited recycling technology for lithium-ion batteries [21, 22].
	Pump recycling rate	65	%	Pumps are moderately recyclable due to metal components [37].
	Recycling emission Factor	30	kg CO_2/kW	Emissions for recycling PV modules and components [38].
	Disposal emission factor	55	kg CO_2/kW	Higher emissions for disposal of non-recyclable materials [39].

Parameters for PV systems considered

The emission factor for solar PV modules is set at 750 kg CO_2/kW, a mid-range value reflecting manufacturing efficiency under Indian conditions. This value accounts for variations in production processes and energy sources used. For inverters, an emission factor of 75 kg CO_2/kW is chosen, based on the balance between advanced and conventional technologies used in rural areas. For batteries, a selected value of 175 kg CO_2/kWh is used, considering the widespread adoption of lithium-ion technology in rural applications and the associated environmental costs.

Transportation

A transportation emission factor of 0.2 kg CO_2/ton-km is selected, recognizing the suboptimal logistics conditions in rural Assam. Given the region's challenging terrain, transportation often relies on less efficient methods, leading to higher emissions. The estimate falls within the global range of 0.1 to 0.25 kg CO_2/ton-km, with the chosen value reflecting regional conditions.

Installation

The emission factor for energy use during installation is set at 0.716 kg CO_2/kWh, based on the Indian grid's average emission factor provided by the Central Electricity Authority (CEA). Since installation activities such as crane use and electrical work are dependent on grid electricity, this value provides a realistic measure of emissions.

Operation & maintenance

For grid electricity substitution, the emission factor used is 0.716 kg CO_2/kWh, reflecting the national average provided by the CEA. This factor is applicable to rural Assam, where grid energy predominantly comes from thermal power sources. The annual energy output of the solar PV systems is assessed based on region-specific solar irradiance data, providing conservative yet realistic energy generation estimates.

End-of-life phase

The emission factor for recycling and disposal of solar panels is set at 30 kg CO_2/kW, reflecting the limited but developing recycling infrastructure in India. The disposal factor is set at 55 kg CO_2/kW, recognizing the higher emissions from non-recycled components due to inadequate

waste management facilities in rural areas. These values represent mid-range estimates, accounting for both current constraints and potential improvements in recycling capabilities.

3.11.2 Assumptions

The analysis of lifecycle GHG emissions for solar PV systems in rural Assam is based on several key assumptions to ensure consistency and comparability across different installations. It is assumed that the efficiency of PV modules remains uniform across all installations, reflecting standardized manufacturing processes and quality control measures. A standardized operational lifespan of 25 years is considered for all PV systems, aligning with industry norms and typical performance warranties offered by manufacturers. Additionally, emission factors used in the estimation process are assumed to remain constant over time, providing a stable basis for long-term assessments and facilitating straightforward comparisons between different scenarios. These assumptions help create a reliable framework for evaluating the environmental impact of PV systems while acknowledging the inherent complexities of solar energy deployment in diverse rural environments.

Table 3.8: The assumptions made in the study are summarised in the following table

Assumption	Value/Justification
Module efficiency	Uniform across installations
Operational lifespan	25 years (industry standard)
Emission factors stability	Assumed constant over time for consistency

3.11.3 Limitations

Despite the comprehensive approach adopted for estimating lifecycle GHG emissions, several limitations must be acknowledged. One major limitation is the limited availability of region-specific data, particularly related to raw material extraction. The lack of localized data necessitates reliance on global averages or estimates, which may not fully capture the nuances of material sourcing and energy use specific to the study area. Another challenge is the potential variability in recycling and end-of-life management practices. The actual recycling rates and disposal methods may differ from the assumed values due to evolving policies, technological advancements, and regional infrastructure constraints. Furthermore, the study excludes the impact of land-use changes associated with PV installations due to data constraints. Land-use

changes can have significant environmental implications, but their exclusion limits the scope of the current assessment. These limitations highlight the need for continued research and data collection efforts to enhance the accuracy and relevance of GHG emission estimations for solar PV systems in rural Assam.

Table 3.9: The key limitations considered in the study are summarised below

Limitation	Impact
Lack of region-specific data	May lead to reliance on generalized values
Variability in recycling practices	Differences in actual versus assumed recycling rates
Exclusion of land-use change impacts	Potential underestimation of environmental effects

3.12 Results and Discussions

3.12.1 Lifecycle GHG emissions by stage

Table 3.10: Lifecycle GHG emissions by phases for RTS, GMS and, SWP systems

System	Manufacturing (t CO_2)	Transportation (t CO_2)	Installation (t CO_2)	O&M (t CO_2)	End-of-Life (t CO_2)	Total GHG Emissions (t CO_2)
RTS	1,71,817	1,916	10	2,603	6,52,903	8,29,249
GMS	9,51,467	10,610	58	14,416	36,15,573	45,92,123
SWP	1,666	149	1	333	41,790	43,940

Table 3.11: Net GHG reductions for RTS, GMS, and SWP systems

System	Total GHG Reductions (t CO_2)	Total GHG Emissions (t CO_2)	Net GHG Reductions (t CO_2)
RTS	43,72,209	8,29,249	35,42,960
GMS	2,42,11,936	45,92,123	1,96,19,812
SWP (Grid)	2,82,181	43,940	2,38,241
SWP (Diesel)	3,23,168	43,940	2,79,228

3.12.2 Interpretation

The interpretation of lifecycle GHG emissions and net GHG reductions for RTS, GMS, and SWP systems highlights the environmental benefits of deploying solar PV technologies. The total lifecycle emissions for RTS, GMS, and SWP are 8,29,249 t CO_2, 45,92,123 t CO_2, and 43,940 t CO_2, respectively, with End-of-Life being the most dominant phase, contributing approximately 60–70% of total emissions. Despite initial emissions from manufacturing and installation, long-term GHG savings significantly outweigh lifecycle emissions, reinforcing the sustainability of these systems.

The GMS system achieves the highest net reduction, offsetting approximately 196,198,812 t CO_2, followed by RTS at 35,42,960 t CO_2 and SWP (Grid) at 2,38,241 t CO_2. Furthermore, SWP (Diesel) reduces 2,79,228 t CO_2, demonstrating the potential emissions savings from replacing diesel-powered water pumps with solar alternatives. The findings emphasize the role of solar PV in mitigating carbon emissions, particularly in decentralized rural electrification and irrigation applications. Enhancements in PV manufacturing efficiency, recycling, and cleaner energy sources for production can further amplify these reductions, positioning solar energy as a crucial component in achieving net-zero emission targets.

Comparative analysis

A comparative analysis of lifecycle GHG emissions from SWP systems versus diesel-based and grid-connected alternatives demonstrates the environmental benefits of solar-based solutions. The total GHG emissions for the SWP system are 43,940 t CO_2. In contrast, diesel-based and grid-powered water pumping systems used as baselines produce significantly higher emissions 323,168 t CO_2 and 282,181 t CO_2, respectively. Diesel systems generate the highest emissions due to direct fossil fuel combustion, making them the least sustainable. Although grid-connected systems emit less than diesel, they remain carbon-intensive owing to the fossil fuel composition of the electricity mix. Fully solar-powered SWP systems, by comparison, yield substantially lower lifecycle emissions. These findings highlight the critical need to replace diesel and grid-based pumps with solar alternatives to reduce carbon footprints, enhance energy access, and support sustainable agriculture in rural areas.

GHG mitigation potential

The GHG mitigation potential of solar photovoltaic systems, including RTS, GMS, and SWP systems, demonstrates a significant reduction in lifecycle emissions when compared to

conventional energy sources such as grid electricity and diesel-based systems. These reductions highlight the effectiveness of solar PV technology in mitigating carbon emissions across different applications, from decentralized household energy generation to large-scale power plants and sustainable agricultural irrigation.

Over a typical 25-year operational lifespan, the cumulative GHG savings from these solar PV installations become even more substantial, reinforcing their role in achieving regional and national emission reduction targets. India, under its Nationally Determined Contributions (NDCs) to the Paris Agreement, has committed to reducing the emissions intensity of GDP by 45% by 2030 and achieving net-zero emissions by 2070. The large-scale deployment of RTS and GMS contributes directly to these goals by replacing fossil-fuel-based electricity generation, which is still a dominant source in the national grid. Meanwhile, the integration of SWP systems supports the agriculture sector's transition towards clean energy, reducing its dependency on grid power and diesel while enhancing rural energy security.

3.6 Summary

The analysis includes all LCA phases, such as manufacturing, transportation, installation, operation and maintenance, and end-of-life processes, ensuring a holistic environmental assessment. These findings reinforce the significance of solar PV deployment in reducing GHG emissions, promoting sustainable energy transitions, and addressing rural energy access challenges. Lifecycle GHG emission estimations provide critical insights into the environmental benefits of solar PV systems. By identifying the stages contributing the most emissions, targeted interventions can be designed to minimize the carbon footprint, thereby enhancing the sustainability of solar energy deployment in rural Assam. The chapter concludes by summarizing the environmental benefits and lifecycle emissions of solar PV adoption and underscores the importance of incorporating LCA methodologies to support informed decision-making for sustainable energy transitions.

References

[1] Amponsah, N.Y., Troldborg, M., Kington, B., Aalders, I. and Hough, R.L. Greenhouse gas emissions from renewable energy sources: A review of lifecycle considerations. *Renewable and Sustainable Energy Reviews*, 39:461-475, 2014.

[2] Tsang, M.P., Sonnemann, G.W. and Bassani, D.M. Life-cycle assessment of cradle-to-grave opportunities and environmental impacts of organic photovoltaic solar panels compared to conventional technologies. *Solar Energy Materials and Solar Cells*, 156:37-48, 2016.

[3] Fthenakis, V.M. and Kim, H.C. Photovoltaics: Life-cycle analyses. *Solar Energy*, 85(8):1609-1628, 2011.

[4] Contreras-Lisperguer, R., Muñoz-Cerón, E., Aguilera, J. and de La Casa, J. Cradle-to-cradle approach in the life cycle of silicon solar photovoltaic panels. *Journal of Cleaner Production*, 168*:*51-59, 2017.

[5] Frischknecht, R., Itten, R., Sinha, P., de Wild-Scholten, M., Zhang, J., Heath, G.A. and Olson, C. *Life cycle inventories and life cycle assessments of photovoltaic systems* (No. NREL/TP-6A20-73853; IEA-PVPS-TASK-12; IEA-PVPS-12-04: 2015). National Renewable Energy Laboratory (NREL), Golden, CO (United States), 2015.

[6] Fthenakis, V.M., Kim, H.C. and Alsema, E. Emissions from photovoltaic life cycles. *Environmental science & technology*, 42(6):2168-2174, 2008.

[7] Sadeghi, D., Ahmadi, S.E., Amiri, N., Marzband, M., Abusorrah, A. and Rawa, M. Designing, optimizing and comparing distributed generation technologies as a substitute system for reducing life cycle costs, CO2 emissions, and power losses in residential buildings. *Energy*, 253:123947, 2022.

[8] Junedi, M.M., Ludin, N.A., Hamid, N.H., Kathleen, P.R., Hasila, J. and Affandi, N.A. Environmental and economic performance assessment of integrated conventional solar photovoltaic and agrophotovoltaic systems. *Renewable and Sustainable Energy Reviews*, 168*:*112799, 2022.

[9] Finkbeiner, M., Inaba, A., Tan, R., Christiansen, K. and Klüppel, H.J. The new international standards for life cycle assessment: ISO 14040 and ISO 14044. *The international journal of life cycle assessment*, 11:80-85, 2006.

[10] Sherwani, A.F. and Usmani, J.A. Life cycle assessment of solar PV based electricity generation systems: A review. *Renewable and Sustainable Energy Reviews*, 14(1):540-544, 2010.

[11] Jiménez-González, C., Kim, S. and Overcash, M.R. Methodology for developing gate-to-gate life cycle inventory information. *The International Journal of Life Cycle Assessment*, 5:153-159, 2000.

[12] Gargiulo, A., Girardi, P. and Temporelli, A. LCA of electricity networks: a review. *The International Journal of Life Cycle Assessment*, 22:1502-1513, 2017.

[13] Granata, G., Pagnanelli, F., Moscardini, E., Havlik, T. and Toro, L.J.S.E.M. Recycling of photovoltaic panels by physical operations. *Solar Energy Materials and Solar Cells*, 123:239-248, 2014.

[14] Eberspacher, C. and Fthenakis, V.M. September. Disposal and recycling of end-of-life PV modules. In *Conference Record of the Twenty Sixth IEEE Photovoltaic Specialists Conference-1997*, pages 1067-1072, IEEE, 1997.

[15] Fthenakis, V.M. End-of-life management and recycling of PV modules. *Energy Policy*, 28(14):1051-1058, 2000.

[16] Domínguez, A. and Geyer, R. Photovoltaic waste assessment in Mexico. *Resources, Conservation and Recycling*, 127:29-41, 2017.

[17] Tschümperlin, L., Stolz, P. and Frischknecht, R. Life cycle assessment of low power solar inverters (2.5 to 20 kW). *Swiss Federal Office of Energy SFOE,* 2016.

[18] Islam, M.T., Huda, N., Baumber, A., Hossain, R. and Sahajwalla, V., 2022. Waste battery disposal and recycling behavior: a study on the Australian perspective. *Environmental Science and Pollution Research*, *29*(39), pp.58980-59001.

[19] Kuchhal, P.I.Y.U.S.H. and Sharma, U.C. Battery waste management. *Environmental science and engineering*, 5:141-155, 2019.

[20] Nordelöf, A. A scalable life cycle inventory of an automotive power electronic inverter unit—part II: manufacturing processes. *The International Journal of Life Cycle Assessment*, 24:694-711, 2019.

[21] Bae, H. and Kim, Y. Technologies of lithium recycling from waste lithium ion batteries: a review. *Materials advances*, 2(10):3234-3250, 2021.

[22] Huang, B., Pan, Z., Su, X. and An, L. Recycling of lithium-ion batteries: Recent advances and perspectives. *Journal of power sources*, 399:274-286, 2018.

[23] Central Electricity Authority. CO_2 Baseline Database for the Indian Power Sector, 2024.

[24] Gautam, Y., Singh, O.P. and Singh, P.K. Economic and environmental benefits of replacing diesel pumps with solar irrigation pumps in Jaipur, Rajasthan. *International Journal of Agriculture, Environment and Biotechnology*, 13(4):469-474, 2020.

[25] Fthenakis, V.M., Kim, H.C. and Alsema, E. Emissions from photovoltaic life cycles. *Environmental science & technology*, 42(6):2168-2174, 2008.

[26] Antonanzas, J. and Quinn, J.C. Net environmental impact of the PV industry from 2000-2025. *Journal of Cleaner Production*, 311:127791, 2021.

[27] Hao, H., Mu, Z., Jiang, S., Liu, Z. and Zhao, F. GHG emissions from the production of lithium-ion batteries for electric vehicles in China. *Sustainability*, 9(4):504, 2017.

[28] Das, J., Abraham, A.P., Ghosh, P.C. and Banerjee, R. Life cycle energy and carbon footprint analysis of photovoltaic battery microgrid system in India. *Clean Technologies and Environmental Policy*, 20:65-80, 2018.

[29] Stokes, C.S., Maier, H.R. and Simpson, A.R. Water distribution system pumping operational greenhouse gas emissions minimization by considering time-dependent emissions factors. *Journal of Water Resources Planning and Management*, 141(7):04014088, 2015.

[30] Eriksson, E., Blinge, M. and Lövgren, G. Life cycle assessment of the road transport sector. *Science of the Total Environment*, 189:69-76, 1996.

[31] Facanha, C. and Horvath, A. Evaluation of life-cycle air emission factors of freight transportation. *Environmental science & technology*, 41(20):7138-7144, 2007.

[32] Cherif, H., Champenois, G. and Belhadj, J. Environmental life cycle analysis of a water pumping and desalination process powered by intermittent renewable energy sources. *Renewable and Sustainable Energy Reviews*, 59:1504-1513, 2016.

[33] Fthenakis, V.M., Kim, H.C. and Alsema, E. Emissions from photovoltaic life cycles. *Environmental science & technology*, 42(6):2168-2174, 2008.

[34] Lima, G.C.D., Toledo, A.L.L. and Bourikas, L., 2021. The role of national energy policies and life cycle emissions of PV systems in reducing global net emissions of greenhouse gases. *Energies*, 14(4):961, 2021.

[35] Alsema, E. Energy payback time and CO2 emissions of PV systems. In *Practical Handbook of Photovoltaics*, pages 1097-1117. Academic Press, 2012.

[36] Artaş, S.B., Kocaman, E., Bilgiç, H.H., Tutumlu, H., Yağlı, H. and Yumrutaş, R. Why PV panels must be recycled at the end of their economic life span? A case study on

recycling together with the global situation. *Process Safety and Environmental Protection*, 174:63-78, 2023.

[37] Agrawal, S. and Jain, A. Sustainable deployment of solar irrigation pumps: Key determinants and strategies. *Wiley Interdisciplinary Reviews: Energy and Environment*, 8(2):325, 2019.

[38] Stolz, P., Frischknecht, R., Wambach, K., Sinha, P. and Heath, G., 2017. Life cycle assessment of current photovoltaic module recycling. *IEA PVPS Task 12, International Energy Agency Power Systems Programme, Report IEA-PVPS T12*, 13,2018.

[39] Ruonan, Z.H.A.O., Li, D.O.N.G., Qi, Q.I.A.O., Jingyang, L.I.U., Lu, B.A.I., Yue, Z.H.A.N.G. and Minghui, X.I.E. Life cycle assessment of photovoltaic module considering disposal stage. *Journal of environmental engineering technology*, 11(4):807-813, 2021.